EXPLORING HYPERSPECTRAL AND VERY HIGH SPATIAL RESOLUTION IMAGERY IN VEGETATION CHARACTERIZATION

KONGWEN ZHANG

A DISSERTATION SUBMITTED TO THE FACULTY OF GRADUATE STUDIES IN PARTIAL FULFILLMENT OF THE REQUIREMENTS FOR THE DEGREE OF

DOCTOR OF PHILOSOPHY

GRADUATE PROGRAM EARTH AND SPACE SCIENCE

YORK UNIVERSITY

TORONTO, ONTARIO

AUGUST 2014

© Kongwen Zhang, 2014

Abstract

This dissertation describes three contributions in characterization of vegetation using remote sensing data, with a focus on hyperspectral and very high spatial resolution imagery. The new and innovative methods developed are: 1) integration of contribution theory into a model inversion approach to obtain high accuracy in canopy biophysical parameter estimation; 2) exploration and adoption of tree crown longitudinal profiles to achieve high accuracy in tree species classification; and 3) evaluation of canopy health state for Emerald Ash Borer (EAB) infestation assessment by intelligent combination of multi-sourced data.

Specifically, the contribution index (CI), which is a simple effective measure of correlations between observations and targeted parameters, has been derived and implemented into remote sensing model inversion for parameter retrieval processing. CI can obtain quantitative and normalized “sensitivity” values for each band using a vegetation canopy model. When including CI as a weight function, the inversion processing would focus more on high contribution bands. As a result, it can significantly improve the accuracy of estimation of the parameters retrieved.

Given the rapid advancement in spatial resolution of remotely sensed aerial imagery during the last decade, interest rises in the potential of very high spatial resolution multispectral imagery in improving the tree species classification. For the first time, the pioneering works on the longitudinal profile of individual tree crowns are revisited and explored in depth with currently available high spatial resolution imagery. It has been revealed that the tree crown longitudinal profile can be used to achieve high accuracy tree

species classification. In addition, it is also shown that using vegetation index combination approach can recover shaded trees from aerial imagery, which is essential for urban canopy studies.

In order to demonstrate the effectiveness of remote sensing for estimation of canopy health state evaluation applications, a case study is conducted. Advanced remote sensing techniques and methodologies are employed to detect the ash Emerald Ash Borer (EAB) infestation at the early stage. The contribution of this study is the innovative development of a data integration methodology; the handling and analysing of the multi-sourced data in order to achieve optimized classification or estimation results. A new generalized workflow is proposed for future similar applications: 1) individual tree segmentation; 2) biophysical parameter retrieval using model inversion and vegetation indices; 3) parameter normalization and conversion; and 4) final evaluation function and result estimation.

I dedicated this research to my beloved wife, June Dai, and to my loveable daughter, Iris. And to all my family and friends, you are all have been very supportive of my research and, whom often provide me with encourage and enthusiasm when I was lacking.

Acknowledgements

I would like to acknowledge, with the deepest appreciation, my supervisor, Dr. Baoxin Hu; my co-supervisor, Dr. Jian-guo Wang; and my supervisory committee member Dr. Spiros Pagitakis. Your guidance was an invaluable source of support during the course of my work.

I also acknowledge, for the financial support through research grants, the Natural Sciences and Engineering Research Council (NSERC) of Canada. I am also indebted to the database of the field campaigns in Ottawa, obtained from a project led by Dr. Elizabeth Pattey, jointly funded by Agriculture & Agri-Food Canada (AAFC), the Canadian Space Agency (CSA) through the Government Related Initiatives Program (GRIP), and GEOmatics for Informed Decisions(GEOIDE). The CHRIS data were provided by ESA through the project led by Dr. Anne Smith of Agriculture and Agri-Food Canada. The high spatial resolution, multi-spectral imagery was supported by the York University library and the help from their staff. The Emerald Ash Borer (EAB) studies' ground support was provided by Ms. Ziya Li and Ms. Meagen Eastwood from Toronto Region Conservation. The ground spectral signature and airborne data of the branch sampling project was provided by the Town of Oakville and the technical support from staff, Mr. Ian Hanon of AMEC.

I would also like to thank the research scientists, staff and graduate students of the Earth Observation Lab and GeoICT Lab for their support and patience with regards

to my work. In particular, I would like to thank Dr. Qingmou Li, Dr. H. Peter White, Dr. Linhai Jin, Dr. Inian Moothy, Mr. Jim Freemantle, Mr. Kun Qian, Mr. Jiangtao Liu, Mr. Roy Soffer, and Mr. Jili Li all of whom offered valuable assistance during my work.

I also really appreciated that Selkirk College (Castlegar, British Columbia, Canada), School of Environmental and Geomatics, provided me with the opportunity to start my teaching career while completing my Ph.D. work.

Also, in particular I would like to thank my friends, Mr. Zoltan Herman, Mr. Alexander Papini, Ms. Jerusha Lederman, and Mr. Justin Robinson, for their editorial help with my manuscripts and final dissertation.

I am grateful to the following examination committee members: Dr. Zheng Hong (George) Zhu, Dr. Costas Armenakis, and Dr. H. Peter White, for their comments and suggestions to improve this dissertation.

A special thanks to my family and friends for being supportive and patient. I wouldn't be who I am today without you.

Finally, I would like to thank York University, the department of Earth and Space Science and Engineering, for their financial assistance and technical support that allowed me to pursue and complete my Ph.D. degree.

TABLE OF CONTENTS

List of Tables

List of Figures

List of Units

Radiance	$Wsr^{-1}m^{-2}$
Irradiance	Wm^{-2}
Leaf area index (LAI)	[ ]
Leaf chlorophyll content a and b (Cab)	μgcm^{-2}
Equivalent water thickness (Cm)	cm
Leaf dry matter (Cw)	μgcm^{-2}
Leaf structure parameter (N)	[ ]
Wavelength	nm
Solar zenith angle	◦
View zenith angle	◦
Reflectance	[ ]
Leaf angle distribution	μgcm^{-2}
Contribution index	[ ]
Position (p)	[ ]

List of Symbols

General model function	F
Parameter vector	X
Observation vector	L
Parameter correction vector	Δx
Jacobian matrix	J
Weighting matrix	P
Initial parameter value vector	x_0
Prediction matrix (H matrix)	H
Diagonal elements vector of H	h_{ii}
Contribution index	CI
Leaf structure parameter	N
Leaf chlorophyll content	Cab
Equivalent water thickness	Cw
Leaf dry matter	Cm
Canopy profile normal distance	d, dm
Canopy profile position ratio	p
Canopy profile first portion	a
Canopy profile second portion	b
Canopy smooth factor	R^2
Individual parameter weight	ω_i
Information from each feature (parameterized)	P_i
Number of features (parameters)	N
Priori-knowledge constant	C
Distance constant	Cd

Abbreviations

ANN	**Artificial Neutral Network**
AMS	**Airborne Multispectral Sensors**
ASD	**Analytical Spectral Device**
AVHRR	**Advance Very High Resolution Radiometer**
AVIRIS	**Airborne Visible-Infrared Imaging Spectraometer**
BRDF	**Bidirectional Reflectance Distribution Function**
BRF	**Bidirectional Reflectance Factor**
Cab	**leaf Chlorophyll content a and b**
CAM5S	**Canadian Advanced Modified 5S**
CASI	**Compact Airborne Spectrographic Imager**
CLUT	**Contribution index implemented Look Up Table**
CHRIS	**Compact High Resolution Imaging Spectrometer**
CI	**Contribution Index**

EAB	**Emerald Ash Borer**
ETM	**Enhanced Thematic Mapping**
FLIGHT	**Forest LIGHT Interaction**
FIFEDOM	**Frequent Image Frames Enhanced Digital Orthorectified Mapping**
GLCM	**Grey-Level Co-occurrence Matrix**
GLOM	**Grey-Level Occurrence Matrix**
GO	**Geometric Optical**
GOES	**Geostationary Operational Environmental Satellite**
GORT	**Geometric Optical Radiative Transfer**
MSS	**Multispectral Scanner**
NDVI	**Normalized Difference Vegetation Index**
TM	**Thematic Mapping**
LAD	**Leaf Angle Distribution**
LAI	**Leaf Area Index**
LDCM	**Landsat Data Continuity Mission**
LiDAR	**Light Detecting and Ranging**
LIBERTY	**Leaf Incorporating Biochemistry Exhibiting Reflectance and Transmittance Yield**

LUT	**Look Up Table**
NDVI	**Normalized Differential Vegetation Index**
OLI	**Operational Land Imager**
PARABOLA	**Portable Apparatus for Rapid Acquisition of Bidirectional Observation of the Land and Atmosphere**
POLDER	**Polarization and Directionality of the Earth's Reflectances**
PROSAIL	**PROSPECT + SAIL**
PROSPECT	**PROperties SPECTra**
RAMI	**Radiation Model Inter-comparison**
RMSE	**Root Mean Square Error**
SAIL/SAILH	**Scattering by Arbitrarily Inclines Leaves / with Hotspot**

Preface

It was a 13 year long, best of my life spending at York University. I had my Bachelor, Master and Ph.D. all three degrees from York University. Hopefully, this Ph.D. degree would be the third, the final decoration on my wall to conclude this student era. It was impossible to express the mixture feeling at this moment. It is definitely a completely relief, but also a bit of lost and confused. All these years, all of the memories have been flashing and rewinding in front of my eyes. I don't even realize how would I end up doing of this and going this far. I had a simple dream when I first stepped on the Canadian soil back in 2001. I quitted my Chinese university life just after one semester and started as an ESL student of a private high school called Madison Academy, which was closed in 2007. I wanted to go back to university so badly, and you would have no idea how difficult it was to apply for university an international student at that time. There was no time for me to waste on any universal English language evaluation exams, such as TOFEL or IELTS. It was York University, provided me an opportunity that to write the York version English test, YELTS. Three months, it was the time took me to get accepted into York University, Engineering program in 2001. I should be considered lucky, maybe. However, I believe the York education philosophy is far more practicality and effective comparing with IELTS I took 5 years later for my immigration application. It was pathetic for some education experts to mark me "competent, average" after had an argument with about the senior society

issue in China. Languages are for communications. Tests are for skill evaluations, not for opinion. The first two years of York study was really the hardest life struggling. All the issues, problems, and crisis happened. I was so lucky to have all these best, nicest and humblest personal around me. It was my friends, my professors and family members to encourage me through that "dark period". I would never forget got my Engineering drawing back with 40% grade, but Dr. Spiros Pagiatakis recognized my afford, which was really solid eight hours work. The third year was my best year. I had found my right position and got used to university life in Canada. It was that year I first met my wife, June. I was thankful for my supervisor of life, Dr. Baoxin Hu giving me the opportunity of working at the research lab, Earth Observation Lab (EOL) at York. It was that summer I found my future direction. I decided to continue on Geomatics engineering, especially Remote Sensing. That decision lead me walk all the way to now, and complete unexpected outcome comparing the initial dream I had that to have a Canadian bachelor degree. It was very grateful to know Dr. Jianguo Wang in my late year of undergraduate. He was like my guardian, like my father at York. His wisdom inspired so much of my life. He would encourage me when I was down, and warm me when I was cocky. My Master degree went fairly smooth, but the Ph.D. degree life had been problematic for me. I got married in 2008 and had my lovely daughter, Iris. The happy, single man had gone since. The social, finical, family press had landed on the man whom was not really ready for it. I failed, almost crashed completely. Once again, it was my friends, my professors and my family helped me and lift me back out of water. I could not be more gratitude to all of them. It was a hard and cold period of life that one man tried to rebound from a crashing failure. At the first semester of 5th year, I had presented an opportunity to start my

teaching career in Selkirk College before the Ph.D. completion. My supervisors, Dr. Hu and Dr. Wang were very understanding and supportive, even it was a not a typical favoured decision. It had proved that it was a dilemma, which I got teaching, research experience, good career, and financial relief, but significantly delaying Ph.D. progress and had suffered over one year of family separation. I would like to apology for the emotional behaviours towards to the end of my Ph.D. completion. It was another critical life experience to me, doubt yourself before doubt the others. Now, I finally put a conclusion to this. I would like to say thank you to everyone whom helped all these years. To anyone actually read this far, thank you for your time.

1 Introduction

This chapter underlines the importance of quantitatively characterizing vegetation canopies. The challenges in such studies are presented, and the research motivation is introduced. It is followed by the research goal and objectives, which aim at developing innovative methodologies to obtain ground vegetation object characteristics precisely and effectively. The contributions of this dissertation are presented next. Finally, the chapter concludes with a summary of the dissertation organization.

1.1 Quantitative characterization of the Earth's vegetation using remote sensing techniques

Vegetation covers approximately 70% of the Earth's land surface and is considered as one of the most fundamental land coverage types (Darvishzadeh, 2008). Reliable and quantitative information of vegetation properties is required to understand, monitor and manage the global environmental changes (e.g., climatic, ecosystem) (Matzler, 2008; Peddle et al., 2007). However, due to the Earth's wide variety of vegetation types and environments (e.g., Arctic tundra, tropical forest, savannah, desert scrub.), it is difficult to characterize its vegetation. Figure 1.1 shows a vegetation example taken from one of testing sites near Thessalon, Ontario, Canada. The left image shows the complex canopy composition (e.g., different species and large variation of heights),

while the right image shows the structure of the canopy' layers. To understand these types of surface objects using traditional *in-situ* survey techniques is very difficult, expensive and labour intensive. This is particularly true in countries like Canada, which combine large areas of vegetation landscapes in extreme winter environments. Therefore, there is an urgent need to develop effective methodologies to monitor their natural resources.

Figure 1.1: The typical canopy of one of testing sites near Thessalon, Ontario, Canada. Left: side view shows the complex canopy composition; Right: upper view from ground shows the canopy's structural variation at different heights.

As defined by Lillesand et al. (2008), "*Remote sensing is the science and art of obtaining information about an object, area, or phenomenon through the analysis of data acquired by a device that is not in contact with the object, area, or phenomenon under investigation*". Remote sensing is being widely recognized as the science that uses a variety of sensors to acquire information and subsequently that can characterize different vegetation types, at various scales, particular at regional, continental and global scales (Atzberger, 2013; Kuenzer et al., 2011). This is due to its global coverage, repeatability, non-destructiveness, high flexibility and relative low cost (Ahamed et al., 2011; Rosenqvist et al., 2003). At large spatial scales, spaceborne remote sensing

sensors scan the entire Earth's surface in a relatively short period of time, normally in days, even hours. Figure 1.2 shows a biomass distribution map from the spaceborne Advanced Very High Resolution Radiometer (AVHRR). The AVHRR is a radiation-detection imager that can be used for remotely observing surface and atmospheric properties, which are critical for environmental monitoring, economic assessment and resource management[1]. To obtain a similar map using traditional ground methods would be a very time consuming and expensive project. For small scale and emergency response tasks, where budgets and time are critical, airborne remote sensing techniques can offer rapid and flexible deployment at a low operational cost (Jensen, 2007).

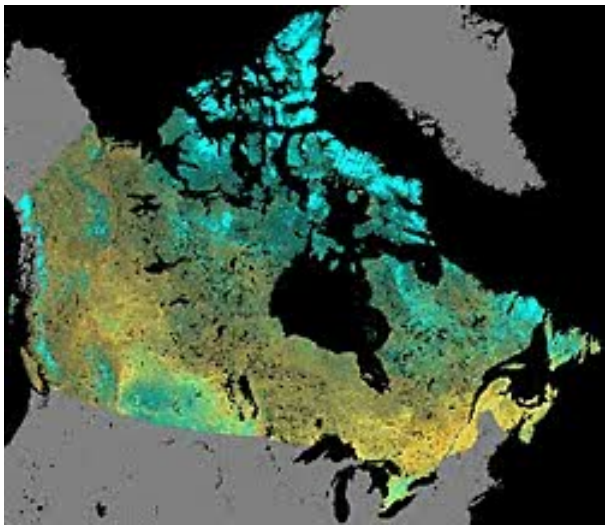

Figure 1.2: A vegetation biomass distribution map from AVHRR (1 km spatial resolution). Green shows higher biomass, while yellow indicates lower biomass. Courtesy of Canada Centre for Remote Sensing (CCRS) and Natural Resource Canada. http://geogratis.cgdi.gc.ca/clf/en?action=noaa. Last access: June 25, 2014. Used under non-commercial purpose permission.

[1]Satellite Products Services Division. Advanced Very High Resolution Radiometer - AVHRR. http://noaasis.noaa.gov/NOAASIS/ml/avhrr.html. Last accessed: August 25, 2014.

From the point of information retrieval, visual interpretation is currently employed by the Canadian forestry sector, which typically provides qualitative evaluation (e.g., vegetation or non-vegetation) and moderate accuracy in species inventory maps (the composition of vegetation species with an area are estimated at typical 60–70 % accuracy). Using very high spatial resolution aerial imagery (Figure 1.3), image analysis specialists would interpret this aerial image by outlining the boundaries of, and assigning the areas' primary tree species. The quality of the boundary lines and measurements from this approach heavily depends on the interpreters' experiences.

Advanced remote sensing methodologies aim to improve quantitative characterization of vegetation properties that can be adopted, for example, for forest inventory updates (Coggins et al., 2013). Significant efforts have been made to develop models and algorithms to extract important vegetation spectral characteristics (e.g., "green peak", "red edge"), angular reflectance distribution (reflectance variability observed at different angles), and temporal variations (e.g., growth, seasonal changes) from remote sensing data (Ozdogan et al., 2010; Weiers et al., 2004).

1.2 Research motivation

Despite the importance of the quantitative characterization of vegetation canopies, extraction of their properties from remote sensing data accurately and efficiently is still challenging. This is due to the complex nature of vegetation canopies (e.g., the same vegetation species may have different spectral signatures and different vegetation species may share some spectral similarity), compounded by the constraints in the physical configurations of sensors and associated observation noise. The recent advances in remote sensing technologies provide data with unprecedented resolution

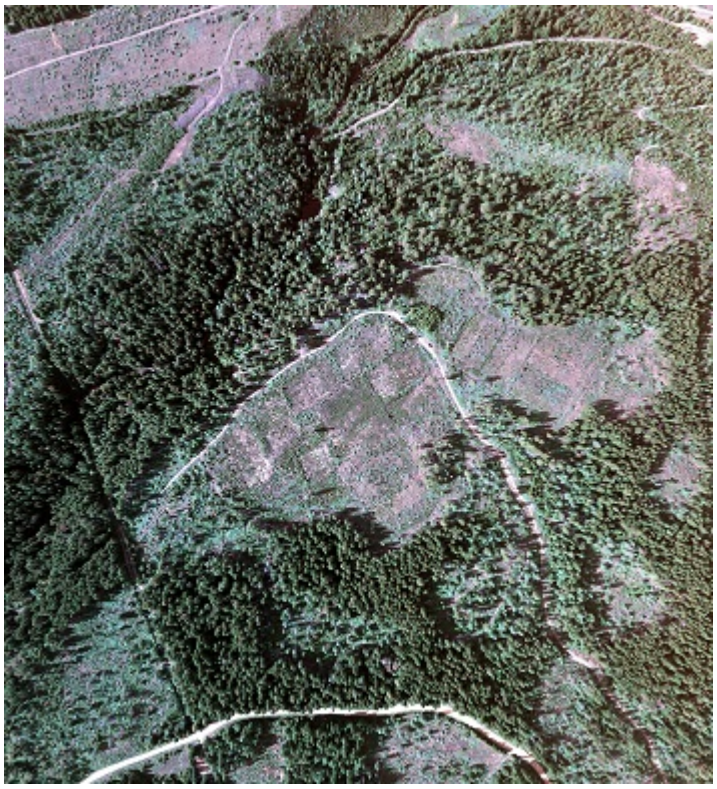

Figure 1.3: A very high spatial resolution aerial imagery over Rover Creek site near Castlegar, British Columbia, Canada. The forest sector uses such images for inventory maintenance by visual interpretation techniques.

in both, spatial and spectral (very high spatial resolution, and hyperspectral sensor, respectively) thus, they provide a good opportunity to improve vegetation characterization. With detailed spectral and spatial information provided by hyperspectral and very high spatial resolution data, subtle difference in the spectral and spatial properties among vegetation canopies can be detected and used. To fully realize the potential of these data sources, advanced methods for data interpretation and analysis are required.

This research focuses on developing innovative state-of-art data analysis and information retrieval methodologies that can be used to accurately and effectively characterize the properties of various vegetation canopies. To improve the accuracy of

vegetation characterization from remote sensing data, one must specify the format of the "interesting information". Only when the information is determined, can existing methods be reviewed, their limitations be revealed, and improvements be proposed. In this study, the focus is on biophysical/biochemical parameter retrieval, vegetation species classification, and tree health state estimation. In most of current existing methods, empirical relationships between vegetation properties and remote sensing observations are established, and validated for specific study areas and with specific data. Strictly speaking, these methods are normally valid on the cases they are developed. Other scenarios require a suitability determination prior to applying them. If it is found not applicable, these methods simply cannot be used. This seriously constrains the effectiveness and usefulness of such methods towards extracting reliable information. Developing data analysis methodologies that are less dependent on the characteristics of a sensor and its observations would significantly improve the effectiveness of remote sensing techniques. Therefore, the ideal method for data processing is the one that evaluates the correlation with the physical model, and can be very flexible on the observation characteristics. In this research, an innovative integration of contribution theory (Hoaglin and Welsch, 1978) into physical model inversion parameter retrieval processing, is developed to derive the contribution index that is: an indicator that evaluates the correlations between observations and parameters of interest solely from physical models, applicable to any data specifications and independently from associated noise. The details are discussed in Chapter 3 of this dissertation.

It is generally accepted that instrumentation development and observation methodology improvements have advanced more rapidly than data processing methodologies and modelling in remote sensing (Atzberger, 2013; Ozdogan et al., 2010). The ad-

vancement in instrumentation development, such as higher computation power and new satellite sensors, provides a large volume of high quality observations which have not yet been fully exploited. For example, increasing spectral and spatial resolution of the observations can capture more spectral and spatial details of ground features. In certain studies, one needs to downscale the data by resampling to reduce their s-patial resolution to a lower value to fit the model applicable scale. This leads to the re-evaluation and improvement of existing methodologies and mathematical models that were limited in the past by data quality. One of the major improvements in remote sensing data quality is in spatial resolution. The spatial resolution of the space borne sensor systems has been improved from the kilometre to the centimetre level, which inspired me to derive critical information from high spatial resolution imagery for use in vegetation characterization. The longitudinal profile of the tree crown has been remodelled for new very high spatial resolution imagery and can deliver critical spatial pattern information for tree species classification. Precise species classification information is the most critical foundation for all vegetation associated studies.

After 40 years of development, a very large volume of remote sensing data has been accumulated. However, these data have been collected by a wide range of sensors under various specifications, and processed and corrected by different methodologies. In most studies, information obtained from remote sensing data is validated by data from other sources, remotely sensed or not (e.g., paper records, maps). While remote sensing has benefited from rich data originating from various of remote sensing platforms, it is a challenge to employ them intelligently, effectively and appropriately. Non-remote sensing data are currently used as ground truthing for final accuracy validation purpose only. It is recognized that they also have potential for including them directly for

processing analysis and interpretation. This inspired my commitment to use multiple sourced data, whether remotely sensed or not, to improve vegetation characterization.

1.3 Research goal, objectives and contribution of this dissertation

The goal of this research is to improve existing and develop new innovative remote sensing data analysis methodologies to fully realize the potential of current high volume, superior quality and multi–sourced remote sensing data to improve the accuracy and precision of vegetation characterization. Simply stated, this dissertation develops state–of–art data processing methodologies to accurately extract vegetation properties using quantitative biophysical parameters, such as tree species, tree heights, and leaf chlorophyll content from high spectral and spatial remotely sensed data.

Accurate retrieval of biophysical parameters is the key to the success of quantitative remote sensing. For example, the retrieval of leaf area index (LAI), tree heights, tree crown sizes and canopy distribution can provide an accurate and detailed description of the targeted canopy. My first focus is to develop an effective, simple and robust methodology that can accurately retrieve biophysical parameters from the observations, which means higher retrieval accuracy than current approaches without extra computation cost. It is also less dependent on observation characteristics, which means the methodologies can be adopted by different retrieval approaches and be applicable on different data. In this study, a contribution index (CI) is designed to quantify the impact of each observation on the retrieval of model parameters. It accounts for the sensitivity of the given observation to the model parameters to be retrieved and the observation uncertainty (e.g., systemic and random errors from the sensors and

measurements).

Tree species classification is critical in forestry studies. The first step of most forestry studies requires tree species information. For example, to investigate whether there are possible infestations of insects or bugs, tree species must be identified first. This is due to the fact that most infestations are species specific. My second focus is to explore and identify new features for species classification improvement that leads to my second significant contribution.

Last, I develop effective integrated data analysis to address the urgent need of intelligently employing large remote sensing data sets. For the same research field, data from non-remotely sensed sources are also collected (e.g., ground survey records, historical documentations). All these data can potentially be used to obtain useful information on the ground target. Multi-sourced data can be processed separately or integrated together. Information derived from different data may or may not be consistent due to differences in information interpretation methodologies and ground object properties. Traditional processing approaches and algorithms are not sufficient to handle multi-sourced data.

The research objectives in this study are:

1) Intelligent integration of a CI towards the improvement of the accuracy of the retrieval of the biophysical parameters of vegetation canopies from hyperspectral remote sensing data.

2) Adoption of innovative spatial features (longitudinal profile of individual tree crowns) derived from very high spatial resolution imagery in order to improve classification accuracy. This is an important but neglected feature that could not be captured in the past due to limitations in image spatial resolution.

3) Development of a data integration and intelligent analysis methodology that requires an innovative approach to integrate multi-sourced data in order to achieve optimized classification or estimation results.

The achievement of the above objectives have generated three peer-reviewed articles published in international journals: the *Canadian Journal of Remote Sensing*, the *Remote Sensing*, and the *Journal of Applied Remote Sensing*, respectively. In addition, the research results have been presented at international conferences, such as the *"Canadian Symposium of Remote Sensing" (CSRS)* and the *"International Geoscience and Remote Sensing Symposium" (IGARSS)*. Chapters 3 to 5 of this dissertation are the based on the published (or accepted) papers.

1.4 Dissertation outline

This is a publication based dissertation, and is organized around published papers. Chapter 1 provides an introduction to this research, including my research motivation, goals, objectives and contributions. Chapter 2 presents the supportive material for a more detailed background related to the three published papers. For all three papers (Chapter 3–5) I am the primary contributor, first and corresponding author. My contributions and roles in these scholarly articles include but are not limited to initial objective development, overall literature reviewing, methodologies development, data processing (including new software development and use of commercial tools), result validations, and manuscript preparation and revisions.

Chapter 3 is the first published paper (Zhang et al., 2011). It constitutes further development of my conference paper, Zhang et al. (2009). It describes a new method I proposed to improve the biophysical parameter retrieval accuracy from hyperspectral

imagery. In this chapter, I introduce the new CI based on contribution theory, which was originally developed for geodetic surveys (Hoaglin and Welsch, 1978) to the standard of Look–Up–Table (LUT) model inversion approach. I evaluate the correlations between observations and targeted parameters prior to the inversion process and take the individual observation noise into consideration. The inversion is performed on the highly correlated and low noise spectral bands. As a result, the inversion accuracy is expected to be higher.

Chapter 4 is the second published paper (Zhang and Hu, 2012). I explore a spatial feature called the "longitudinal profile", which is an intensity section of the individual tree crown tops from very high spatial resolution imagery. I derive spatial information from it, and use it to improve tree species classification accuracy. The approach for extracting longitudinal profiles is developed in this chapter based on the pioneer work of Fourier et al. (1995). The significant improvement of the spatial resolution of the multispectral imagery enables tree crown spatial pattern identification for species classification improvement.

Chapter 5 is the third published paper (Zhang et al., 2014). It is the in-depth development of my conference paper, Zhang et al. (2012). It reports a case study that integrates multi–sourced data to evaluate the health state of ash trees in the town of Oakville, Ontario, Canada. Current remote sensing data provide a lot of information, but from different sensors, in different formats (e.g., spectral and spatial), and of different quality (with or without multiple corrections and calibrations). In this case study, I include non–remote sensing data, such as paper community maps and documents. Existing classification approaches were not found sufficient handle all the data assimilation intelligently. The data are constrained to fit into standard models, which cause information loss. I conclude the research contributions with a case study in early detection of Emerald Ash Borer (EAB) infestation of ash trees in southern Ontario. My case study demonstrates an approach that can intelligently integrate all information retrieved from multi-sourced data, and apply it to increase the possibility of detecting EAB infestation in its early stages.

Chapter 6 concludes the research work, highlights the contribution and points out limitations and possible areas for future investigations.

2 General background

This chapter provides details of supportive material of the conducted research. It is organized in three major sections: 1) it begins by introducing remote sensing in general; 2) it is then followed by detailed descriptions of major sources and types of remote sensing data; 3) the topics on the current remote sensing data processing, analysis and interpretation are presented. Part 1 provides a general understanding and an overall big picture of remote sensing. Since a few types of remote sensing data are used in my studies, it is important to have a compensative review of different remote sensing sensors and their data, which is why part 2 is presented. The model inversion approach and information retrieval is one of the main focus, therefore, it is necessary to include a review for different models and information retrieval methodologies, which is part 3.

In the introduction section, the history of the development of remote sensing is reviewed; the primary characteristics of remote sensing are identified; and the general workflow of remote sensing data acquisition, transmission and analysis are presented. Then, the two main components of remote sensing, namely instrument development and data analysis are discussed, leading to the next two major sections of this chapter namely, different data sources and data analysis and interpretation (data mining).

In the data source section, the focus is on the data used in this research, namely multi/hyperspectral, multi-angular data, and high/very high spatial resolution im-

agery. Multi/hyperspectral data are very similar, differing mainly in the number of the bands, which is defined as *"the specific wavelength intervals in the electromagnetic spectrum of remote sensing instrument"* (Jensen, 2007).

The information retrieval procedure is normally divided into two steps: the feature extraction and the information extraction. A spectral feature in multi/hyperspectral data can be the reflectance in an individual bands or individual band or result of transforming the reflectance values associated with multiple bands. In the context of high spatial resolution imagery, spatial features, such as texture, can be extracted to describe the spatial patterns of vegetation canopies. "Information", is understood as "facts derived from observations that can be provided or learned about someone or something". For example, the hyperspectral data requires remote sensing expertise to understand and process; however, the tree heights as information derived from hyperspectral data can be easily understood by everyone. The information extraction process is briefly introduced with forward modelling and radiative transfer models, and in the retrieval of biophysical parameters, which includes the vegetation index, model inversion approaches, and species classification. The forward modelling of radiative transfer models is using mathematical equations to simulate the observations via a designed set of parameters, while the model inversion (or inverse modelling) are refereed to the procedure that determines the optimal parameter set that produces the most similar spectra comparing with the observed one. The contribution analysis is a very important methodology and it is adopted throughout this research.

2.1 Introduction to remote sensing

Remote sensing science has its roots in photography (Jensen, 2000). However, remote sensing was not considered a branch of science, rather it was regarded only as a tool or a method in data collection (Matzler, 2008). The term "Remote Sensing" was coined by the geographers at the US Office of Naval Research in the 1960s at about the time when the "spy satellites" were beginning to move out of the military sphere and into the civilian milieu (Cracknell and Hayes, 2007). Any definition of remote sensing, e.g., by Lillesand et al. (2008), includes two important characteristics: remotely acquired data and dedicated data analysis methodologies. Remote sensing data acquisition is conducted by instruments not physically in contact with the target of study. This unique attribute has allowed remote sensing to gain wide recognition and adoption in a variety of fields, particularly in Earth surface vegetation studies (e.g., forest and agriculture). It is unobtrusive, which means it does not disturb the object or area of interest and can have very high flexibility in terms of access ability (Ahamed et al., 2011; Pu and Gong, 2000). In this study, the focus of remote sensing is on the Earth surface objects, which primarily involves interactions of incident radiation on the targets of interest. It is different from the another important remote sensing branch namely, atmospheric remote sensing, which is of interest mainly in the atmospheric energy and aerosol interaction. However, the overall remote sensing data acquisition and analysis is a lengthy and complicated process, and it is shown in Figure 2.1. In Figure 2.1, step A is energy source or illumination, B is radiation and the atmosphere, C is interaction with the target, D is recording of energy by the sensor, E is transmission, reception, and processing, F is interpretation and analysis and G is applications (Canada Centre for Remote Sensing (CCRS)).

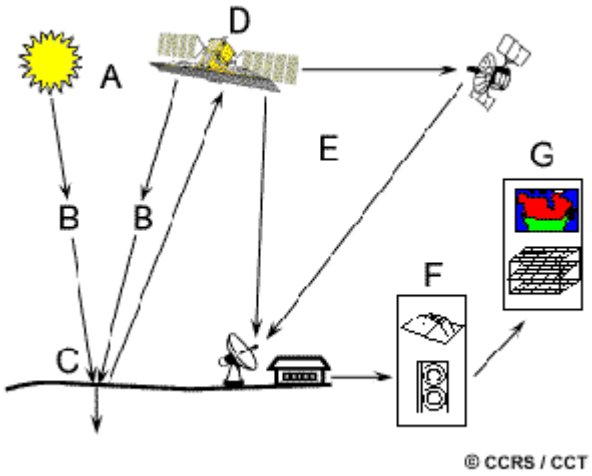

Figure 2.1: From step A to G, the overall data acquisition, processing and analysis procedures of remote sensing provided by CCRS. [Courtesy of CCRS. Used under non-commercial purpose permission. http://www.nrcan.gc.ca/earth-sciences/geomatics/satellite-imagery-air-photos/satellite-imagery-products/educational-resources/14621. Last access: August 25, 2014]

This chapter is organized in two main components: instrumentation and data processing and analysis (Matzler, 2008). The instrumentation component addresses the question: How is the reflected or emitted electromagnetic energy from ground targets recorded by a device or sensor, such as camera, multispectral scanner, hyperspectral scanner, RADAR (RAdio Detection And Ranging), and LiDAR (Light Detection And Ranging). The data analysis component aims to answer the following question: How can we extract biophysical parameters of surface objects from remotely sensed data to solve important problems? (Jensen, 2007).

2.2 Different remote sensing data sources

Remote sensing of the Earth's surface, whether land or ocean is carried out using a variety of different instruments. These instruments work in a range of different wavelengths (e.g., visible (420 - 680 nm), near inferred (800 - 1000 nm)) bands of the electromagnetic radiation spectrum and employ various recording techniques or systems, such as cameras, multispectral scanners, sonar, radar, and LiDAR (Cracknell and Hayes, 2007). As a result, there are many different types and forms of remote sensing data available. They are divided into different classes by their wavelengths, such as visible and thermal instruments. They can also be categorized by their platforms, which are ground based, airborne and spaceborne (satellite based). In most cases, they are characterized by their attributes, such as spectral and spatial resolutions.

Let us start with a general comparison between multi/hyperspectral remote sensing. They are arguably the most popular data in remote sensing and have been used throughout this research. They are normally mentioned together due to their similarity. They both target on the spectral signature of ground targets, which means that they measure the reflected radiance at different wavelengths. Radiance is the measure of radiation flux that passes through or is emitted from a surface and falls within a given solid angle in a specified direction. The unit of radiance is normally $Wsr^{-1}m^{-2}$. Irradiance is the power of electromagnetic radiation per unit area incident on a surface, which has a unit of W/m^2. Reflectance is the ability of a surface to reflect electromagnetic radiation, and is measured by the ratio of the reflected flux to the incident flux, thus it is a fraction of 0 to 1 or a percentage (Jensen, 2007). The primary differences between multi/hyperspectral data are the number of spectral bands (e.g., ETM+ 6 bands vs. CASI 63 bands), discrete vs. continuous, and bandwidth (broad

(> 10 nm) vs. narrow (< 5 nm)) as shown in Figure 2.2. For vegetation studies, multi/hyperspectral data capture the spectral characteristics of vegetation canopies, which are primarily affected by the internal and external structure and biophysical and biochemical parameters of the plants, such as leaf pigments, leaf water content, and leaf dry matter (Gates et al., 1965; Goel and Grier, 1988; Jacquemoud et al., 1995). Compared with multispectral remote sensing data, hyperspectral data cover more spectral details due to the additional bands. For most vegetation studies, some bands, such as green, blue, red and NIR, are much more important than others. Using hyperspectral data, there is no need to identify the band during the data acquisition phase, which means more potential for future data analysis, but at a trade-off of data acquisition cost and complexity.

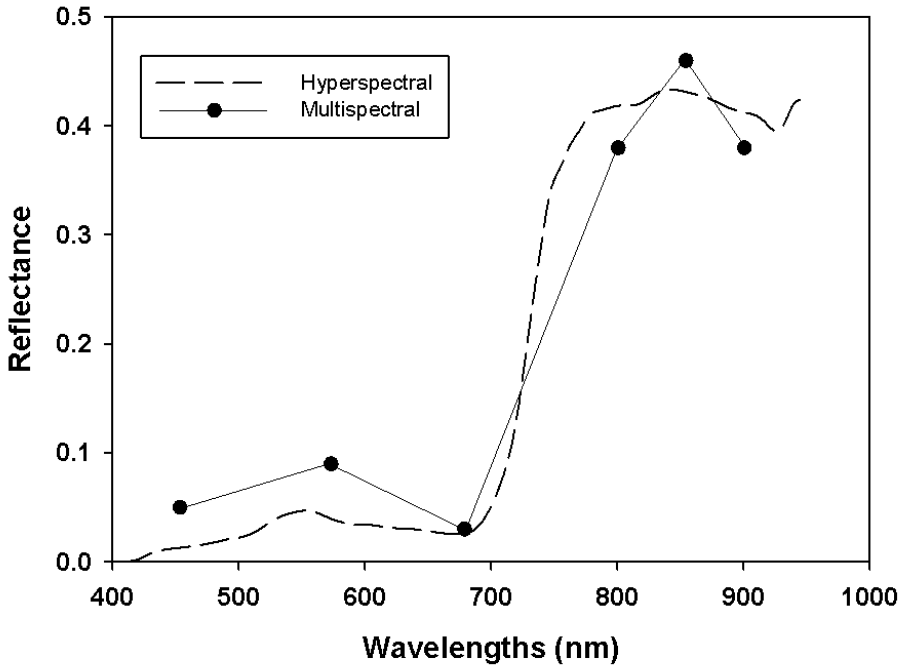

Figure 2.2: Visual differences between discrete and continuous spectra of the same target (typical alive green vegetation) in ETM+ (6) multispectral and CASI (62) hyperspectral bands.

2.2.1 Multispectral remote sensing data

A multispectral image is a collection of several monochrome images of the same scene, each of which is taken at discrete and broad bands of bandwidth greater than 10 nm (Jensen, 2000). Normally, multispectral images have only a few bands (e.g., ETM+ six spectral, one thermal and one panchromatic bands) and broad bandwidth as shown in Figure 2.2.

The first satellite-based multispectral sensor was the Multispectral Scanner Sensor (MSS) on board Landsat 1. Landsat 1 was the first Earth-observing satellite launched by NASA on July 23, 1972, to study and monitor our planet's landmasses. The MSS recorded data in four spectral bands: green (500 - 600 nm), red (600 - 700 nm), and two infrared bands (700 - 800 and 800 - 1100 nm) at spatial resolution of 79 metres (green, red and near-infrared) and 240 metres for thermal. As stated on NASA website: "*[MSS] To help understand the data and to explore the potential applications of this new (multispectral) technology ...*" Later, improved versions of sensors were launched on newer Landsat missions, from MSS, to Thematic Mapping (TM) and Enhanced Thermal Mapping Plus (ETM+) sensors (Jensen, 2000; Lillesand et al., 2008). The Landsat program provides in the longest global Earth observation data series, which are essential for climate change studies and other environmental concerns (Gray and Song, 2013). The latest Landsat 8 was launched on February 11, 2013 through the Landsat Data Continuity Mission (LDCM) with the new multispectral sensor called Operational Land Imager (OLI) on payload.

Other satellite based multispectral sensors include, but not limited to Moderate Resolution Imaging Spectroradiometer (MODIS), Geostationary Operational Environmental Satellite (GOES), Advanced Very High Resolution Radiometer (AVHRR),

Systeme Pour l'Observation de la Terre (SPOT) (Jensen, 2007; Lillesand et al., 2008).

2.2.2 Hyperspectral remote sensing data

Hyperspectral remote sensors collect dozens or hundreds of narrow, adjacent, contiguous spectral bands simultaneously. A typical hyperspectral spectrum of live green vegetation and soil is shown in Figure 2.3. In Figure 2.3, the hyperspectral spectrum captures the very fine detail curves of the different ground targets, which in this case, are live green vegetation and soil. These two curves show very obvious differences through out the entire wavelength range, which allows for a good recognition and separability of these two types of ground targets. Generally speaking, the broad concept of hyperspectral remote sensing combines conventional imaging, spectroscopy, and radiometry to produce images together with spectral signatures associated with any spatial resolution elements (pixel) (Thenkabail et al., 2012). These sensors can discriminate between ground surface features that have absorption and reflection characteristics and can be easily diagnosed over narrow wavelength internals, and the conventional multispectral scanners where such characteristics are "lost" within the relatively coarse bandwidths of the various bands (Lillesand et al., 2008).

Most hyperspectral sensors are airborne, such as the Airborne Visible-Infrared Imaging Spectraometer (AVIRIS) (224 bands, $400 < \lambda < 2450$ nm at approximately 9.6 nm interval), the Compacted Airborne Spectrographic Imager (CASI) (288 bands/62 bands, two modes, $400 < \lambda < 1050$ nm at 1.9 nm / 5 nm interval) (O'Neill et al., 1997), and PROBE-1 (128 bands, $400 < \lambda < 2500$ nm at 11 – 18 nm interval) (Lillesand et al., 2008). Some well known satellite-borne hyperspectral sensors are the Hyperion (220 bands, $400 < \lambda < 2500$ nm at approximately 1 nm interval) (Jensen, 2007),

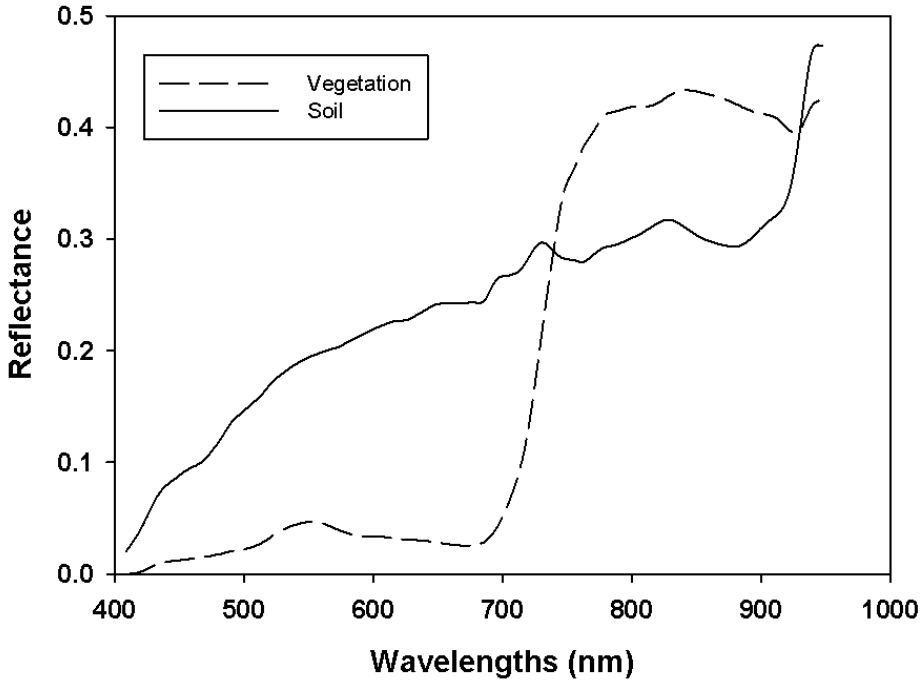

Figure 2.3: The hyperspectral spectra of typical live green vegetation and soil. Notice the obvious spectral curve differences through the entire range, which can be used to distinguish these two types of ground objects.

and the Compact High Resolution Imaging Spectrometer (CHRIS) (Two modes: 19 bands/ 18 meters resolution or 63 bands/36 meters resolution $415 < \lambda < 1050$ nm at different bandwidths) (Cutter, 2000; Smith et al., 2005).

Hyperspectral data are used in various classification studies, such as mineralogy, soil, vegetation and atmosphere (Pu and Gong, 2000; Thenkabail, 2001). However, these studies focus on different spectral regions (e.g., mineral spectra interests 400–2400 nm region; vegetation spectra targets more at 400–1000 nm). Since hyperspectral data come in large data volumes and dimensions, they have unique characteristics to understand, process and analyze, such as very detailed spectral features of the ground

target, very high data redundancy and complicated correlations between bands. In this study, a new methodology is developed to evaluate the correlations between the spectral bands and the target parameters in order to adopt the model inversion on these most "important" and "sensitive" observations. As a result, using this methodology improvement of the overall parameter retrieval accuracy from the hyperspectral data can be guaranteed. In this research I am using hyperspectral data from CASI and CHRIS to demonstrate the effectiveness of this new methodology.

2.2.3 High and very high spatial resolution imagery

High (sub-metre to metre level) and very high (sub-metre to centimetre level) spatial resolution imagery mainly focuses on the spatial details of the ground targets (Rich et al., 2010; Wulder et al., 2004). It retrieves and interprets information from imagery using spatial pattern recognition, which detects similar patterns to "known" features. Therefore, it was initially recognized more as a computer science question rather than a remote sensing analysis and interpretation one, e.g., how to identify if the shapes are the same; how to extract the shape (Klassen et al., 2004; Kulikova, 2009; Larsen and Rudemo, 1998, 2004; St-Louis et al., 1998). However, spatial information, such as the side and top shape, texture, profiles (vertical sections), and patterns of tree crown, which can all be determined by remote sensing image processing techniques, have been considered as key visual criteria when extracting information from imagery for vegetation and forestry applications (Franklin et al., 2001; Tso and Mather, 2009).

Historically, fine spatial resolution satellite imagery (at the level of tens of metres) had been reportedly used in land cover mapping at the regional and global scale, but not at the scale of individual crowns (Aplin et al., 1999). The limited spatial resolution

was the primary issue at that time. As a result, the focus was on improving the spatial resolution of the sensors. In 1999, the first IKONOS commercial high spatial resolution satellite (0.82 m at panchromatic (450–900 nm) band) was launched. In 2001, Quickbird provided 0.61 metre spatial resolution satellite images to the public. Later, WorldView-1 (2007) and -2 (2009) offered 0.46 metre spatial resolution imagery[2]. In 2008, GeoEye-1 (0.46 metre) was put in use[3]. In 2011, AIRBUS Defence and Space Pleiades-1A satellite sensor (0.5 metre spatial resolution) was successfully launched[4]. Recently (2014), GeoEye-2 was announced to be renamed as WorldView-4 and will be launched in 2016[5]. At the same time, due to rapid development, airborne imagery can provide much higher spatial resolution than the satellite based sensors, at a much lower cost and higher flexibility. Airborne sensors can presently achieve a spatial resolution at centimetre level with a budget of a few thousand dollars (2012 Canadian dollars). High and very high spatial resolution imagery provides new possibilities for remote sensing imagery data analysis.

Technically, high and very high spatial resolution imagery can be considered as multispectral imagery as well. In most cases, the high spatial resolution imagery has at least three spectral bands (e.g., the natural colours: Red (600 – 700 nm), Green (500 – 600 nm), and Blue (400 – 500 nm)). Recent high spatial resolution imagery also includes NIR (800 – 1000 nm). The spatial details of the high spatial resolution imagery naturally can be used as additional evidence to support the spectral features in surface object classification, such as tree species classification. However, it is rarely

[2]http://www.satimagingcorp.com/satellite-sensors/worldview-2/

[3]http://www.satimagingcorp.com/satellite-sensors/geoeye-1/

[4]http://www.satimagingcorp.com/satellite-sensors/pleiades-1/

[5]http://www.satimagingcorp.com/satellite-sensors/geoeye-2/

used in synergy with multispectral data in imagery classification. This was due to the fact that majority of botanist's tree shape recognition literature is based on tree side-views rather than crown top views.

In most remote sensing data, only a portion of the tree crown (top view) is visible in imagery, which made the reproduction of the tree shape difficult. The spatial information that can be used in imagery classification is the 2D top view. Therefore, the classification mainly depended on the experience of the imagery interpreters. Another challenge of using tree top shape is the within class variation, which means the trees of the same species are generally similar, but there are noticeable differences between individuals. It is difficult to identify a consistent feature, and its measurement, that can represent the unique characteristic of a tree species. Tree shape comparison should be considered as a fuzzy process, which requires a high flexibility around a known feature. Simply stated, in order to successfully employ high/very high spatial resolution data, I need to answer the following two questions: 1) what feature is to be measured? and 2) how to quantify this feature in a consistent, effective and accurate matter?

In this study, I employed an object oriented approach to improve the tree species classification. The object oriented approach has two main advantages comparing to the traditional pixel based methods: 1) it combines the spectral and spatial information together instead of using solely conventional statistical results (Matinfar et al., 2007); 2) it eliminates the surrounding background interference. Figure 2.4 illustrates these two advantages. From Figure 2.4.b, it is obvious that pixel based methods considering each individual pixel as isolated elements. The statical results are based on entire image or a subset of it. No spatial correlations were taken into account. While Figure 2.4.c shows the object oriented approach takes the entire tree crown as basic elements,

which enable the calculation of the spatial correlation with these tree crowns. The non-object enclosed area of the rest of the image can be completely filtered out, which provides minimum background interference.

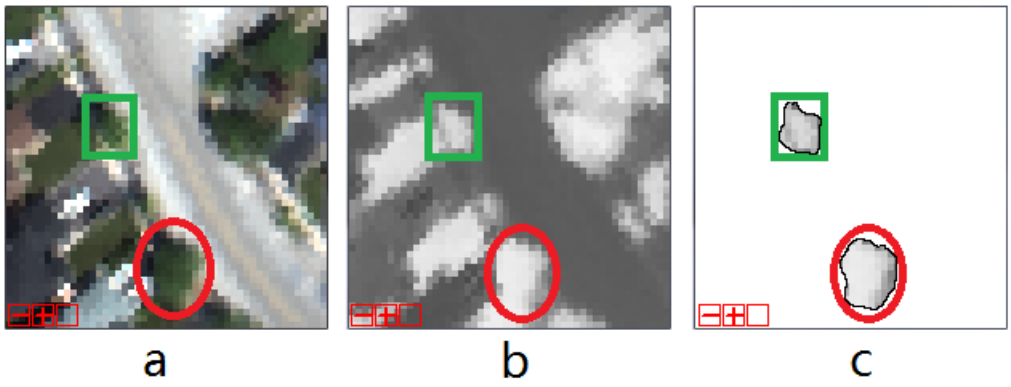

Figure 2.4: A graphic demonstration of the advantages of using object oriented approach comparing to traditional pixel based methods. a) original true color image; b) pixel based brightness value; 3) after segmentation tree objects with background filtered out.

2.2.4 Multi-angular remote sensing data

Early research has demonstrated that vegetated surfaces are not true lambertian surfaces, which are defined as an ideal "matte" or diffusely reflecting surface (Kimes, 1983). The fundamental physical property governing the reflectance behaviours a surface object is it bidirectional reflectance distribution function (BRDF) (Asrar, 1989). Simply speaking, the reflectance value of the same surface target at different illumination and view angles are different. Despite the well defined concept of BRDF, it is impossible to be truely directly measured due to the fact that infinitesimal elements of solid angle do not include measurable amounts of radiant flux (Nicodemus et al., 1977). Instead, bidirectional reflectance factor (BRF) is commonly used (Bruegge et al., 2001). BRF is defined as the ratio of the radiant flux actually reflected by a

sample surface to that which would be reflected into the same reflected beam geometry by an ideal perfectly diffuse standard surface irradiated in exactly the same ways as sample (Nicodemus et al., 1977). It is an integration of radiant flux over finite solid angles of incidence and exitance yields the "reflectance factor" (Asrar, 1989), that is used to estimate the BRDF at specific angle and over a period of time. It is considered as the standard field measurement, which estimates the BRDF at specific angles (Leblanc and Chen, 2000; Walter-Shen and Biehl, 1990).

Multi-angular sensors and their data are designed for obtaining adequate sampling needed to analyse the BRDF of the surface objects, which is shown in Figure 2.5 (Kimes, 1983; Suits, 1972). The main differences between them and non-multi-angular sensors is the multi-angular sensors are capable of taking data at different angles simultaneously since multi-sensors are mounted and operated at the same time, while other sensors need to reposition themselves at different view angles to collect "multiple angled" data.

Many multiangular sensors have been developed, such as satellite based Multi-angle Imaging Spectro Radiometer (MISR) (Wu et al., 2011)), Portable Apparatus for Rapid Acquisition of Bidirectional Observation of the Land and Atmosphere (PARABOLA) (Bruegge et al. (2000); Chen and Leblanc (2001)), Compact High Resolution Imaging Spectrometer (CHRIS) (Cutter, 2000; Smith et al., 2005) and airborne ones e.g., Polarization and Directionality of the Earth's Reflectances (POLDER) (Chen and Leblanc, 2001; Lallart et al., 2008), Frequent Image Frames Enhanced Digital Ortho-rectified Mapping (FIFEDOM) (Hu et al., 2007). CHRIS data is originally designed to take advantage of both high spectral resolution and multiangular views when observing the Earth's surface (Barnsley et al., 2004; Hu et al., 2009; Smith et al., 2005).

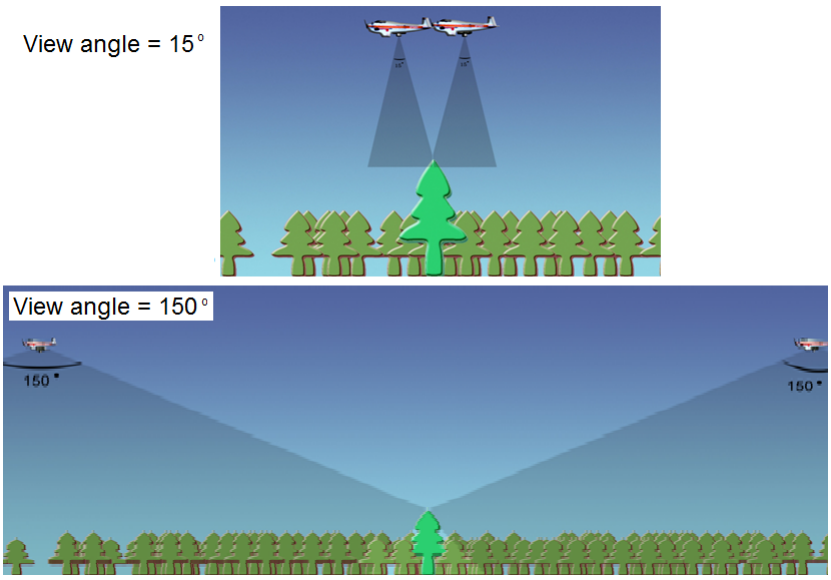

Figure 2.5: The basic concept of multi-angular remote sensing. The same ground target (e.g., a tree), will be captured multiple times at different observation angles.

2.2.5 Data fusion

It is worth mentioning a very important and popular topic called data fusion. Data fusion in remote sensing normally referring to combination of image data from more than one types of sensors (Lillesand et al., 2008). The main objective of data fusion is to produce a fused result that provides the most detailed and reliable information possible. Therefore, it normally involves improvement in spatial resolution of the multispectral/hyperspectral images. There are three different levels of data fusion 1) pixel level; 2) feature level; 3) information level. Classic remote sensing data fusion methods focus on pixel level, e.g., Brovey method, High pass filter, IHS (Intensity-Hue-Saturation) and PCA (Principal Component Analysis) basis (Jensen, 2007). In 2012, Jing and Cheng (2012) summarized and reviewed all existing pixel based approaches, and provided detailed discussion and comparison validations. The feature

and information level data fusion are more popular in social and economic studies. In this study, I explored the potential of integrating remotely sensed and non-remotely sensed data at feature/information level to deliver accurate environmental assessment.

2.3 Information retrieval from remote sensing data

Humans are adept at interpreting objects, from visual contact, photo or spectral interpretation. At the early stage, image analysis was mainly done by visual interpretation. In modern remote sensing, "observation" is defined as the processed measurements from remote sensing sensors after essential corrections, such as atmospheric, geometric and radiometric, normally in the form of reflectance or radiance and stored digitally. Therefore, data analysis component of remote sensing will answer the question about how to extract information from remotely sensed observations.

However, atmospheric effect, the interaction of direct solar radiation and of the radiation reflected from the target with the atmospheric constituents interfere with this process of remote sensing (Asrar, 1989), should be considered and corrected first. The atmospheric gases and aerosols as well as clouds, scatter and absorb solar radiation, which results in the modification of the reflected radiation from the ground targets, particulary critical for visible and near infrared bands. First, it affects the spectral and spatial distribution of the radiation incident on the surface. Second, radiance being reflected is attenuated. Third, atmospheric scattered radiance, called path radiance, is added to the transmitted radiance. Therefore, properly atmospheric correction can improve the quality of remote sensing data. It is normally conducted by two steps: 1) estimate of the atmospheric characteristics, e.g., optical depth; 2) apply inversion to correct image from measured radiance (Kaufman1978, 1978). In particular, there are

three different approaches to correct the atmospheric effects, 1) single/multiple scattering atmospheric correction, which is an approach that uses mathematical algorithm to model the radiance scattering and absorption of all parties along the path, e.g., 5S model (Simulation of the Satellite Signal in the Solar Spectrum). 2) dark-target atmospheric correction, which is most suitable to the clear sky when Rayleigh atmosphere dominates since Rayleigh scattering dominates. Therefore, the clear-deep water has a very low spectral reflectance in the short wavelength region, which can be used as control for corrections. 3) direct digital number to reflectance transformation, which is used when control ground references are available and empirical corrections can be calculated (Gong et al., 2008).

There are two major steps in remote sensing data analysis procedures: the feature selection and the information extraction. Since including all available bands from remote sensing data, such as hyperspectral data which are highly redundant and complicated can make the data analysis process extremely slow, very computational expensive and in some cases, less accurate. Therefore, feature selection is an essential step for remote sensing data analysis.

Data analysis can be parametric or non-parametric. The parametric methods are much more explicit and accurate compared to the non-parametric ones. There are two groups of parametric information extraction methods: The first group includes deterministic radiative transfer models. These are process based models that utilize my knowledge about the optical interaction of target material to inference on characteristics I am interested in. Typically, a model is trained with known data (a.k.a. training data) on the optical property of interest (Meroni et al., 2004; Verhoef and Back, 2003). The second group is based on statistical methods. These methods typically utilize a

subset of features to develop a quantitative model or classification protocol. In this group, if the target characteristic can be presented numerical and the output is quantitative, the common approach is a decision support system using a mathematical relationship (Atzberger, 2013), e.g., estimation of variables, such as leaf area index (LAI), which is the total one-sided area of leaf tissue per unit ground surface area. (Chen et al., 1997; Watson, 1947). In the studies which require LAI of whole stands, a surcharge for understory and litter has to be added to the LAI of trees to obtain the integrated total LAI of a given forest stand, which is also known as canopy LAI. Detailed review of different methods for LAI definitions and measurements can be found Breda (2003). The assessments of biophysical parameters of different vegetation surfaces, such as crops (Atzberger, 2013; Haboudane et al., 2004; Jacquemoud et al., 1995), and forest (Cosmopoulos and King, 2004; Morsdorf et al., 2009; Omari et al., 2013), are essential for estimating productivity, provision of critical information for local agencies, and delivery of timely updates for environmental monitoring. Otherwise, if the target is characteristic is categorical, it is normally using a classification approach (Thenkabail et al., 2012). The relationships within the remote sensing data analysis procedures can be graphically represented as in Figure 2.6 in simplified form.

Both feature and information extractions can be supervised or unsupervised. Supervised means prior knowledge or training data are used to identify a group of best features and to train a classier on target characteristics, including divergence measurement, and correlation between features and ground. While unsupervised methods are based on one or more feature characteristics, such as variance, entropy and other natural grouping within the data (Mitra et al., 2002).

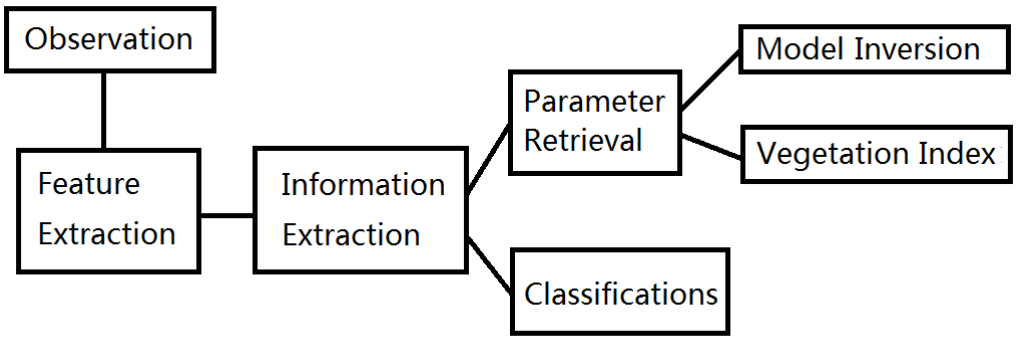

Figure 2.6: The major steps of remote sensing data mining procedures and associated methods covered in this chapter.

2.3.1 Introduction to physical vegetation models

Many physical models have been developed in the past few decades for forestry and agriculture applications (Liang, 2008). These models describe the radiative transfer processing from a light source, such as the Sun, through the canopy and back to the sensor. This effort is normally referred to as the forward or the direct mode of the model (White, 1999). The model reproduces and simulates the ground object property, such as reflectance by parameterising the interaction between solar radiance and the ground target into a function of a set of designed variables (Datcu and Schwarz, 1998; Matzler, 2008; Wang, 2012). Since most of vegetation models (except Monte Carlo simulation model) always produce the same output from a given set of initial parameters, they can be considered as deterministic systems, which are defined as no randomness is involved.

Due to their complexity, these models have assumptions that can not reliably describe the environmental conditions and the canopy characteristics. Therefore, they are normally dedicated to a specific targeted object and have an applicable range.

Goel and Grier (1988) and most recently White (1999) gave a detailed descriptions of different types of model development, which includes assumptions, strengths and weaknesses.

In general, vegetation models can be divided into two categories by their scales, namely canopy and leaf level. In canopy level models, the canopy can be classified by shape assumptions, turbid medium models, geometric models, hybrid models and Monte Carlo simulation models (Moorthy et al., 2008; White, 1999). The evolution of the vegetation canopy modelling over the past 40 years is shown in Figure 2.7 illustrating that models have become more and more sophisticated and complicated, and can represent more details, e.g., at the early stage the surface object were assumed to be represented by a flat infinite slab, while the most recent models can distinguish individual trees with different sizes and shapes.

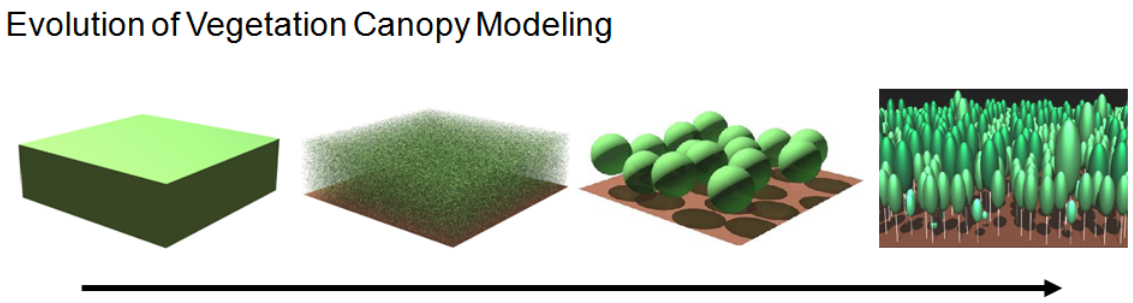

Figure 2.7: The evolution of the vegetation canopy modelling, from simple to more complicated and realistic models. [Moorthy et al. (2008). Courtesy of Dr. Inian Moorthy. Used under author's permission.]

The turbid medium models assume that the canopy is horizontally uniform, which has plane-parallel layers. The vegetation elements within the layers are treated as small, randomly distributed particles. Radiative transfer occurs only between layer-

s, which depends on the depth of the vegetation. Therefore, they are also referred as volume scattering models. LAI is a critical variable in these models. The LAI explicitly represents the depth of the vegetation, which shows an almost exponential change of reflectance value with increasing saturation (Chen et al., 1997). Leaf angle distribution (LAD) is also an important parameter of these models, which determines leaf inclination and orientation. Although, LAD is normally fixed to a commonly used value for model simplicity, the angular behaviour of the model depends on it. Two well-known models in this class are the Suits (Suits, 1972) and SAIL (Scattering by Arbitrarily Inclined Leaves) models (Verhoef, 1984). The Suits model idealized the canopy as a homogeneous mixture of horizontal and vertical diffusely (Lambertian) reflecting and transmitting panels, which can be described by six parameters, ρ(reflectance), τ(transmittance), LAI, $\rho_{(s)}$ (soil reflectance), SKYL (Sky lighting), and ALA (average leaf angle). SAIL model extended Suits model, which considered LAD. However, SAIL model used a 13 distinct inclination angles intervals to approximate the LAD. SAIL is a low computation cost, effective model, generally success in homogeneous agricultural crops, e.g., corn, wheat, and soy bean (Haboudane et al., 2004; Jacquemoud et al., 2009; Pena-Barragan et al., 2011) and the densest forest canopy, e.g., mature deciduous forest (Li and Strahler, 1986; Peddle et al., 2007; Zarco-Tejada et al., 2001).

Geometric models were initially introduced by Terjund and Louie (1974). The architecture of forest canopies is described by four major components: the sunlit crown, sunlit understory (an assumed isotropic vegetative bottom layer), shaded crown and shaded understory (Nicodemus, 1982). Each component has an average reflectance factor representing the whole canopy. Therefore, canopy reflectance is a weighted sum

of the four component reflectances. Taking the simplest geometric optical model, with no transmission occurring through the crown and no multiple scattering within the canopy, the shaded components do not contribute to the total reflectance, except for the effect of the diffused sky viewed by them (White et al., 2002). An example of this type of models is GO (Geometric Optical) model (Li and Strahler, 1986, 1992). The common assumptions are the components are all Lambertian surface in nature, which do not have angular dependencies (Toutin, 2004).

The hybird model is a combination of the turbid medium and geometric optical models. The turbid medium models have an generalized description of multiple scatting between layers, which is referred as optical, but lack element geometry. The pure geometric optical model focuses on the canopy's discontinuous structure, but ignores energy loss. By combining them together, multiple scattering within crowns and between leaves are well modelled. Therefore, this combination leads to a better simulation result and more potential applications. It can cover homogeneous and inhomogeneous areas, and also can represent sparse or dense forest canopy. An example of this type of models is GORT (Geometric Optical Radiative Transfer) model (Li et al., 1995). These models are more general when comparing them with pure turbid medium or GO models. However, they are normally much more complicated and computationally intensive. More importantly, they require more variables, which require detailed knowledge of the canopy. These variables are not easily obtainable from ground measurements or from remotely sensed data. Since hybird models deal with turbid vertical distribution and the horizontal discontinuities of the leaf medium, they are also called 2-scale models in literature (Li et al., 1995; White, 1999).

The Monte Carlo simulation model was developed from the turbid medium mod-

el, which was based on the integral equation describing the turbid medium surface (Antyufeev and Marshak, 1990a,b). It is the most complex and most computationally expensive model type. Instead of mathematically simplifying the canopy using various assumptions, the model implements a realistic canopy using a ray tracing algorithm , which means each photon is traced along its complete interaction course with the atmosphere and ground objects, until it is finally absorbed elsewhere or detected by the sensor (Henderson et al., 2003). The concept of this approach has been discussed for a long period of time. However, the implementation of such a model is not trivial. Two widely used Monte Carlo simulation models are the DART (Discrete Anisotropic Radiative Transfer) (Barbezat and Jacot, 1998; Gastellu-Etchegorry et al., 1996) and FLIGHT (Forest LIGHT Interaction) models (North, 1996). It is the most realistic simulation one can have, but at the cost of computation power. The accuracy of the models is directly related to the number of simulations performed (Goel and Grier, 1988).

Many models have been improved and modified from their original forms. A good example is SAILH (Kuusk, 1985). It is a SAIL model with additional hot spot consideration. Hotspot is the surface reflection phenomenon happening around the Sun's illumination direction (Chen and Cihlar, 1997). Simply put, the hotspot peak (local maximum) is in the backscattering direction and minimum in the forward scattering direction due to the BRF anisotropic behaviour (Kimes, 1983). Also, the new GORT model, added inter-crown multiple scattering into the classical GORT model (Ni et al., 1999). Another example is Chen and LeBlanc's 4-scale bidirectional reflection model, which was used to simulate the Canadian Boreal forest canopy (Chen and Leblanc, 1997; Chen et al., 1997). The 4 Scale model added two more scales

(dimensions and variables), which were two considerations in GORT models, namely the tree and leaf distributions. The main differences from GORT are: assumption of random distribution, the multiple mutual shadowing effect, and the effect of the sunlit background being modelled using a canopy gap size distribution function (Chen and Leblanc, 1997).

The inter-comparison between models has been used to validate new models, such as the Radiation Model Inter-comparison (RAMI) initiative (Pinty et al., 2001, 2004; Widlowski et al., 2011, 2007). This effort has demonstrated that model selection should consider the given study area, data set and the canopy parameters being evaluated. In the case of homogeneous areas, the turbid medium SAIL model provides the best result at minimum cost. In the case of coarse-resolution data, canopy parameters are limited. The model with less parameters would be expected to have faster performance than a more complex model.

In the category of leaf level models, the two more commonly accepted models are PROSPECT (Jacquemoud and Baret, 1990) for deciduous and LIBERTY (Dawson et al., 1998) for conifers. PROSPECT was developed based on Allen's generalized "plate model" radiative transfer model (Allen and Richardson, 1968). It describes two types of interactions, scattering and absorption, employing a total of five parameters to simulate the 400 nm to 2500 nm vegetation photosynthetic range. The scattering was described by using leaf mesophyll structure parameter (N) and spectral refractive index (n). The absorption was modelled by using equivalent water content (Cw), leaf chlorophyll content (Cab), and dry matter (Cm). It is arguably the most successful and most validated leaf level model to-date e.g., Jacquemoud et al. (2000, 1995, 2009); le Maire et al. (2004); Moorthy et al. (2008).

LIBERTY stands for Leaf Incorporating Biochemistry Exhibiting Reflectance and Transmittance Yield. It has been also developed based on the radiative transfer model to determine leaf level optical properties, including reflectance and transmittance. The fundamental difference between LIBERTY and PROSPECT is that LIBERTY does not assume the leaf is a flat plate with distinct layers. It considers the shape and size of the leaves, such as pine needles. In my studies, PROSPECT is preferred, which is used in Chapter 3 and 5. The main reason is the canopy and leaf type found in my study areas are more suitable and better validated by PROSPECT.

It is quite popular to have canopy and leaf model coupled together for model inversion biophysical parameters retrieval. The coupling of two different levels of models can add further leaf level detail characteristics to the canopy studies. The 5-scale model was introduced, in which the LIBERTY model was added to the 4 scale model to enhance the leaf reflectance detail by merging it with leaf model incorporating biochemistry exhibiting reflectance and transmittance yields (Chen and Leblanc, 2001; Dawson et al., 1998; Leblanc and Chen, 2000; Peddle et al., 2007). The PROSAIL (PROSPECT + SAIL) model was employed in many studies, which have been successful in retrieving leaf level biophysical parameters in close canopy (Jacquemoud et al., 1995, 2009; le Maire et al., 2004). Due to this reason, PROSAIL is also used in my study (Chapter 3) and is found very successful. Recently, Omari et al. (2013) used proFLAIR (PROSPECT + FLAIR) to retrieve canopy LAI, Cab and canopy integrated chlorophyll content (LAI $\times$ Cab).

2.3.2 Parameter retrieval using vegetation model: model inversion

Since remotely sensed parameters are typically non-direct measurements, data processing involves solving inversion problems (Jacquemoud et al., 2000; Liang, 2008). *"Physically based models of vegetation reflectance serve as a basis for extracting vegetation variables using directional and spectral data from modern sensors"* (Kimes et al., 2000). In most cases, it is not possible to establish a complete inversion physical model (Goel and Strebel, 1983; Goel and Thompson, 1984; Liang, 2008; Wang, 2012). The inverse function of the forward model is almost impossible due to multiple integration functions and assumptions involved in the model. When it is difficult to obtain a direct empirical relationship between the features, e.g., hyperspectral bands and the targeted parameters, the forward model is then used in the inversion processing (Datcu and Schwarz, 1998; Matzler, 2008; Peddle et al., 2007). The solution is then proposed as: the observed spectrum is compared with a series of simulated model spectra to estimate the best parameter composition which can minimize the cost of a merit function (Liang, 2008). Inversion methods based on physical models are generally effective, as physical models are generally designed to provide rigorous and reasonably accurate mathematical descriptions of the major processes of solar radiation passing through vegetation canopies (Kimes et al., 2000).

The comparison process of modelled and observed spectrum is an optimization procedure. The classic approaches are iteration and Look–Up–Table (LUT). The iteration method repeats model runs, predicts parameter changes and updates the initial parameters to reduce the cost of the merit function. It is computationally effective and typically fast. However, it requires a parameter change prediction calculation and also requires a good initial value estimation. This method may have convergence

problems (Mueller et al., 2009). LUT are less computationally effective when applying to a detailed search. However, LUT is much more stable and robust (Rivera et al., 2013). It can provide a global search result without any convergence issues.

As mentioned earlier, vegetation models are normally non-linear and contain a number of variables. The models also pose limitations and implicit restrictions to their inversion. Different combinations of parameters may provide similar spectra output, a case known as "ill-posed" model inversion. It is stated that "*the inverse solution is not always unique as various combinations of canopy parameters may yield almost similar spectrum*" (Darvishzadeh, 2008). A parameter combo would be identified as the "solution", which may not necessarily be the most accurate; in some cases, it can be completely false. e.g., the iteration approach has "local minimum" convergence problem. Therefore, the question is not finding the differences, rather, "what is the cause of the differences".

Due to the fact that the model inversion requires minimizing a merit function, different wavelengths respond independently to specific parameters. Therefore, the optimization process plays a very important role, but is often overlooked (Wang, 1987). The current most popular optimization method is the least squares approach, which minimize the following merit function:

$$\Phi = \sum P_i(x_i - l_i)^2, \tag{2.1}$$

where P_i, x_i and l_i are the weight, the modelled and the observed of the i^{th} observation throughout this chapter, respectively.

In the past few decades, many merit functions have been proposed, such as Equation 2.2 and 2.3 (Cracknell and Hayes, 2007; Liang, 2008). These merit functions are generally successful in their respective applications only. Least square or partial least

squares approaches are much more accurate, scalable and robust (Gong et al., 2008, 1995).

$$\Phi = \sum (\frac{x_i - l_i}{x_i + l_i})^2 \tag{2.2}$$

$$\Phi = \sum absP_i(x_i - l_i) \tag{2.3}$$

2.3.3 Vegetation index

Using vegetation index (VI) to estimate the biophysical parameters is an important and popular approach for remote sensing data analysis. It identifies the empirical relationships between the spectral reflectance with targeted parameters using certain mathematical models (Baret and Guyot, 1991; Brown et al., 2000; Haboudane et al., 2004, 2002). Classic vegetation indices, like Green Red Index (GRI) (Tucker, 1979) and Normalized Difference Vegetation Index (NDVI) (Rouse et al., 1973), have been used for decades and they are effectively validated indices and represent certain characteristics of surface vegetation. However, these indices were developed from the broad band multispectral data, which may provide inadequate or limited information (Thenkabail et al., 2012). More indices have been developed for hyperspectral data, such as Modified Triangle Vegetation Index (MTVI2) for quantitative vegetation estimation (Broge and Leblanc, 2000; Haboudane et al., 2004), photochemical reflectance index (PRI) for indicating vegetation general stress (Gamon and Bond, 2013; Merzlyak et al., 1999) and multi-angular vegetation indices for capturing the vegetation structural angular differences, such as Hotspot-DarkSpot index (HDS)(Chen et al., 2003, 2005). The biophysical parameters then can be presented as a simple expression of the associated

index, such as LAI can be presented by MTVI2 (Haboudane et al., 2004). The ground vegetation can be roughly classified using NDVI. Typically, if NDVI over 0.5 means clear evidence of green alive vegetation within the scene, while less than 0.2 indicates very unlikely vegetation existence.

$$GRI = \frac{R_{Green} - R_{Red}}{R_{Green} + R_{Red}} \tag{2.4}$$

$$NDVI = \frac{R_{NIR} - R_{Red}}{R_{NIR} + R_{Red}} \tag{2.5}$$

$$MTVI2 = \frac{1.5[1.2(R_{800} - R_{550}) - 2.5(R_{670} - R_{550})]}{\sqrt{(2R_{800} + 1)^2 - (6R_{800} - 5\sqrt{R_{670}}) - 0.5}} \tag{2.6}$$

$$PRI = \frac{R_{531} - R_{570}}{R_{531} + R_{570}} \tag{2.7}$$

$$HDS = \frac{\rho_{HS} - \rho_{DS}}{\rho_{DS}} \tag{2.8}$$

$$LAI = 0.2227exp(3.6566MTVI2), \tag{2.9}$$

where R indicates reflectance or radiance measurement and the subscripts indicates central bandwidth in names or value, e.g., NIR represents Near Infra-red range bands, typically around 800 nm; 570 means the actual central wavelength. ρ_{HS} and ρ_{DS} are the reflectance at hotspot and darkspot, typically are along the solar plane, in the backscatter and forescatter direction respectively.

The advantages of using VI are simple, effective, repeatable and low cost in processing time and power. VI's depend on appropriately selecting bands such that at

least one is sensitive and highly variable to range of the parameter, and the other that represents a baseline or region not sensitive to changes in the parameter. A ratio of such bands provides an index sensitive to the parameter of interest. There have been significantly efforts that focused on how to effectively and accurately select the most sensitive bands for vegetation indices, such as theoretical/prior knowledge and sensitivity studies. The theoretical/prior knowledge based approach uses the understanding of chemical constitution of the object, such as chlorophyll content, nitrogen and carotenoid, to select, combine and construct the VI (Thenkabail et al., 2012). The sensitivity study intends to identify the bands showing a high variation responding to a small initial change (Bowyer and Danson, 2004). Both approaches have been developed for years and have been well demonstrated in the literature.

However, using VI to retrieve biophysical parameters has some limitations, which are typically dependent on sites and data and intend to get saturated. VI are known to be impacted (or influenced) by a variety of conditions, such as by atmospheric contributions, by background contributions to the spectral BRF, by view/illumination geometry, and by a lack of dynamic range at extremes of the parameter. Training and coefficient reassessment of VI is a must in most of these cases. The VI are very sensitive to observation uncertainties, particularly observation noises, errors and outliers (Hoberg et al., 2007). They are also limited to their designed scale and other implicit and explicitly assumptions.

In this study, VI are adopted in a few innovative ways throughout this research. In Chapter 4, GRI (Equation 2.4) is used with NDVI (Equation 2.5) to recover shadow covered urban trees to improve the segmentation result. In Chapter 5, three indices are selected from a list of candidates to provide the simple, effective and robust information

representing leaf chlorophyll content variation of individual trees.

2.3.4 Image classification

Image classification is another important branch of information retrieval. The image pixels are categorized into information classes by certain analysis approaches. In classification studies, information is presented in a set of classes which characterizes the surface from the remotely sensed images. Classes can be defined from available spectral libraries or from training (Veganzones et al., 2008). Image classification involves statistical calculations, but obtaining quantitative information e.g., numerical estimations is not the objective of classification. Rather, the final assignment of information or specific themes into clusters (statistically similar pixel groups) is the goal. The simplest method uses a threshold approach to assign the information classes based on some features e.g., using NDVI to separate vegetated and non vegetated surfaces. Therefore, image classification can be closely related to inversion and parameter retrieval if the biophysical parameters are used as features.

Both supervised and unsupervised techniques are developed for classification (Jensen, 2000). The classical supervised approaches are "minimum distance", "parallelepiped", "maximum likelihood", "decision tree" and Artificial Neural Network (ANN) (Hayes et al., 1988; Lillesand et al., 2008; Quinlan, 1993). The supervised classification uses a training set of ground classes to generate known identities and all unknown pixels are classified into them. On the other hand, the unsupervised classification automatically generates clusters (statistically similar groups) and assigns them into information classes. The traditional unsupervised approaches are "K-mean" and "ISODATA" (Jensen, 2007). The basic difference between these two techniques is the information assigning

stage. The supervised approach determines the information classes before comparing them with unknown pixels, while unsupervised approaches generate statistically separated clusters for information class assignment in post-processing.

Since classification methods must be applied on some features, the selection of features plays a critical role in the classification result. However, traditional remote sensing classification focuses almost only on spectral (multi/hyperspectral) information, and little on other information. With higher spectral, spatial and temporal resolution remote sensing data becoming available, it is important to explore the possibility of developing new features to improve classification. Obviously, it would be best to integrate them all together to maximize the data potential in classification. However, the challenge is the existing classification methods offer very limited multi-sourced data handling. The classical methods developed based on the single information type cases, e.g., multispectral, thermal and LiDAR. The traditional methods normally also requires dimension reduction when handling high dimensional data, e.g., Principal Component Analysis (PCA), mathematically transforms the high dimensional and correlated bands into a few non-correlated information bands.

In this dissertation, I improve the classification in two main aspects, namely new feature exploration and data assimilation. Instead of mining deeper into the well established spectral features, I explore the spatial information and use one innovative feature called "longitudinal profile" to demonstrate that the classification accuracy can be significantly improved by introducing new dimension of information, e.g., spatial information. I also explore the potential of multi-source remote sensing data in the tree health state classification. I independently develop a four step schema to extract different information from multiple data sources with a wide range of characteristics,

and assemble them into a final evaluation function to deliver classification results.

2.3.5 Contribution analysis and contribution index

The contribution analysis in geodetic survey, determining the coordinates using distances and angular observations, is based on the correlation between parameters and observation and the measurement accuracy of the observations. It calculates a contribution index (CI) to quantify the "contribution" of each observation (e.g., angle or distance measurements) and to the estimated targeted parameters. The CI of each observation is derived based on the prediction matrix, which is initially defined in linear model analysis (Chatterjee and Hadi, 1988; Hoaglin and Welsch, 1978; Wang, 1987). If a generalized model is presented as follows:

$$L = F(x) + V, \tag{2.10}$$

where F is the general function of the model with the parameters x; L is the n-dimensional observation vector; x is the m-dimensional parameter vector; and V is the n-dimensional residual vector, which describes the difference between the modelled and observed canopy reflectance. Based on the least squares principle, parameter correction vector x can be estimated through an iterative process. At each iteration the vector can be estimated by

$$\hat{\delta x} = (J^T P J)^{-1} J^T P (L - F(x_0)), \tag{2.11}$$

where J is an $n \times m$ dimensional Jacobian matrix whose elements are the partial derivatives of the model with respect to the parameters at their initial values for this iteration (x_0). P is the weight matrix of the observations and is proportional to the

inverse of the covariance matrix of the observations. The prediction matrix (H) is defined as follows (Chatterjee and Hadi, 1988; Hoaglin and Welsch, 1978):

$$H = J(J^T P J)^{-1} J^T P \tag{2.12}$$

The H matrix is idempotent and its diagonal elements (h_{ii}) have values from 0 to 1 and with a sum equal to the degrees of freedom of the system of equations. If the i^{th} observation is totally redundant ($h_{ii} = 0$), it does not contribute to the determination of the model variables. On the other hand, if the i^{th} observation is necessary $h_{ii} = 1$, the i^{th} observation is high leverage and has a significant impact on the determination of the model parameters (Chatterjee and Hadi, 1988; Wang, 1987). As a result, if this observation is excluded, either the inversion would fail or the result would not be reliable. The CI of each observation to the model inversion is defined as the normalized diagonal elements of H shown as:

$$CI_i = \frac{h_{ii}}{\sum_{j=1}^{n} h_{jj}} \tag{2.13}$$

Let us look at a simple sample (Figure 2.8), which was originally published in Wang (1987) and used in Zhang et al. (2009). In this simple triangular survey, there are A, B, C and D four stations. A and B stations form the baseline. The number 0 to 8 indicates the angular measurements. The task is to estimate the coordinates (x and y position) of station D. In other words, x_D and y_D are the two targeted parameters. Station C is added to improve the observation accuracy. Obviously, it is easy to sense that this design is problematic. Station C is not in an ideal position. However, how to accurately quantify this problem? The proposed solution is CI (Equation 2.13).

Table 2.1: The CI results from the simple sample. All results were originally published in Wang (1987).[Wang (1987). Courtesy of Dr. Jian-guo Wang. Used under author's permission.]

Angle number	**CI**
0	0.075
1	0.195
2	0.436
3	0.609
4	0.603
5	0.443
6	0.601
7	0.588
8	0.441

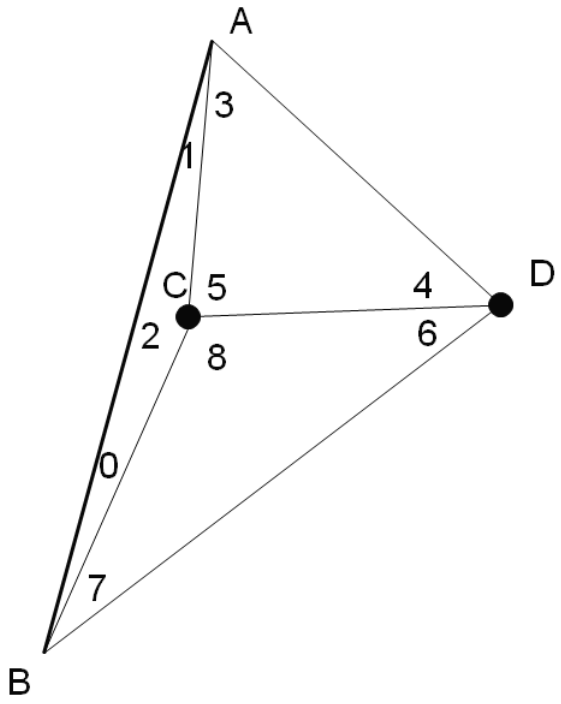

Figure 2.8: A simple example of triangular network survey, which visually demonstrates the practical value of the contribution index. A, B, C and D are the station points, and numbers 0 to 8 represent angular measurements. The objective is to determine the coordinates of station D, x_D and y_D. [Wang (1987). Courtesy of Dr. Jian-guo Wang. Used under author's permission.]

If I calculate all CI as shown in Equation(2.13), the results are given in Table 2.1. From Table 2.1, one can easily identify the problematic measurements, which are 0 and 1. It is determined due to two reasons: 1) the absolute CI value of measurement 0 and 1 is low, any value less than 0.25 should be concerned; 2) these two have much lower value to the average of the rest, which are about 1/7 and 2/5, respectively. If one measurement cannot score a high absolute CI value, it at least needs to be comparable to the other observations (e.g., $= /-$ 50% of the average). Clearly, these two measurements are affected by poor geometric positioning of station C. In triangle ABC, angular measurement 2 is dominating. Even assuming the measurement errors

are the same, the contribution of angular measurement 2 is much more significant than 0 an 1. In practice, the position of C makes angular measurements of 0 and 1 very small, which is difficult to be accurately measured. Since the measurements 4 and 5 have good CI values (around 0.5 absolute value and above average relatively), one potential solution is shifting the station C toward D. This makes sense due to the fact that this would result in increasing angle 0 and 1, which potentially improves the angular observation quality. Another solution is reducing or excluding the measurements 0 and 1 from the final D coordinate calculation, since they are not "significant" and of low accuracy.

In my study, I adopt CI in the model inversion using hyperspectral data to retrieve biophysical parameters. The CIs are calculated to determine the "contribution" of each band to the targeted parameters, such as LAI. The CI is used as weighting to justify the focus of the "cost" comparison in inversion to "important" and accurate bands. As a result, the accuracy of retrieved parameters is improved. Some other sensitivity studies may also propose similar weights. However, the CI is found much more stable comparing to general local sensitivities approaches (e.g., monitoring the responses changes with a small initial input differences) and much more flexible and low computation cost comparing to global sensitivities methods (e.g., considering a compensative analysis with significant requirements in parameters and conditions).

3 Improving the retrieval of the biophysical parameters of vegetation canopies by using the contribution index

This chapter is based on the published journal paper:

Zhang, K., Hu, B., Wang, J., Pattey, E., and Smith, A. M. (2011) "Improving the Retrieval of the Biophysical Parameters of Vegetation Canopies by using the Contribution Index". *Canadian Journal of Remote Sensing*, 37(6): 643-652.

It is a further development of the conference paper:

Zhang, K., Hu, B., Wang, J., and Smith, A., (2009) "Improving the canopy model inversion using a weighting function", proceedings of the 30th Canadian Symposium of Remote Sensing (CSRS), Lethbridge, AB.

Republication permission granted by Editor in Chief of Canadian Journal of Remote Sensing on July 31, 2013.

3.1 Introduction

Biophysical parameters of vegetation canopies, such as leaf area index (LAI) and leaf chlorophyll content, are routinely required for environmental monitoring and sustainable resources management. The retrieval of these parameters from remote sensing data has been an active research topic for decades and has led to many techniques e.g., Jacquemoud et al. (2009). One approach is to establish the relationships between in situ measurements and vegetation indices e.g., Baret and Guyot (1991); Brown et al. (2000); Haboudane et al. (2004, 2002). The relationships are typically dependant on sites and data. As a contrast, the methods based on physical model inversion are more general and effective, as a physical model provides rigorous and reasonable accurate mathematical descriptions of the major processes of solar radiation passing through vegetation canopies (Kimes et al., 2000). However, such a model is normally complex and nonlinear and contains a number of variables (Liang, 2008). To accurately and robustly invert the physical models to retrieve the biophysical parameters of vegetation canopies from remote sensing data, a robust inversion strategy is required.

One of the key issues in the physical model inversion is the determination of a reliable merit function that usually quantifies the misfit between the observed reflectance and the simulated reflectance calculated by a canopy model, which requires estimation or prior-knowledge of related biophysical parameters. Traditionally, the merit function is defined in Equation (3.1)(Goel and Strebel, 1983; Goel and Thompson, 1984; Jacquemoud et al., 2000; Kimes et al., 2000).

$$C = \sum_{i=1}^{n_b} \omega_i (l_{i,obs} - l_{i,mod})^2, \tag{3.1}$$

where n_b represents the number of observations; $l_{i,obs}$ and $l_{i,mod}$ are the i^{th} observed

and modelled canopy reflectance, respectively; and ω_i is a weight, which is normally related to the uncertainty of the i^{th} observation.

Because a canopy model is nonlinear and observed data are not noise free, the traditional merit function may have multiple local minima and (or) a wide flat global minimum, which is sometimes also referred to as "valley"(Kimes et al., 2000). To obtain a robust and stable solution, a priori knowledge is usually used to regularize the inversion process. The most commonly used a priori knowledge is the estimated mean values and standard deviations of the model variables e.g., Li et al. (1998); Makowski et al. (2006). The merit function with such a priori knowledge presented can be described as follows (Privette et al., 1996):

$$C = \sum_{i=1}^{n_b} \omega_i (l_{i,obs} - l_{i,mod})^2 + \sum_{j=1}^{m} (\frac{x_j - x_j^0}{\sigma_j})^2 \tag{3.2}$$

In Equation (3.2), m is the number of parameters targeted; x_j and x_j^0 are the retrieved and expected parameter values, respectively; ω_i is the weight of the observation i; and σ_j is the estimated standard deviation of the parameter j. The other a priori knowledge that has been exploited is the sensitivity of a given observation to the model parameters (Kimes et al., 2000). For example, Privette et al. (1996) weighted each observation in the merit function based on the first derivative of this observation with respect to a particular model parameter. The weighted merit function had steep gradients than the traditional merit function and thus generated rapid and accurate model inversion. However, this method was able to successfully retrieve only one parameter at a time (Privette et al., 1996).

In this study, a contribution index (CI) was designed to quantify the impact of each observation on the retrieval of model parameters. It accounted for the sensitivity of the given observation to the model parameters to be retrieved and their uncertainty. The

CI was used in the merit function to weight each observation. The Look–Up–Table (LUT) method was used in this study because of its robustness and stability, although it was not the fastest algorithm. To validate the proposed CI based merit function, the LUT inversion method was implemented to invert the coupled PROSPECT (Jacquemoud and Baret, 1990) and SAIL (Verhoef, 1984) models using both the simulated and real data from the Compact Airborne Spectrographic Imager (CASI) and the Compact High Resolution Imaging Spectrometer (CHRIS).

3.2 Study areas and data used

Two study areas were selected for this study. The first one ($45°18'N$, $75°45'W$) is located at the former Greenbelt Farm of Agriculture and Agri-Food Canada, Ottawa, Canada. Over three successive years, from 1999 to 2001, different field crops such as corn, wheat, and soybean, were grown on approximately 30 ha till-drained fields. During the 2001 growing season, the CASI images were acquired during three different deployments on 13 June, 26 June, and 19 July (Haboudane et al., 2004). These images covered from 408 to 947 nm with a spatial resolution of 2 m by 2 m.

The processing of CASI imagery included the following steps: raw data to radiance transformation, atmospheric corrections and reflectance retrieval, removal of aircraft motion effects and geo-referencing, and flat field adjustments of surface reflectance spectra. The hyperspectral digital images collected by CASI were inverted to at-sensor radiance using calibration coefficients determined in the laboratory. The CAM5S atmospheric correction model (O'Neill et al., 1997) was then used to transform the at-sensor radiance to at-ground reflectance. To perform this operation, an estimate of aerosol optical depth at 550 nm was derived from ground sun-photometer

measurements.

Reflectance spectra of asphalt and concrete within CASI imagery were used to calculate coefficients that adequately compensated for residual effects of atmospheric water and oxygen absorption, and therefore were used to perform the flat field calibration. Data regarding geographic position, illumination and viewing geometry, as well as ground and sensor altitudes were derived both from aircraft navigation data recordings and ground measurements using a differential global positioning system. Simultaneous to CASI data acquisition, LAI was measured using both a destructive method using LI-3100 leaf area meter (LI-COR, Lincoln, USA) and an indirect method using a LAI-2000 leaf area meter (LI-COR); the leaf chlorophyll contents were quantified analytically. Details of this data acquisition and processing were presented in Pattey et al. (2001) and Strachan et al. (2002).

The second study area is located near Lethbridge, Alberta, Canada ($49°43'N$, $112°8'W$). The CHRIS data were acquired over this study area in June and July, 2004 with a spatial resolution of 36 m and 62 spectral bands covering from 410 nm to 1002 nm. The test site was planted with spring wheat in April. Simultaneous with the CHRIS data acquisition, LAI values were measured using LAI-2000 area meter. The at-sensor radiance data provided by the European Space Agency (ESA) were inverted to at surface reflectance using the CAM5S atmospheric correction model (O'Neill et al., 1997). The drop-out and strips in the data were removed using the Geomatica software v10.0 (PCI Geomatics, Canada). Details on the data acquisition and processing were presented in Smith et al. (2005).

3.3 The CI and the CI-based merit function

As mentioned previously, because the canopy reflectance observed at different wavelengths and angles is not equally sensitive to the model parameters for the retrieval of the model parameters and because the observations have different uncertainties, it is important to weight each observation differently in the merit function depending on its contribution to the retrieval of the model parameters.

In this study, the CI of each observation was derived based on the prediction matrix, which was initially defined in linear model analysis (Chatterjee and Hadi, 1988; Hoaglin and Welsch, 1978; Wang, 1987). The prediction matrix is described in the context of a canopy model inversion. A canopy model can be generalized as shown in Equation 2.10. Based on the least squares principle, parameter correction vector x can be solved through an iterative process. At each iteration the vector can be estimated as Equation 2.11. The prediction matrix (H) is defined as Equation 2.12 (Chatterjee and Hadi, 1988; Hoaglin and Welsch, 1978). However, in this study, it should be referred as contribution prediction matrix, which is the base for deriving CI.

The H matrix is idempotent and its diagonal elements (h_{ii}) have values from 0 to 1 and with a sum equal to the degree of freedom of the system of concern. If the i^{th} observation is totally redundant $h_{ii} = 0$. In such a case, this observation does not contribute to the determination of the model variables. On the other hand, if the i^{th} observation is necessary $h_{ii} = 1$. In this case, the i^{th} observation is high leverage (Chatterjee and Hadi, 1988; Wang, 1987) and has a significant impact on the determination of the model variables. As a result, if this observation is excluded, either the inversion would fail or the result would not be reliable.

The CI of each observation to the model inversion is defined as the normalized

diagonal elements of the prediction matrix shown in Equation 2.13. Therefore, the CI-based merit function is expressed as follows:

$$C_{CI} = \sum_{i=1}^{n_b} CI_i (l_{i,obs} - l_{i,mod})^2 \tag{3.3}$$

Clearly, we used CI to replace the standard weighting function and this "new" cost function would be the cost function used in this study. As shown in Equations 2.12 and 2.13, the CI of each observation accounts for its uncertainty via the matrix P and its sensitivity to the parameters to be retrieved via the matrix J. The CI based merit function is expected to have sharp gradients and generates stable inversion results. To demonstrate this, the data simulated by the coupled PROSPECT and SAIL model were used. Both PROSPECT and SAIL models were well validated and are widely used for homogeneous vegetation canopies, such as crops (Jacquemoud et al., 1995, 2009). The input parameters together with their values for the simulations are summarized in Tables 3.1 and 3.2. These intervals are set to maximize the retrieval accuracy while considering the computation time.

Based on the simulation data, the CI of each band in the spectral region from 400 nm to 1000 nm and with a bandwidth 10 nm was calculated in terms of the retrieval of LAI, leaf chlorophyll content, and dry matter content.

The following points can be summarized from the results (Figure 3.1):

(i) The CI value of each band was mainly determined by leaf chlorophyll content and LAI.

(ii) The leaf dry matter content, illustrated by the solid (0.03 μgcm^{-2}) and dashed lines (0.003 μgcm^{-2}) had almost no impact on CI for a wide range of C_{ab} and LAI values, except for certain bands, such as 550 nm and 800 nm etc.

(iii) For similar LAI value, the increase of leaf chlorophyll content affected different-

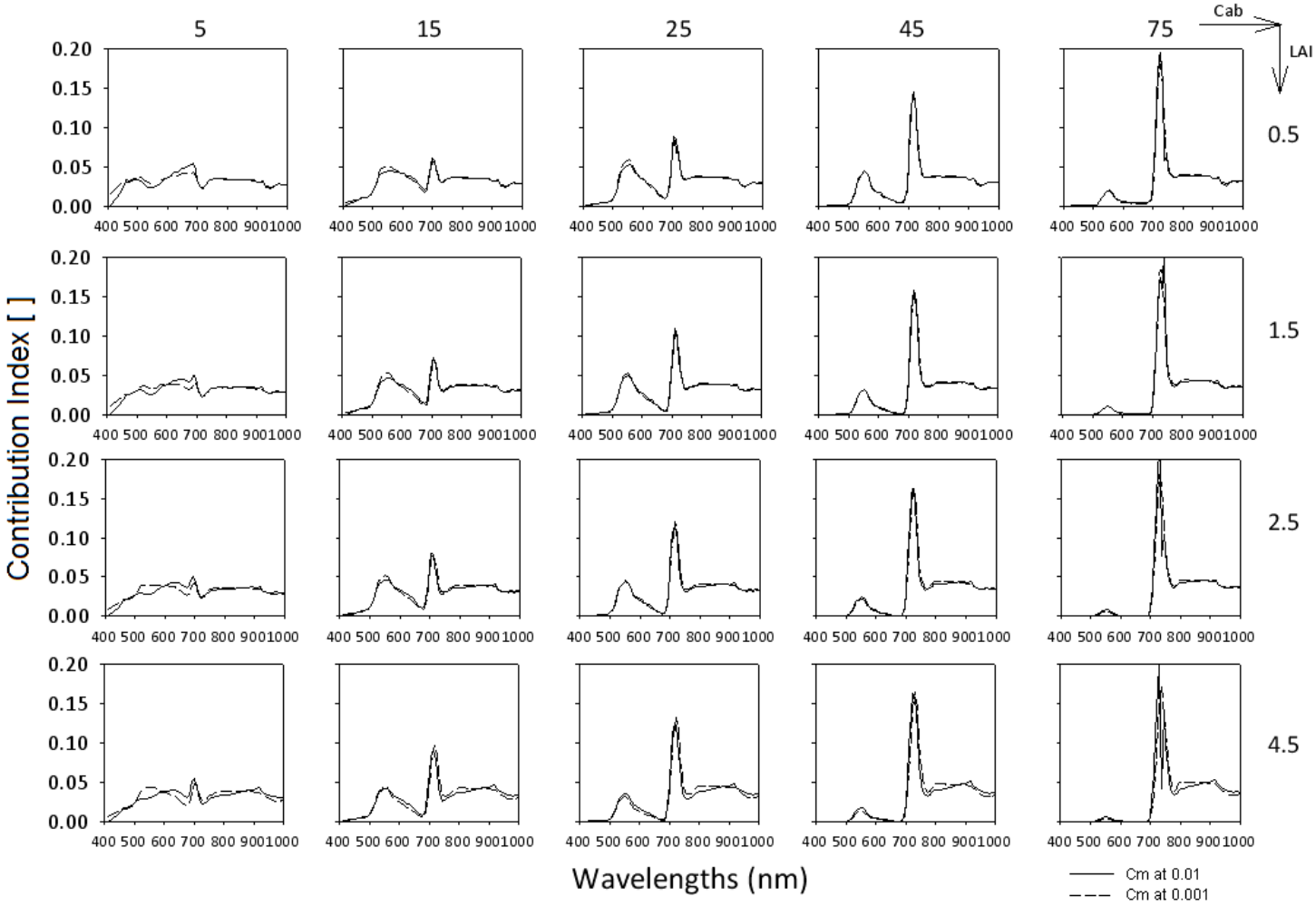

Figure 3.1: The CI of canopy reflectance in the visible and near-infrared region for a series of LAI and leaf chlorophyll content values at dry matter content at 0.001 μgcm^{-2} and 0.01 μgcm^{-2} for a canopy with spherical leaf angle distribution.

Table 3.1: The input parameters of the PROSPECT model (Haboudane et al., 2004)

Parameters	**Values**
Leaf structure parameter (N)	1.4*
Leaf chlorophyll content ($C_{ab}; \mu g cm^{-2}$)	5 - 80 at interval of 1
Equivalent water thickness ($C_w; cm$)	0.0015
Leaf dry matter per area ($C_m; \mu g cm^{-2}$))	0.001-0.005 at interval of 0.0005

* is recommended value by Moorthy et al. (2008).

Table 3.2: The input parameters of the SAIL model

Parameters	**Values**
LAI []	0.1 - 8 at interval of 0.1
Solar Zenith angle (°)	35 and 45
View Zenith angle (°)	0
Soil reflectance	from measurement, with 5% tolerance
Leaf angle distribution ($C_m; \mu g cm^{-2}$))	horizontal (soybean) /
	spherical (wheat, corn)

ly CI in the visible region (450-670 nm) and the red edge region (680-780 nm). When the leaf chlorophyll content was low, the CI curve was relatively low and flat. For leaf chlorophyll content $\geq$ 15 μgcm^{-2}, two CI peaks formed, one in the visible band and another one in the red edge region. The magnitudes of the peaks were directly proportional to the value of leaf chlorophyll content until the leaf chlorophyll content reached about 50 μgcm^{-2} where it plateaued. For the CI peak in the red edge region, the position of the peak moved toward higher wavelengths when leaf chlorophyll content increased. The position of the CI peak in the red edge region changed from 718 nm (with Cab 25 μgcm^{-2}), 724 nm (Cab 45 μgcm^{-2}), to 730 nm (Cab 75 μgcm^{-2}) for LAI = 1.5. These observations were consistent with the reported effects of leaf chlorophyll content on the canopy reflectance in the literature e.g., Cho and Skidmore (2006); Clevers et al. (2002); Dawson and Curran (1998).

(iv) For a given leaf chlorophyll content, the CI values in the visible wavebands were inversely proportional to LAI. In the red edge region, the magnitudes of CI peaks increased with an increase in both leaf chlorophyll content and LAI. Increasing LAI is equivalent to stacking more leaves, which usually tends to also increase leaf chlorophyll signal.

(v) It is interesting to look at the cases with the leaf chlorophyll content values at 15 μgcm^{-2}. The general shapes of the CIs with different LAIs were very similar. They all had double peaks. The values of the two peaks were almost the same, which is very unique compared with the cases with larger leaf chlorophyll content values. For the cases where leaf chlorophyll content was greater than 15 μgcm^{-2}, the peaks in the red edge were always higher than those in the green region and the greater LAI, the greater the differences. This implies that canopy reflectance in the green region

is equally important as that in the red edge to characterize crops which are either young (low LAI, low leaf chlorophyll content) or mature but stressed (high LAI, low leaf chlorophyll content).

By adding the CI of each band to the merit function, a strong dependence of the model inversion on the canopy reflectance emerged in the spectral band sensitive to the model parameters. Therefore, the CI based merit function is expected to improve the inversion accuracy by reducing the size of the valley. To illustrate this effect, the contour plots of the traditional (Equation 3.1 and with $\omega_i = 1$) and CI based merit functions (Equation 2.13 and with P = I) for LAI 2.5 and leaf chlorophyll content 45 $\mu g cm^{-2}$ at two different dry matter content values are presented in Figure 3.2. The valley, which caused ambiguity in the retrieval of LAI and leaf chlorophyll content, is clearly shown in both the traditional and CI-based merit function. However, the CI-based merit functions have a much smaller valley area, which is expected to generate more reliable and accurate model inversion results. It is due to the fact that LAI and Cab only responses to certain spectral bands significantly. By including all available observations equally, a lot of "non-important" bands do not contribute much information in the final retrieval of these two parameters, but introducing measurement random errors regardlessly. The CI justify the focus of the inversion by weighting the bands accordingly, which basically reducing the unnecessary noise. It can also be observed from Figure 3.2 that the semi-major axis of the contours coincides with the axis representing the leaf chlorophyll content. As a result, the uncertainty in the retrieved leaf chlorophyll content is expected to be larger than for LAI.

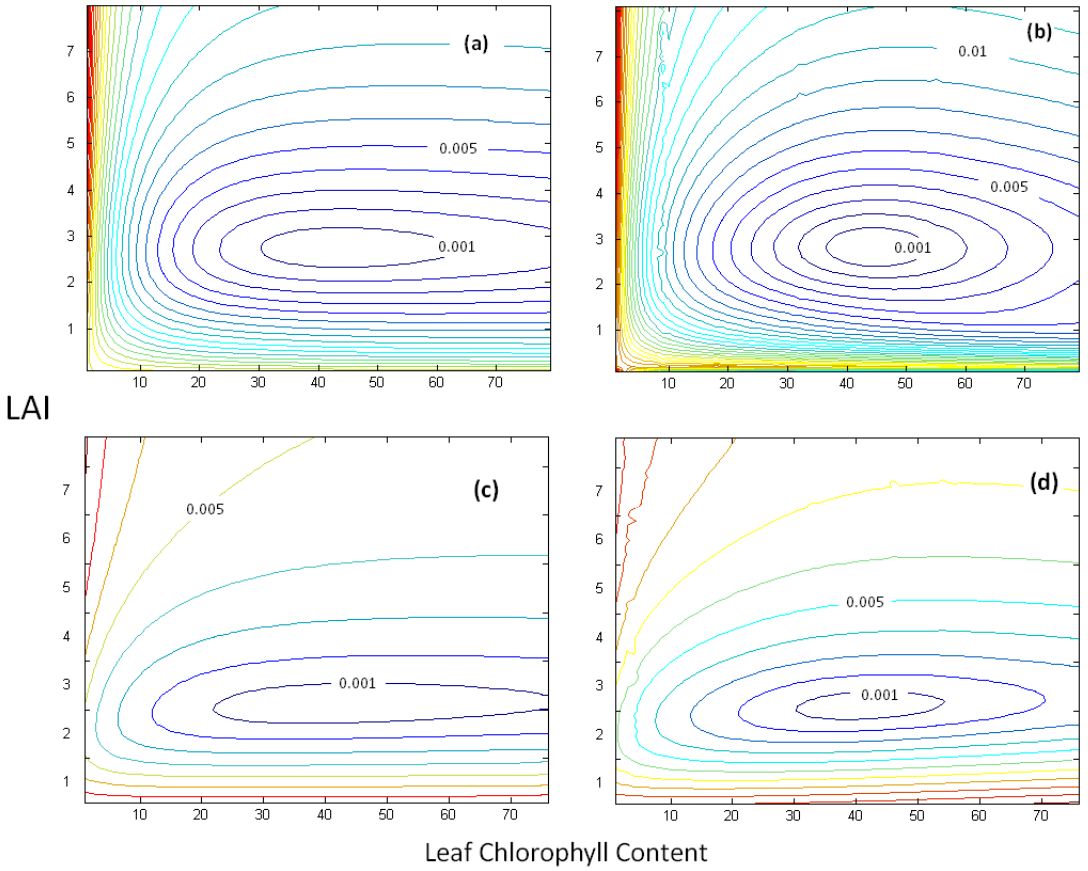

Figure 3.2: Contour plots of traditional merit function, (a) and (c), and CI based merit function with the CI, (b) and (d), with respect to LAI and leaf chlorophyll content at different dry matter level, 0.001 μgcm^{-2} for (a) and (b) and 0.01 μgcm^{-2}, for (c) and (d). The true value of LAI is 2.5 and leaf chlorophyll content is 45 μgcm^{-2}.

3.4 Retrieval of vegetation parameters using the CI based merit function

3.4.1 Retrieved of LAI and leaf chlorophyll content from simulated data

A comprehensive simulation study was conducted to further investigate how the CI-based merit function improved the retrieval of model parameters. Different LAI (0.5-8 at a step of 0.1) and leaf chlorophyll content (5-80 μgcm^{-2} at a step of 1 μgcm^{-2}) at different dry matter contents were paired up to generate simulated canopy reflectance using the PROSPECT and SAIL model. The inversions were conducted using the LUT method and the traditional merit function in Equation 3.1 and with $\omega_i = 1$ (referred to as LUT) and CI-based merit functions with P = I (referred to as CLUT). The uncertainty in the observed data were not considered in the LUT and CLUT methods at this stage. Examples of retrieved LAI and leaf chlorophyll content for increasing Cab and varying LAI are presented in Table 3.3. Because the dry matter content can be retrieved accurately using both the LUT and CLUT methods, its results are not listed in Table 3.3. The CLUT method significantly outperformed the LUT one for LAI ranging from 2.5 to 4.5 and leaf chlorophyll content from 25 to 45 μgcm^{-2} (i.e., cases 7, 8 and 9). These are the value intervals showing large variations of the CI among the bands (Figure 3.1). As expected, the CLUT generated better inversion results than the LUT method by giving more weight to the spectral bands important in the model inversion.

The CLUT did not improve the retrieval of LAI and leaf chlorophyll when both were small (i.e., cases 1 and 2). This is because the CI of each band is similar (Figure 3.1), which leads to similar merit functions for LUT and CLUT.

Table 3.3: Retrieved LAI and chlorophyll content values using Look–Up–Table inversion based on traditional merit function (LUT) and contribution index merit function (CLUT) for increasing chlorophyll content and varying LAI. Uncertainties of the observations were neglected at this stage.

Case No.	**True LAI**	**True** C_{ab}	**LUT LAI**	**LUT** C_{ab}	**CLUT LAI**	**CLUT** C_{ab}
1	0.5	5	0.5	12	0.5	12
2	1.5	5	1.8	15	1.7	10
3	2.5	5	2.8	7	2.6	5
4	2.5	15	2.8	18	2.6	18
5	0.5	25	0.6	31	0.5	29
6	6.5	25	7.0	35	6.8	24
7	2.5	45	2.8	40	2.6	44
8	3.5	45	3.9	40	3.7	44
9	4.5	55	5.2	40	4.7	52
10	5.5	75	6.1	55	5.7	72

3.4.2 Retrieval of LAI and leaf chlorophyll content using CASI imagery

The CLUT method was also applied to the CASI images to retrieve LAI, leaf chlorophyll content, and dry matter content using the coupled PROSPECT and SAIL model in this study. Based on (Haboudane et al., 2004), we kept the model variable N = 1.4 and Cw = 0.009 cm. The ranges of other parameters were the same as those listed in Tables 3.1 and 3.2. Because the in situ leaf dry matter content was not measured, only retrieved LAI and leaf chlorophyll content were validated against the field measurements. The comparisons were carried out on the basis of the growth stage and crop type, and the results are shown in Figures 3.3 - 3.5.

From Figures 3.3 and 3.4, it is clear that for all of the cases analyzed, the CLUT method performed better than the LUT in terms of the root mean square error (RMSE) and R^2 between the retrieved and measured LAI. The best performance of the CLUT was obtained for the CASI image acquired early in the growing season on 13 June (Figure 3.3). The R^2 increased by 14% from 0.81 (LUT) to 0.92 (CLUT) while RMSE was reduced by 20% from 0.55 to 0.44. The improvements were more limited for the CASI images acquired on 26 June (R^2 increased by 33% from 0.39 to 0.52) and on 19 July (R^2 increased by 2% from 0.84 to 0.86). The RMSE was reduced by 10% for both cases. For wheat (Figure 3.4), the improved CLUT performance increased R^2 by 14% from 0.56 to 0.64, and reduced the RMSE by 8%. For soybean, the R^2 values were very high around 0.98 for both the LUT and CLUT methods, but a smaller RMSE was obtained with the CLUT method. Similar results were observed for corn.

Although the overall performance of both inversion methods was marginal for retrieving the leaf chlorophyll content (Figure 3.5), the CLUT also outperformed the LUT method. Due to limited ground sample measures, a detailed analysis for individ-

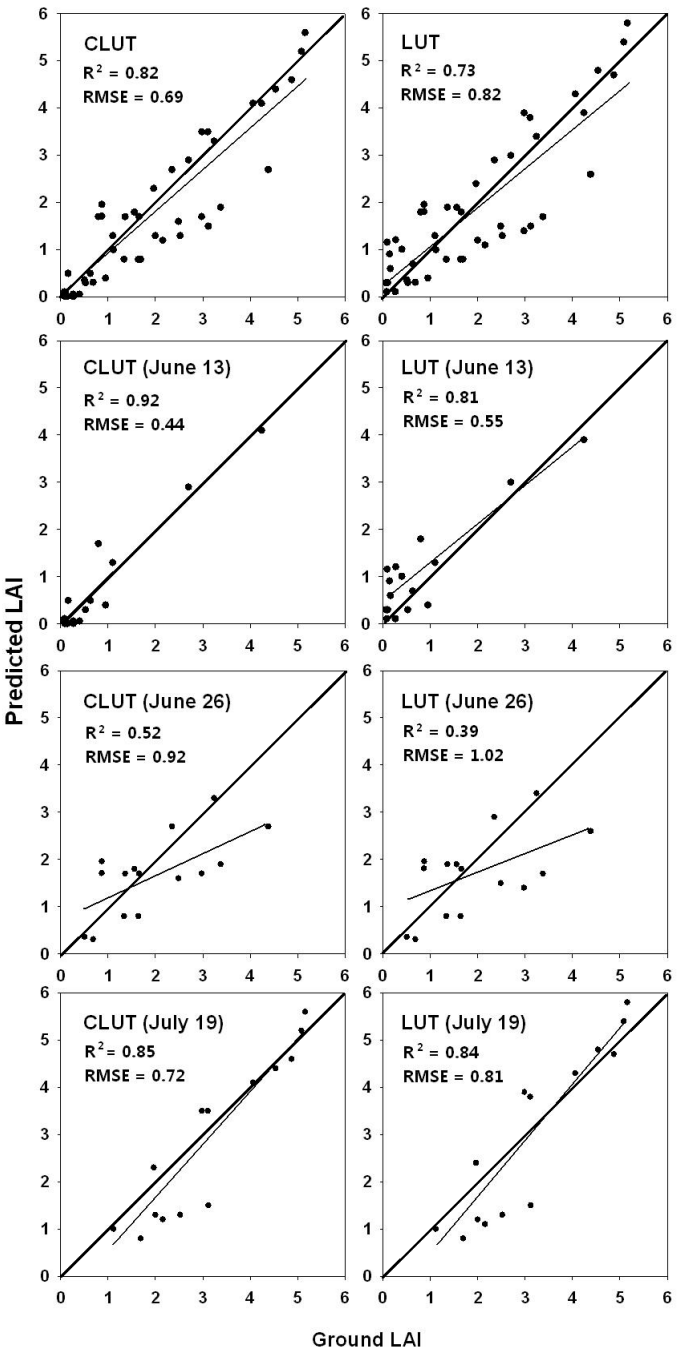

Figure 3.3: Relationship between the measured LAI and LAI retrieved from the 2001 CASI data. From top to bottom: overall,13 June, 26 June, and 19 July, using the CLUT and LUT methods. 1:1 line is added to have a visual comparison.

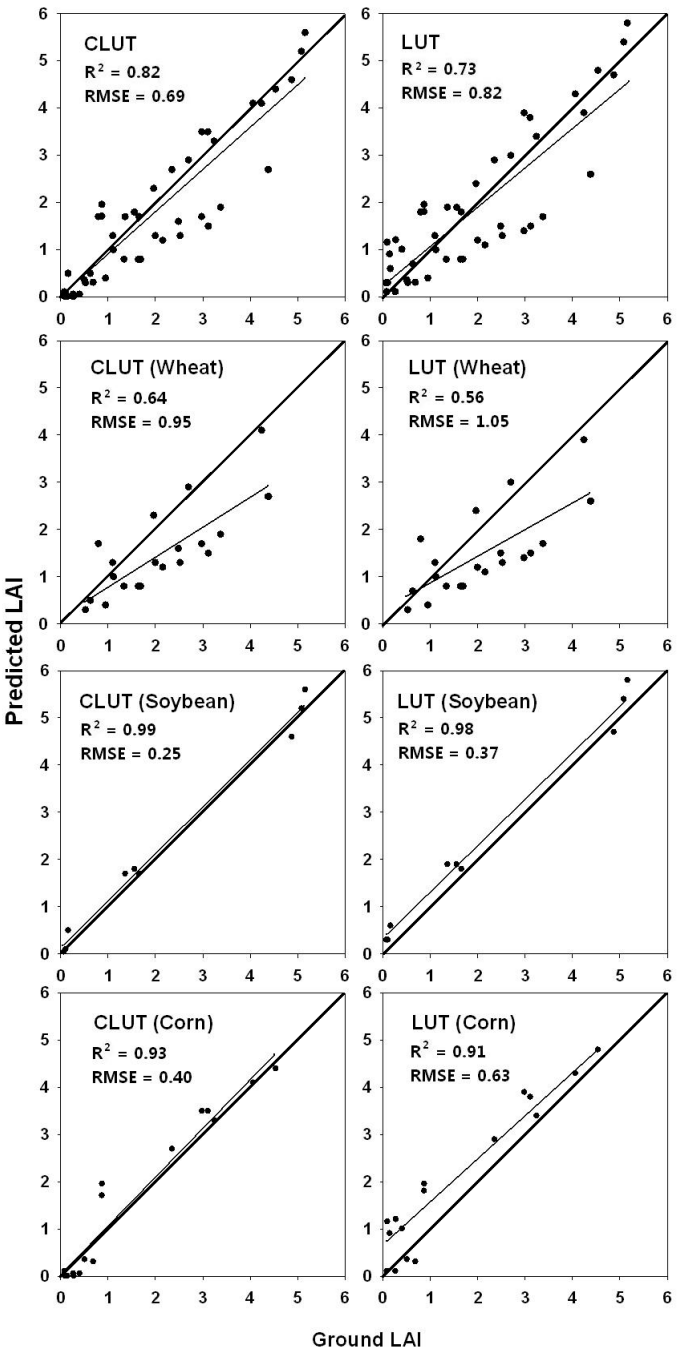

Figure 3.4: Relationship between the measured LAI and LAI retrieved from the 2001 CASI data for different crops. From top to bottom: overall, wheat, soybean, and corn using the CLUT and LUT methods. 1:1 line is added to have a visual comparison.

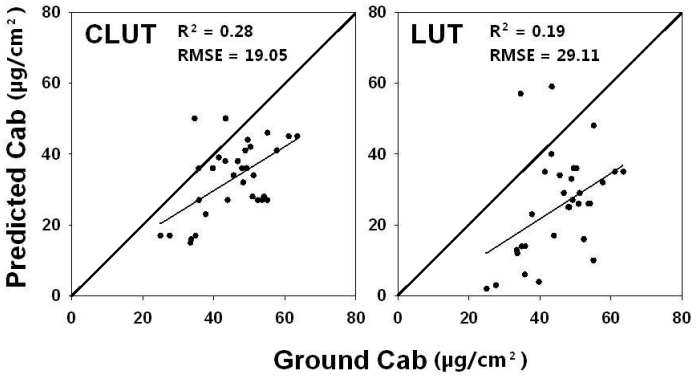

Figure 3.5: Relationship between the measured leaf chlorophyll content and leaf chlorophyll content retrieved from the CASI data. 1:1 line is added to have a visual comparison.

ual growth stages and crops could not be carried out. For all of the data available, the R^2 between the predicted and ground measured leaf chlorophyll content was 0.28 for CLUT and 0.19 for LUT, while the RMSE was 19.05 and 29.11 μgcm^{-2} , respectively.

The lower performance result for leaf chlorophyll content (Figure 3.5) compared with the LAI (Figures 3.3 and 3.4) could be explained by the smaller range of leaf chlorophyll content values while LAI values covered a much wider range. In addition, as implied by the direction of the semi-major of the merit function contours in Figure 3.2, the ambiguity in the retrieval of the leaf chlorophyll content is expected to be much greater than in the retrieval of LAI.

3.4.3 Retrieval of LAI from CHRIS imagery

In this study, the CLUT method was further tested with the CHRIS imagery. Compared with the CASI imagery, the signal-to-noise of the CHRIS imagery was relatively low (around 300:1). As a result, the effect of considering the uncertainties in the

observed data on the retrieval of LAI was investigated. The standard deviation of the reflectance values of a homogeneous soil area in the images was calculated for each spectral band and taken as a measure of the observation uncertainty at the corresponding band. For clarification, we denoted the LUT method using the merit function defined in Equation 3.1 and ω_i with as the inverse of the uncertainty of the observation as NLUT (Noise considered), and the CNLUT method with the CI of each observation accounting for both its uncertainty characterized by P taken as the inverse of the uncertainty of the observation and sensitivity to the parameters.The LUT, CLUT, NLUT, and CNLUT methods were first used to retrieve LAI using the only nadir observations in this study. Due to the lack of laboratory measured data of leaf chlorophyll content and dry matter content, only the retrieved LAI values were validated and the results are shown in Figure 3.6.

Significant improvements on the retrieval of LAI were obtained using both CLUT and CNLUT methods at nadir (Figure 3.6) compared with the LUT and NLUT methods. It demonstrated that weighting an observation in the merit function based on its sensitivity to the retrieved parameters could significantly improve the retrieval accuracy. Indeed, the CLUT method improved the R^2 from 85% to 91% and reduced the RMSE from 1.60 to 1.34. Considering the uncertainty in each observation in the model inversion had a limited impact for improving the inversion accuracy, compared with accounting for the sensitivity of each observation on model parameters. The increase of R^2 between the retrieved and measured LAI was marginal between CLUT and CNLUT methods (i.e., from 0.91 to 0.92), but the RMSE reduction from 1.34 to 0.92 was more significant. The NLUT method failed to improve the RMSE between the retrieved and measured LAI compared to LUT.

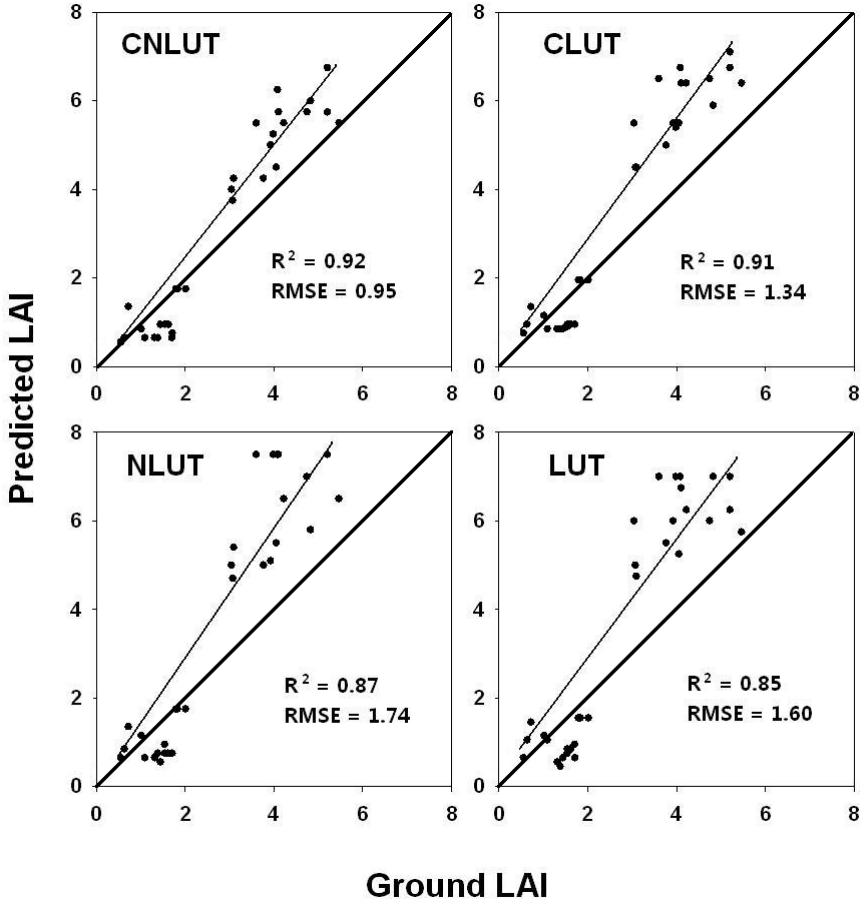

Figure 3.6: Relationship between the measured LAI and that retrieved from the 2004 CHRIS data using nadir only data. 1:1 line is added to have a visual comparison.

The LUT, CLUT, CNLUT, and NLUT were used with nadir and off-nadir observations together to investigate how off-nadir observations affect the model inversion. Due to the imagery co-registration issue obtained at the large fly-by zenith angles (FZA) ($\pm 55°$) images, the data acquired at the FZA ($\pm 36°$) were kept in the inversion. The results are shown in Figure 3.7. It is clear from Figure 3.7 that CNLUT had the best performance among all four approaches in terms of both R^2 and RMSE; and the approaches with the CI based merit functions performed better than others without considering the sensitivity of observations to model parameters (CNLUT vs. NLUT and CLUT vs. LUT). Compared with the retrieval results based on only nadir observations (Figure 3.6), the results in Figure 3.7 also show that the off-nadir observations (Figure 3.7) improved the retrieval accuracy by reducing the RMSE from 0.95 (nadir only) to 0.58. The multiple angular acquisitions reduced the tendency to overpredict the LAI. However, despite the popularity, using PROSAIL model may not be the optimal approach due to its relative simple assumption of ground structure. Other model, e.g., proFLAIR (Omari et al., 2013), would possibly serve the same even better role. In this study, we just want to have a simple, effective and clear demonstration of the significance of CI in model inversion.

3.5 Summary and conclusions

The impact of the CI of each observation on the retrieval of parameters of interest in a physical canopy model was studied. The CI quantifies the sensitivity of each observation to the targeted parameters. The experiment, based on the simulated data, showed that the changes of CI values with the spectral band in terms of the retrieval of LAI and leaf chlorophyll content were consistent with the reported effects

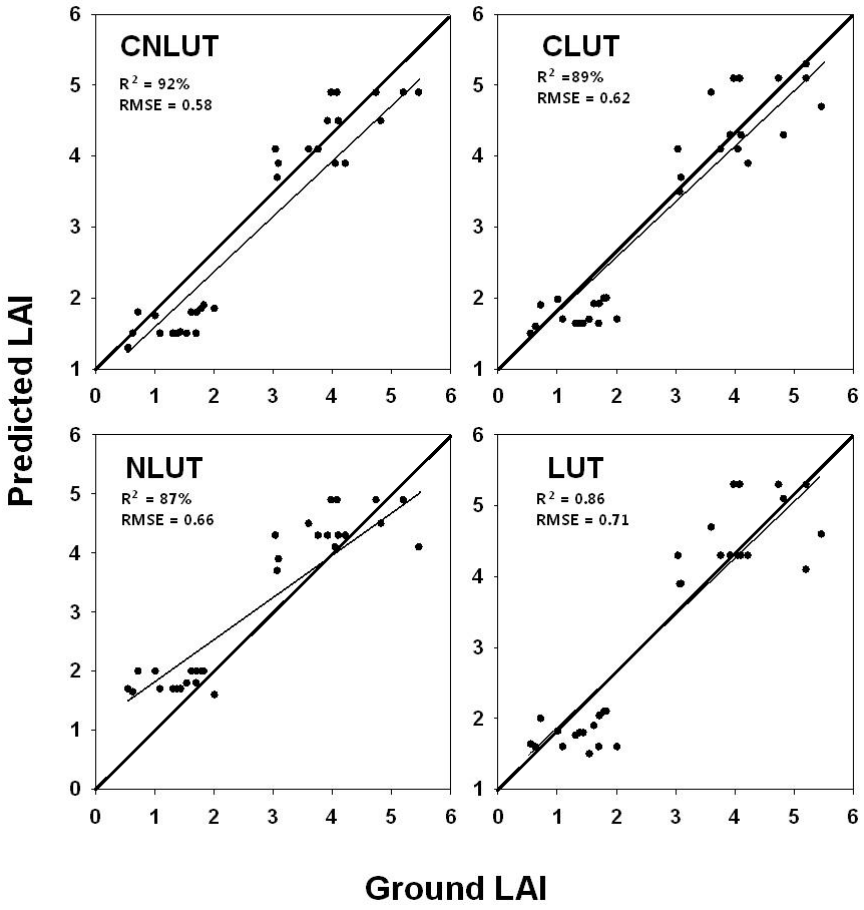

Figure 3.7: Relationship between the measured LAI and LAI retrieved from the 2004 CHRIS data using three angular observations. 1:1 line is added to have a visual comparison.

of LAI and leaf chlorophyll content on the canopy reflectance in the literature. The CI also takes into consideration of the uncertainty (noise) in each observation. A high noise level in an observation would lower its weight in the inversion process. As a result, by adding the CI of each observation in the merit function, the inversion was concentrated on important and reliable observations, which led to an improvement in retrieval results. Based on the simulated data, it was demonstrated that adding CI to the merit function could reduce its valley area, which is expected to reduce the uncertainty in the retrieved parameters.

After implementing the CI-based merit function into the LUT method, the CLUT method was tested using both simulated data and CASI and CHRIS data. The results showed that weighting observations in the merit function based on their sensitivity to the model parameters was effective, and the CLUT method outperformed the traditional LUT method in terms of the RMSE and R^2 between the retrieved and measured LAI and leaf chlorophyll content. The CI-based merit function was validated with the LUT inversion method, but it could be used with other optimization inversion techniques, such as the iteration approach. The LUT method was used in this study because of its robustness and stability, although it was not the fastest algorithm. The LUT method guaranteed a simple and fair comparison. Other optimization techniques, such as iteration approaches, could also adopt the CI-based merit function, but preliminary work is required to take into account the initial values influence and convergence issues. The CI-based merit function can also be implemented with other coupled canopy-leaf models. This study demonstrated the CI potential in inversion improvement and the coupled PROSPECT and SAIL model was selected because of its popularity, stability, and robustness. The CI merit function itself is derived from

prediction matrix, which was totally independent from the models used. However, the CI values were calculated based on given models, which means the contributions of the observations to parameters have to follow the assumptions of the selected models and vary depending on the model performances. In future work, the CI-based model inversion method will be further tested based on different models and for different environments.

4 Individual urban tree species classification using very high spatial resolution airborne multi-spectral imagery using longitudinal profiles

This chapter is based on the published journal paper:

Zhang, K., and Hu, B. (2012) "Individual urban tree species classification using very high spatial resolution airborne multi-spectral imagery using longitudinal profiles". *Remote Sensing*, 4, 1741-1757

Remote Sensing is a MDPI open access journal which permits reproduction for non-commercial purposes.

4.1 Introduction

In recent years, researchers have become more aware of the importance of detailed land characteristics in urban systems (Tooke et al., 2009). Trees comprise a critical component of urban ecosystems and directly impact human habitations. Individual trees each exert significant influence over their environment; a tree's roots may affect underground utility systems; branches may affect surrounding power lines, and certain species of flowering trees when in bloom may cause serious allergies in local inhabitants. In addition, depending on species, a tree may serve as home for a variety of animals and insects which in turn exert significant ecological influence and may represent a source of potential hazard for residents. Accurate tree species classification is therefore an essential component to urban studies, city forest inventories, ecology management, and other urban planning applications.

Traditionally, identification of tree species is conducted through photo interpretation assessment of aerial photographs by an interpreter. This technique relies heavily on the breadth of the interpreter's experience in applying spatial discrimination criteria (Fourier et al., 1995; Waser et al., 2011) and is therefore more likely to be qualitative in nature. The classification is then used to identify tree species. Classification uses the features of the objects, sometimes also known as criteria (Franklin et al., 2001) or descriptor (Brandtberg, 2002). The ideal features should present the highest separability of the targeted objects, which means they have the highest within-class similarity and minimum overlap inter-class. The commonly used features are spectral signatures, texture, vegetation indices (VI) and shape information etc. It can be generally divided into two approaches: the pixel-based and the object-based. The former uses pixel-based features to determine the similarity, while the latter requires segmentation

first and uses the grouped pixels to generate features.

The spectral signature is the most commonly used feature. A compilation of articles of commonly used procedures, issues and applications for spectral signature comparison can be found in Hill and Leckie (1998). Leckie et al. (2003) extended the spectral signature algorithm to eight and ten band CASI imagery to facilitate classification of old growth conifer sites along the west coast of Canada. Erikson (2004) used empirically radiometric and morphologic developed parameters to classify the four common species in Sweden. Larsen (2007) obtained an individual 3-dimensional tree map using image geometry and contrast to identify each tree through comparison to a set of known species. However, the accuracy of spectral signature classification remains relatively low, normally less than 50% due to the high variation within-class and the high similarity inter-class. VI can be considered as an extension of spectral signature. The difference is the VI is normally dedicated to special parameters through its "formula". VI usually serves as a filter before or as additional information in classification. In Pena-Barragan et al. (2011), the VI and spectral features were put together for inversion and NDVI was reported contributing around 50% to the model.

Texture is considered as key visual criteria when extracting information from imagery for vegetation and forestry applications (Franklin et al., 2001). In Coburn and Roberts (2004), four main texture approaches were identified: statistical, geometrical, model-based and signal processing. According to Gebreslasie et al. (2011), the most popular texture approach is the statistical approach, which considers local spatial or spectral variability. However, different criteria have been used for variety of studies. In Haralick (2011); St-Louis et al. (1998), grey-level occurrence matrix (GLOM) and grey-level co-occurrence matrix (GLCM) were introduced to recognize patterns. In

Dawson and Parsons (1994), the standard deviation, entropy, run lengths and "fractal" (a scale-invariant object) roughness were investigated for their separability for urban derelict lands. In Franklin et al. (2001), the first and second order variance and homogeneity were found to be effective in distinguishing the forest age class from IKONOS imagery. In Rich et al. (2010), texture metrics mean Euclidean distance, variance and mean were used to capture the disturbance severity across a windstorm damaged vegetation structure from IKONOS imagery. In Klassen et al. (2004), GLCM homogeneity, dissimilarity and entropy were cooperated within an object with other object-based information to identify the crops from ASTER imagery. In Coburn and Roberts (2004), a total of 12 features, mean, variance, entropy, correlation, contrast and second moment of GLOM and GLCM were used to extract the structural attribute of Eucalyptus plantation forest from IKONOS imagery. Texture features are rarely used by themselves. They are more commonly used as additional information combined with the spectral signature. It normally provides an extra dimension of measurements and improves the classification by 5%–15% compared to spectral only cases.

Despite that the shape of a tree has long been recognised as significant in identifying tree species, shape information is rarely used information in multi-spectral imagery classification (Fourier et al., 1995). This is due to the fact that most botanist's shape reorganizations are based on the side view of a tree. In most of the Remote Sensing forest study, only a portion of the tree tops are visible in the imagery, which makes the reproduce of the tree shape difficult. The shape information that can be used in imagery classification is 2D top view shape. The classification mainly depends on the experiences of the imagery interpreters. On the other hand, when shape information

is relatively easy to obtain, such as in LiDAR data, shape has been recognized as the primary classification parameters. Brandtberg (2002) used the convex and concave contour to describe the shady side curvatures. Based on the development of the Planar shape recognizing (Klassen et al., 2004), the "shape space" had been reported as a potential of the classification improvement in Kulikova (2009), which the planar shape represented by the angle function was explored. Shape information is proved to be useful in term of improving classification result on top of conventional spectral and texture information.

Segmentation of individual trees has been an ongoing research field for years (Erikson, 2004). A variety of approaches exist with an objective towards auto-locating of trees and individual crown boundary. It is commonly achieved from the analysis of high resolution spatial imagery (Leckie et al., 2004). The popular methods are, but not limited to, the template matching approaches (Larsen, 1997; Larsen and Rudemo, 1998, 2004), the valley following approach (Gougeon, 1995; Gougeon and Leckie, 2003), the local-maxima (Wulder et al., 2004), texture grouping (Warner et al., 1998), the use of morphological operators (Barbezat and Jacot, 1998), and joining of convex edges (Brandtberg and Walter, 1998). Since the segmentation is not the focus of this study, an automatic processing was tested using the watershed approach proposed by Jing et al. (2011) for a potential of large size image processing. Even the overall segmentation accuracy was over 80%, the main errors occurred when a few trees group together. For these grouped trees, a manual detailed segmentation of collected ground validation data is necessary to enhance the accuracy. This type of manual delineation accounts for less than 10% of trees validated.

This study proposes a new classification feature derived from directional profiles

for surmounting challenges associated with applying tree species classification schemes in urban settings. It was inspired by the unique growing conditions of urban trees;

(1) A main error resulting from using forest classification schemes as a proxy to urban individual tree classification is the miscounting of the number of trees covered by the shadows of neighbouring buildings. In a forest setting, man-made structures are rarely present and shadows of neighbouring trees normally do not cover the entirety of surrounding trees. In this study, in order to accurately identify urban tree species on an individual basis, a scheme is made prior to segmentation to recover undetected tree masked by building shadows;

(2) Urban trees are much more isolated than forest trees, making it easier to define their boundaries. Urban trees typically experience less competition for resources than their forest counterparts. Consequently, urban trees are not as constrained and are more likely to grow to the capacity of their genetically determined shape and size. In contrast to forest scenarios, high resolution spatial imagery within the urban setting is capable of capturing entire single trees instead of just tree tops or canopies. Shape information for urban trees is therefore very specific and useful in the identification of individual tree species. In this study, new vegetation parameters based on longitudinal profiles of tree crowns, which derived from shape information of trees, were developed and supplied to construct a new decision tree to uniquely distinguish species.

Trees growing on Keele campus of York University (Toronto, ON) can be considered as typical, temporal climate urban trees and are used as test cases for this study.

4.2 High spatial resolution imagery and ground data collection

4.2.1 Airborne high resolution spatial imagery

The main Image used for this analysis is 6 cm by 6 cm high spatial resolution multi-spectral airborne imagery taken by Air Sensing Inc. on 1 August 2007 in sunny, clear conditions. The data was supplied by the York University Map Library in its raw format. The image comprises four spectral bands: Blue (460 nm), Green (570 nm), Red (670 nm) and NIR (800 nm). The image was captured at the flight height of 390 metres (1282 feet). The image covers York University (Ontario, Canada) Keele campus, which is shown in Figure 4.1.

4.2.2 Ground data collections

A total of 213 trees on campus were documented using camera and measuring tape. The physical parameters, such as tree heights and crown sizes were measured or interpreted from images. They were identified using tree guide books (Farrar, 1995; Kershaw, 2001; Sibley, 2009) or by consulting with field experts. There are a wide variety of tree species available on the York Campus. The six popular and important species selected are Maple, Ash, Birch, Oak, Spruce and Pine shown in Figure 4.2. The documented trees were 32 Maples (*Acer rubrum*, *Acer platanoides*), 30 Ash (*Fraxinus pennsylvanica*), 14 Birch (*Betula lenta*), 26 Oak (*Quercus rubra*), 15 Spruce (*Picea abies*) and 25 Pine (*Pinus banksiana*, *Pinus resinosa* and *Pinus sylvestris*). The rest were the trees belonging to other species, which were not classified.

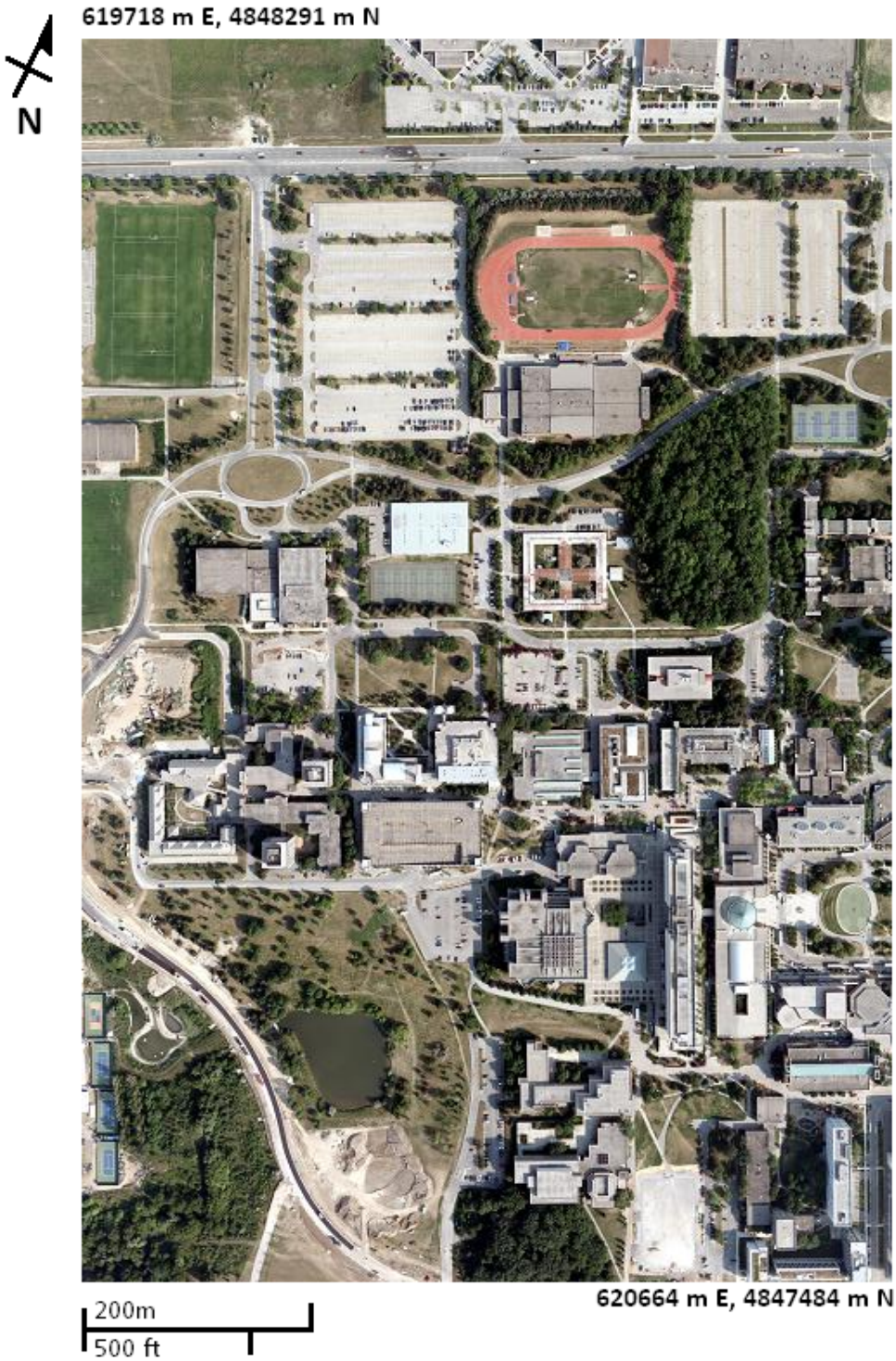

Figure 4.1: True colour high spatial resolution image of York University, Toronto, Ontario, Canada.

Figure 4.2: Top left to right: Maple, Ash, and Birch; bottom left to right: Oak, Spruce, and Pine.

4.3 Methodology

4.3.1 Shadow tree recovery

The main cause of missing out trees covered by shadows casted from nearby buildings from the imagery was the conventional usage of the Normalized Differential Vegetation Index (NDVI), which is shown in Equation (4.1). Most segmentation and classification approaches use NDVI to separate vegetation and non-vegetation surface as the pre-processing mask. For forest trees with dense canopy, this shows positive results. Forest trees are normally not fully covered by other trees' shadow. In fact, only a portion of tree top is captured by imagery. However, as discussed in Section 4.1, the isolated trees in urban environment can cause a complete failure due to the shadow of nearby buildings. Since the shadow blocks the direct illumination, the light sources for the shadowed area are the nearby surrounding scattering. The NIR band is most significantly affected, which leads to a much lower value of NDVI. Any segmentation or classification methods using NDVI to classify the vegetation and non-vegetation surfaces would therefore give a false result.

$$NDVI = \frac{NIR - R}{NIR + R} \tag{4.1}$$

where NIR and R represents the Near-infrared and Red reflectance, respectively.

The threshold value for NDVI was determined experimentally. In this study, NDVI < 0.2 is used to classify the non-vegetation surface. The NDVI of 0.2 was selected as a trade-off between separating the trees from the background non-vegetation surface and preserving as much shaded trees as possible. However, all trees within a building shadow suffered some level of crown loss in this step. In urban cases, whole or partial

trees are missed due to this inappropriate classification, as shown in Figure 4.3(b). Figure 4.3 is a subset of the campus image, which within the ellipse circled area had over 15 ash trees. The NDVI mask had missed half of the ash trees due to the shadow of the nearby Ross Building. Keep in mind that in forest applications, the shadow from nearby objects other than trees rarely exists.

To solve this issue, a ratio version of the green radiance index is used: Greenness Index (GI) (Tucker, 1979), which can be expressed as:

$$GI = \frac{G}{G + B + R} \tag{4.2}$$

where B, G and R represents the Blue, Green and Red reflectance, respectively.

Figure 4.3(c) shows the performance of the GI for the same area. It was clear that for the NDVI missed trees, GI had recovered.

Using ratio to create vegetation index is a simple but effective approach that Gitelson and Merzlyak used to successfully retrieve leaf chlorophyll content (Gitelson and Merzlyak, 1996). GI is the green percentage of the pixel, which represents the greenness of the objects. If the object is green, then the GI is at least greater than 0.33. Since shadow covered trees are still more visually greenish, it can be detected by GI. As a result, for the trees that NDVI missed due to the shadows, GI gives a chance to recover them. Also due to the fact the living vegetation has a relatively low reflectance value in the visible ranges, it is much lower and less sensitive to GI than arbitrary green objects. Therefore, GI should be kept as low as possible.

However, GI also has its limitations. First of all, it may also detect the artificial green objects, such as green roof, pipes, etc. Second, it would miss the non-green leaf trees, such as Red Maple. Figure 4.3(c) is also a good sample to illustrate these

weaknesses. For the green squared area, the green pipes on top of the roof were picked up, while the NDVI result did not have this error. For the red squared area, the GI missed the red maple due to leaf colour, while the NDVI result easily picked them up.

Therefore, a few filtering and smoothing approaches were used in separating the green artificial objects from the tree pixels and merged with the NDVI output. Figure 4.3(d) is the final processed segmentation image. This process can be summarized as three steps: (1) Filtering small segments less than 20 pixels (0.72 m^2) on both NDVI and GI images. This step removed any detected small objects not likely to be a tree due to the size, which significantly filtered out the background grass and other small non-tree vegetation objects; (2) Merge NDVI and GI images; (3) Smooth the merged image, mainly the edge and filling the gaps within the segments. This output segmentation image is used as filter in the next step, shape signature collection. Therefore, it is very important to keep the tree crown completeness.

4.3.2 Classification

Since urban trees have a much more complete tree top view, whole tree shape information is available and can be potentially important. In this study, longitudinal profiles (further referred to as profile) of the tree crown tops were also investigated. These profiles were obtained from the following procedures. As shown in Figure 4.4, a red maple tree was used to demonstrate the procedure step by step. Step A: obtain the intensity profile of the crown by recording all the values along the direction of the Sun Azimuth angle from a segmented tree. Step B: cut off the edges (drop all zero value pixels) and convert the end to end section to tree perimeter using image scale and spatial resolution. The first a few pixels may have been impacted by the nearby tree

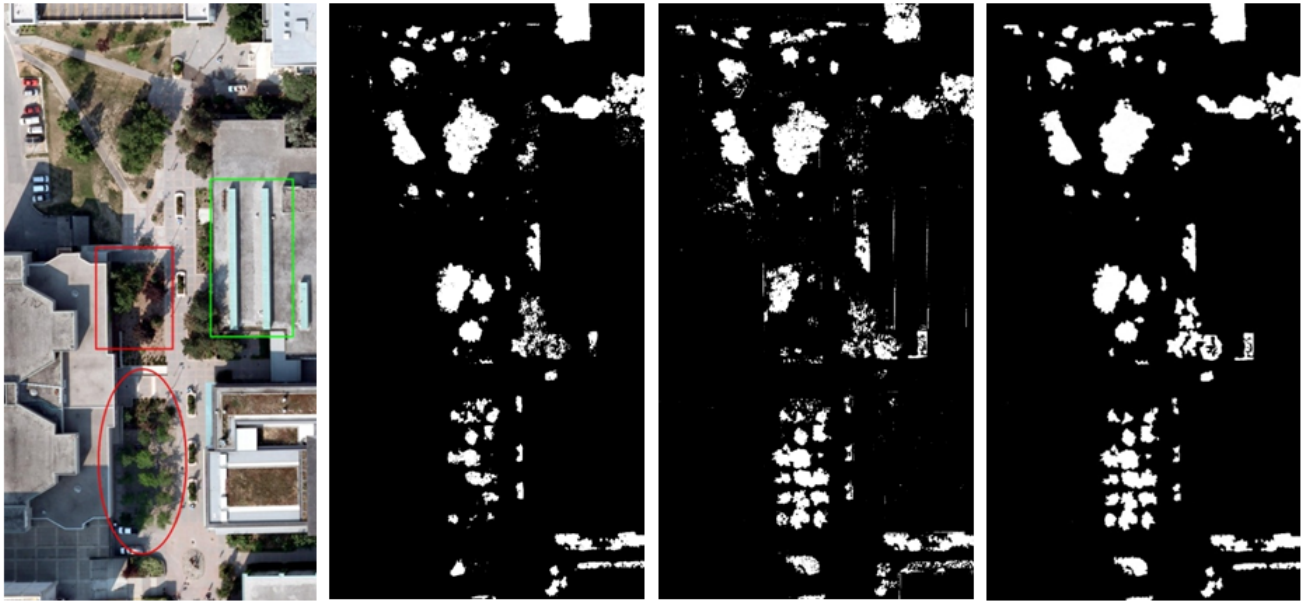

Figure 4.3: From left to right (a) the true color original image with location indication; (b) the NDVI filtering image; (c) the GI filtering image; (d) the NDVI+GI merged image with smoothing and shape filtering.

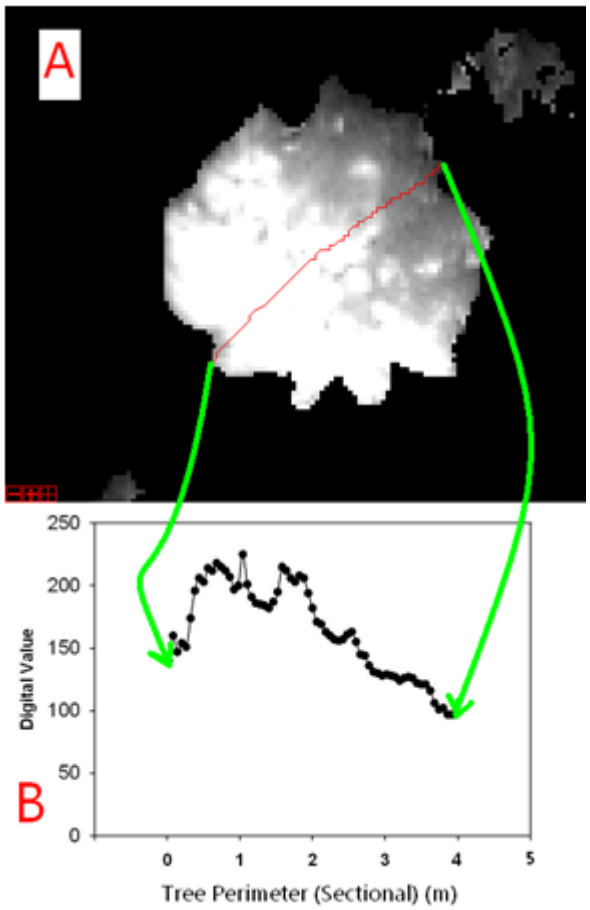

Figure 4.4: The illustrated procedure of obtaining longitudinal profile of a tree crown.

shadows. A first derivation of the raw curve was calculated and the first high peak was eliminated. This step was later proved to significantly improve the robustness of the algorithm. This study was inspired by some pioneer work done by (Fourier et al., 1995), which was mainly limited by the low spatial resolution of the image at that time and coined the term "longitudinal profile" for potential tree species classification. The longitudinal profiles of the different tree species in NIR band are summarized and shown in Figure 4.5.

The outlines of these plots are determined by the geometry of the illumination and viewing condition, and the tree shape. Therefore, it is essential to determine the effect

of geometry of the illumination condition, especially Solar Zenith Angle (SZA) (Puttonen et al., 2010). In this study, the SZA were determined by two different approaches, direct retrieval from the dataset and calculated from the field measurements, such as street-lamp height and its shadow distance. It was $50° \pm 3°$. From Figure 4.5, there is one common feature through out all species. There is always, some more obvious than others, a turning point to separate the profile into two portions. The first portion is generally higher than the second in value, which represents the sunlit and shadowed tree crown surfaces of the same tree. From simple geometry calculation, it is easy to find that SZA directly impacts on the location of this turning point, which in theory, an approximation of the tangent line of the incoming ray of the tree crown surface. It can be approximated by the Equation (4.3) (Jensen, 2005):

$$da = dm \times \frac{1 - sin(SZA)}{2} \tag{4.3}$$

where da is the distance away from the beginning of the profile, dm is the diameter of the tree.

This estimation has a pretty good agreement with the observations, which provided a possibility of correcting all the images obtained from different SZA to a normalized value range. However, this is not the focus of this study. Within one image, the SZA is assumed to be the same for the entire image and any variations caused by the SZA are ignored.

Back to Figure 4.5, these profiles represent a few key features of the trees at a fixed SZA, such as the general outlines of the tree shape, the smoothness of the leaves surface etc. To quantify profiles geometrics, linear best fit, second order polynomial and modified free-form curve approximation were calculated from the profiles in this

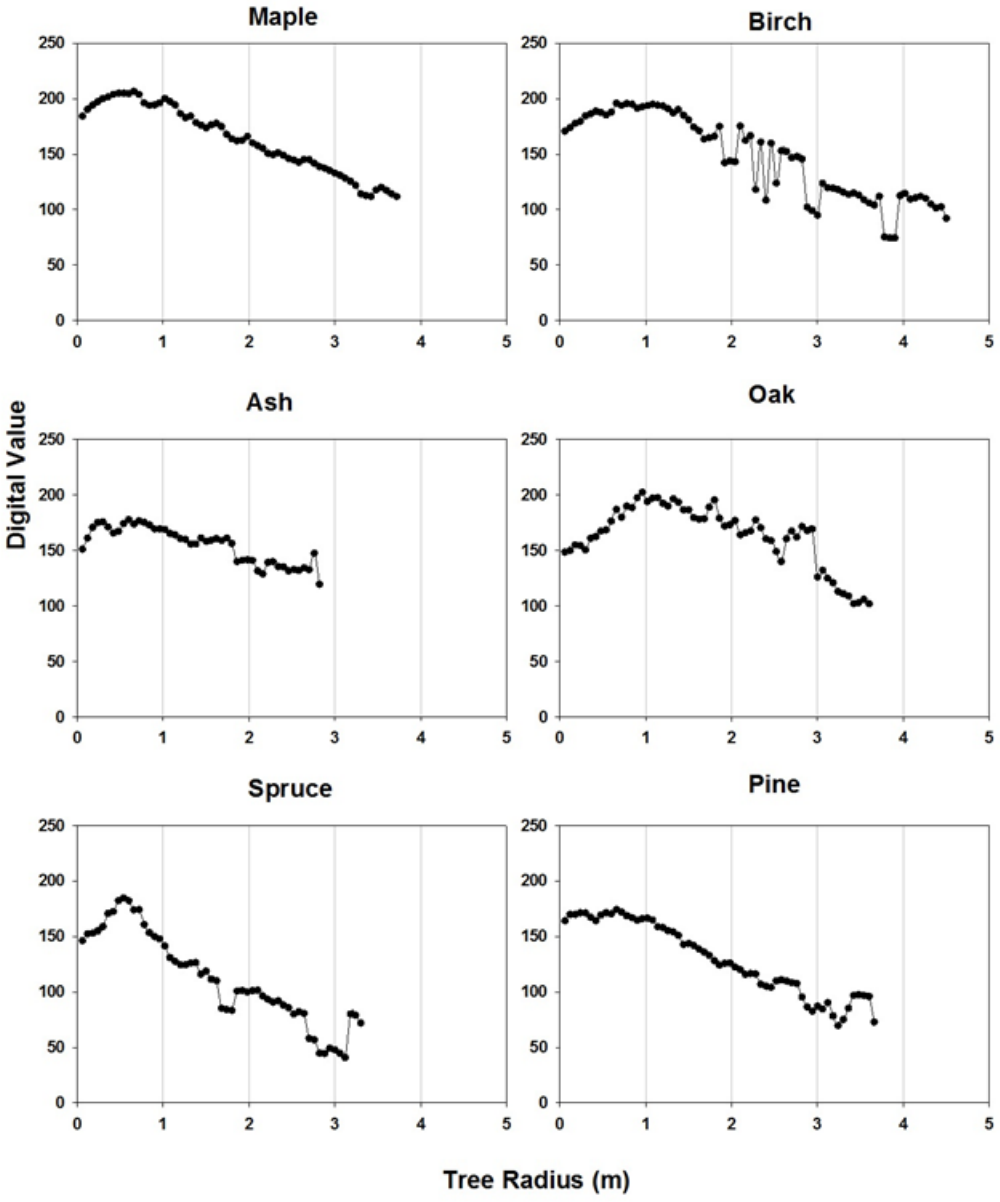

Figure 4.5: The longitudinal profiles of the six different species.

study. Characterizing free-form curves, such as Bezier curves, B-spline curves are classic problem in geometric design. Numerous methods have been proposed in the past decades (Chen et al., 2010; Chuang and Kao, 1999; Shih, 2008; Yuksel et al., 2011). One of the popular approaches is to sample the given curve as a sequence of points and approximate the distance between the points. An important goal for this approach is to reduce the number of the control points that are used. In this study, since the curves are much simpler and known and predictable regulations, a modified approach adapting the concept of forming triangles in the Vectorization (Zhang et al., 1998) was used. Instead of assigning multi-nodes, only one inter-curve node was used, and minimizing the linear fit of the both sides of the triangle, which is illustrated in Figure 4.6. Two parameters were calculated the normal distance (d) from the node to the baseline, which is the link of the two end points and the position (p) given as the ratio of the two segments of a and b, which can be expressed as:

$$p = \frac{a}{b} \tag{4.4}$$

If the curve is flat, close to a linear fit, the d value is fairly low and p value is negative. If the curve is irregular, the d value is dramatic increased and the p is close to 1. If the curve is left skewed, the p value is less than 1 while the right skewed curve will result a greater than 1 value.

In this study, a knowledge-based decision tree was constructed. Decision tree classification is considered a fairly robust and reliable approach (Heumann, 2012). All available parameters, including spectral information, texture information, tree size and height, and geometry of profiles were taken into consideration. However, only the most effective ones were used in the end. The selection of the tree nodes were based

on the following criteria: (1) try to pick minimum one feature from each category; (2) try to use the ones have clearly distinguished features than others; (3) try to minimize the number of the decision tree nodes used.

All spectral bands were included as candidates. Due to the atmospheric absorption, the visible bands suffered significant signal strength loss. Only the NIR band was selected. Figure 4.7 shows the mean, upper and lower values of each species. The NIR at value of 160 and 150 was used to separate the conifer and deciduous with Oak exception. Any value between 150 and 160 are subject to further evaluation. The GRI (Equation (4.5)) (Tucker, 1979) had shown the most effective in separate Conifer and deciduous trees amount the vegetation indices, mainly competing with NDVI. The NIR and GRI combination can identify the strong featured conifer and deciduous trees. The spectral and VI information was used as the first level of screening.

$$GRI = \frac{G - R}{G + R} \tag{4.5}$$

It is not too difficult to separate deciduous from the conifers. However, it could be quite challenge to distinguish the Pine and Spruce. A combination conditions of "left skewed" ($0 < p < 1/3$) and "high d value" ($d > 100$) was used in this study. An interesting left skewed peak was noticed from the Spruce but not in Pine.

To separate the four deciduous tree species, the "left skewed" criteria was first used ($0 < p < 1/2$). The "left skewed" mainly separates the Maple/Birch and Ash/Oak groups. In this study, the Ash are mainly young trees, as such they share a highly complex crown structure with the Oaks. The next criteria examined was "if the curve is flat" ($d < 25$). The Maple has low d value due to their big leaves and mature. The Ash have a low d due to their young age and relative smaller size.

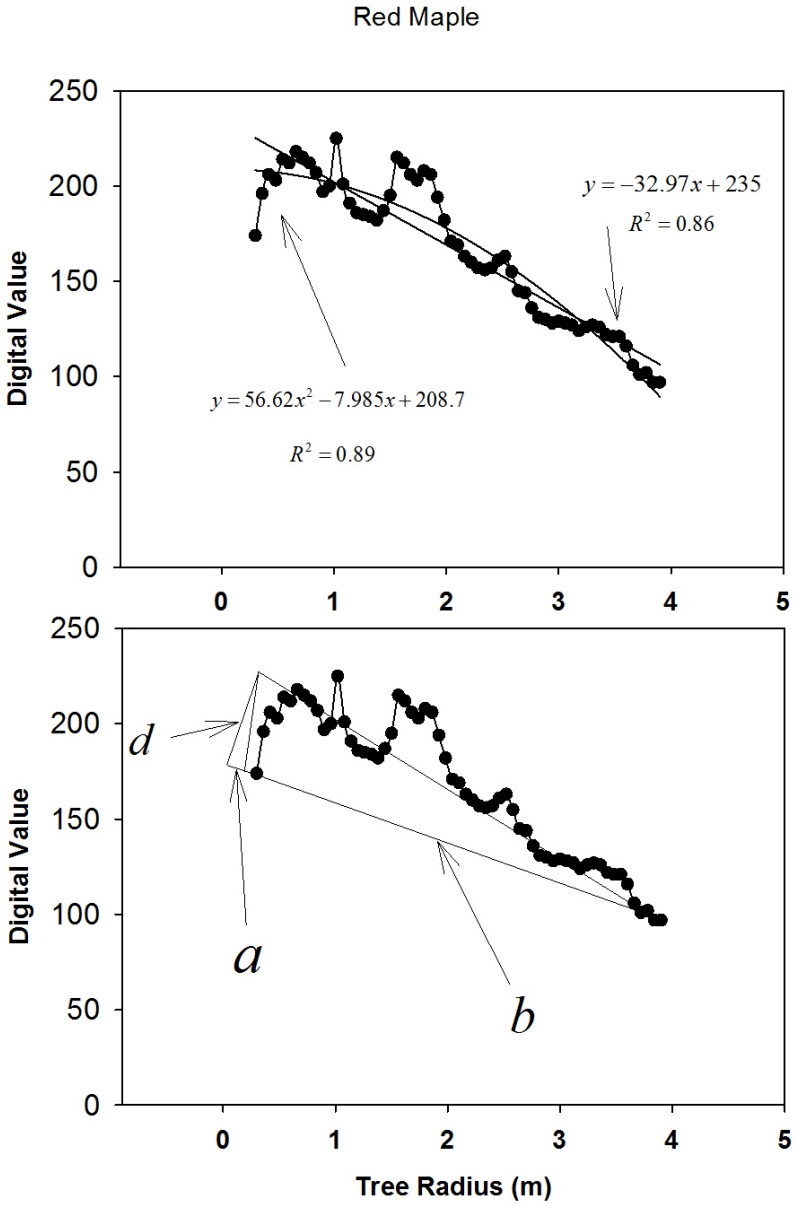

Figure 4.6: (Top): the linear and second order polynomial fit; (Bottom): the single node triangles in the Vectorization of the profiles.

This separation is confirmed also by looking at the linear regression R^2. The Maple broad leaf generates a much smoother surface than the Ash; therefore, its R^2 is over 0.8. Ash would hardly exceed 0.7. All four species can be separated at this stage, however, the result can be ensured by further examining the second order polynomial fit regression coefficient. The final "knowledge-based" decision tree is shown in Figure 4.8. There is an external terminator (iteration counter) to settle the rare cases, which the same node has been visited twice. This only can happen for "highly spectrally mixed" cases, which is most likely caused by the Oak inter-class variety. Therefore, these special cases were signed to Oak to keep no "undecided" cases.

The decision tree can also be constructed base on statistical analysis of the dataset. One of the approaches was based on the "gain criterion", which originated from Hunts information theory (Hunt, 1966). This mathematical decision tree construction was also conducted in this study as comparison. The results were obtained using the commercial software C5.0 (a commercial decision tree classification software) (Hayes et al., 1988; Quinlan, 1993) under the license of York University Earth Observation Laboratory.

4.4 Results and discussion

Out of the overall 200 trees observed on the ground, 142 trees belonged to the 6 selected species. It was first to generate a "knowledge-based" decision tree by randomly picking 50% of the data (70 trees total were picked due to the round up in numbers in different species).This random picking had been repeated a few times, and no significant variation was found. All 142 trees were then analysed by this "knowledge-based" decision tree to generate classification result, which is shown in Table 4.1. The overall

Table 4.1: Classification result using knowledge-based tree.

Species	***Maple***	***Ash***	***Spruce***	***Pine***	***Oak***	***Birch***
Maple	29	1	0	0	0	2
Ash	3	25	0	0	1	1
Spruce	0	0	10	3	0	2
Pine	0	0	4	20	1	0
Oak	1	0	0	0	24	1
Birch	0	0	2	0	0	12

$OA = 84.5\%$

accuracy (OA) was 84.5% and the Cohen's Kappa Coefficient is 80.6%. An indication map is shown in Figure 4.9.

To compare the result, commercial decision tree software C5.0 was used to generate its trees and classification results. Since C5.0 requires training data, the 142 trees used in the "knowledge-based" tree classification were then divided approximately equally into two groups. One group (70 trees) was used as training while the other (72 trees) was used as validation. To better demonstrate the differences contributions of different information. Different information compounds were used and different results were generated.

First of all, only the 4 bands spectral signature approach was used for classification, which is referred as 4 bands signature approach. Results are shown in Table 4.2. The features used were Blue band (100%), NIR band (100%), Green band (50%) and Red Band (32%). Percentage indicated which level and how many times this feature was used. 100% means it was used in first level, all the candidates go through this node. The overall accuracy (OA) was 48.6 % and the Cohen's Kappa Coefficient is 35.7%.

Next, the vegetation indices and texture information was added to the band signa-

Table 4.2: The C5.0 decision classification results with 4-band spectral information only.

Species	***Maple***	***Ash***	***Spruce***	***Pine***	***Oak***	***Birch***
Maple	10	3	0	0	0	3
Ash	1	11	0	0	3	0
Spruce	3	3	2	0	0	0
Pine	0	2	0	10	1	0
Oak	6	5	0	0	1	1
Birch	3	0	2	0	1	1

$OA = 48.6\%$

tures approach. Results are shown in Table 4.3. The feature used were NDVI (100%), Blue band texture (60%), size (57%) and GRI (37%). The overall accuracy (OA) was 75.0% and the Cohen's Kappa Coefficient is 68.7%.

Last, the profile derived indices were added to the data, which makes it a combination of profile, vegetation indices, textures and band signatures. The results are shown in Table 4.4. The features used were d (100%), p (100%), NDVI (88%), GRI (55%) and linear R^2 (27%). The overall accuracy (OA) was 86.1% and the Cohen's Kappa Coefficient is 82.6%.

The normal distance (d), position ratio (p) and linear R^2 are mainly derived from the profile information. NDVI and GRI are also important and selected in Table 4.4 as expected. It was surprising that the texture was completely ignored in the C5.0 decision tree. The benefits of introducing profile-based information are obvious. The classification result improved on every species comparing to Table 4.3, which includes all information except profiles. Table 4.3 delivers a decent 75% total accuracy. It shows the similar trend of classification selected as the "knowledge-based" tree, which tries to keep away from directly using spectral bands. The features were vegetation

Table 4.3: The C5.0 decision tree classification result with spectral, VI and Texture information.

Species	***Maple***	***Ash***	***Spruce***	***Pine***	***Oak***	***Birch***
Maple	13	2	0	0	0	1
Ash	0	12	0	0	3	0
Spruce	1	1	6	0	0	0
Pine	0	1	1	10	1	0
Oak	1	1	0	0	9	2
Birch	1	0	1	0	1	4

$OA = 75.0\%$

Table 4.4: The C5.0 decision tree classification results with all information (Spectral, texture, profiles *etc.*) together.

Species	***Maple***	***Ash***	***Spruce***	***Pine***	***Oak***	***Birch***
Maple	14	1	0	0	0	1
Ash	0	14	0	0	1	0
Spruce	0	1	7	0	0	0
Pine	0	1	0	12	0	0
Oak	0	1	0	0	11	1
Birch	1	0	2	0	0	4

$OA = 86.1\%$

index (NDVI and GRI), the physical parameter (size) and spatial information (texture). This strongly agrees with the initial motivation and inspiration of this study. For uncalibrated imagery with nearby building shadow issues, spectral information is the least reliable. The information that are independent of spectral information will minimize the negative impact and will be expected to improve classification.

4.5 Summery and conclusions

As the results shown in Section 4.4, the longitudinal profiles have been proved to be valuable additional information to improve the individual tree species classification when using very high spatial resolution airborne imagery. For both designed and C5.0 generated decision trees, the accuracy of overall classification results involving profiles were at 84.5% and 86.1%, which are much better than trees generated from non-profile included cases (75% or less). The longitudinal profiles approach is typically suitable for high spatial resolution imagery in the urban environment. It was clear that the shapes of trees are strong signatures of tree species recognition. In urban environment, trees tend to grow into their natural shape due to low competition. Trees are more isolated and have clear boundaries. The end to end longitudinal profiles are not as difficult to obtain as in forestry cases. The profile information can directly represent tree shape, which is a more favourable side view. It is not affected by the nearby building shadow, which brings more robustness to the spectral signature issues. It also can quickly estimate the level of the tree crown variation, which is highly correlated with texture and leaf size and shapes without spectral variation problems. These features are very important for non-calibrated high spatial resolution imagery without calibrations.

In this study, one important improvement is the separation of Pine and Spruce,

which directly results from including profile information in the classification. The Pine and Spruce have similar spectra and both have needle leaves, which can be a challenge for spectral classification, but the high spatial resolution profile can capture the needle orientation and branch differences to improve the classification. For other species, Maple was the most stable specie that can be estimated at a reasonable accuracy (62.5% or higher), followed by Ash. In this study, most Maple and Ash trees on the ground are in the similar growth stage. Most Maple were mature and healthy, therefore, it was expected to have a reasonable retrieval accuracy. On the other hand, Ash were young, healthy but suffer significantly from the shadow issue. Once the GI was implemented to reduce the segmentation error, profile information can strongly compensate the spectral differences caused by the shadow.

In forestry cases, trees are subjected to high competition with neighbour trees. Airborne imagery normally can only see the top of crowns, which is the focus of the current shape recognition studies. The competitive growing condition dramatically changes the outline of the trees, increasing the difficulty of effectively using the shape information in classification.

Due to the volume of the ground data, limited validations were conducted. The profile can not get away from the biggest challenge in species classification using remote sensing data, the variability in the properties derived from remote sensing data between trees with the same species caused by various factors (within class variability), and the inter-class similarity. It should be applied with the other information together to maximize the classification accuracy. Coefficients reassessment and "knowledge-based" tree modification may be needed if applying this method to a new study area. The results were more of a demonstration of the potential of using longitudinal profiles

in classification. More validation work is needed in the future studies. The end to end profiles are specifically designed for urban tree cases in this study. However, it is still potentially possible to apply it in forestry study, which would use top portion only. It means partial profile to reconstruct the side view tree shape is valuable in the future investigation.

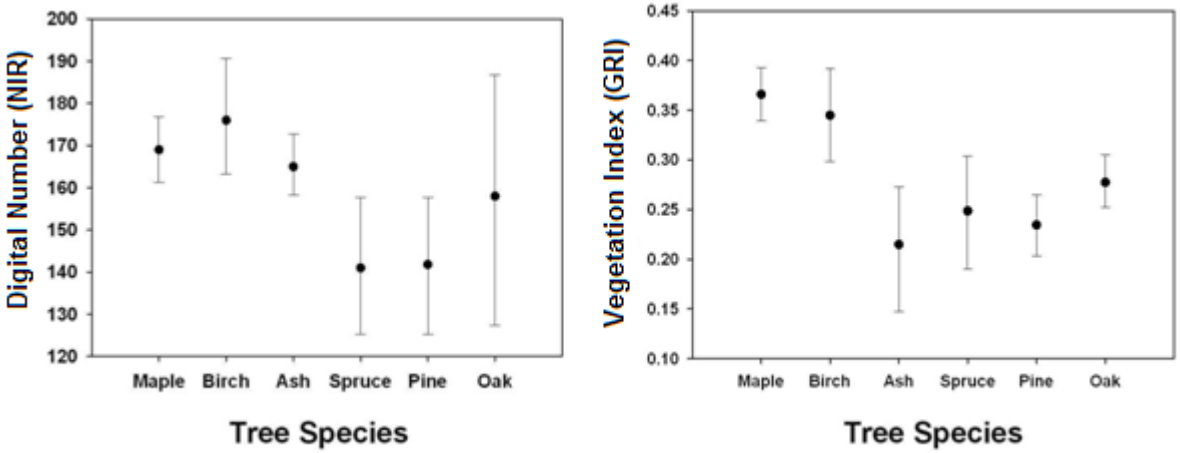

Figure 4.7: The NIR (Left) and GRI (Right) mean and maximum/minimum boundaries for six tree species.

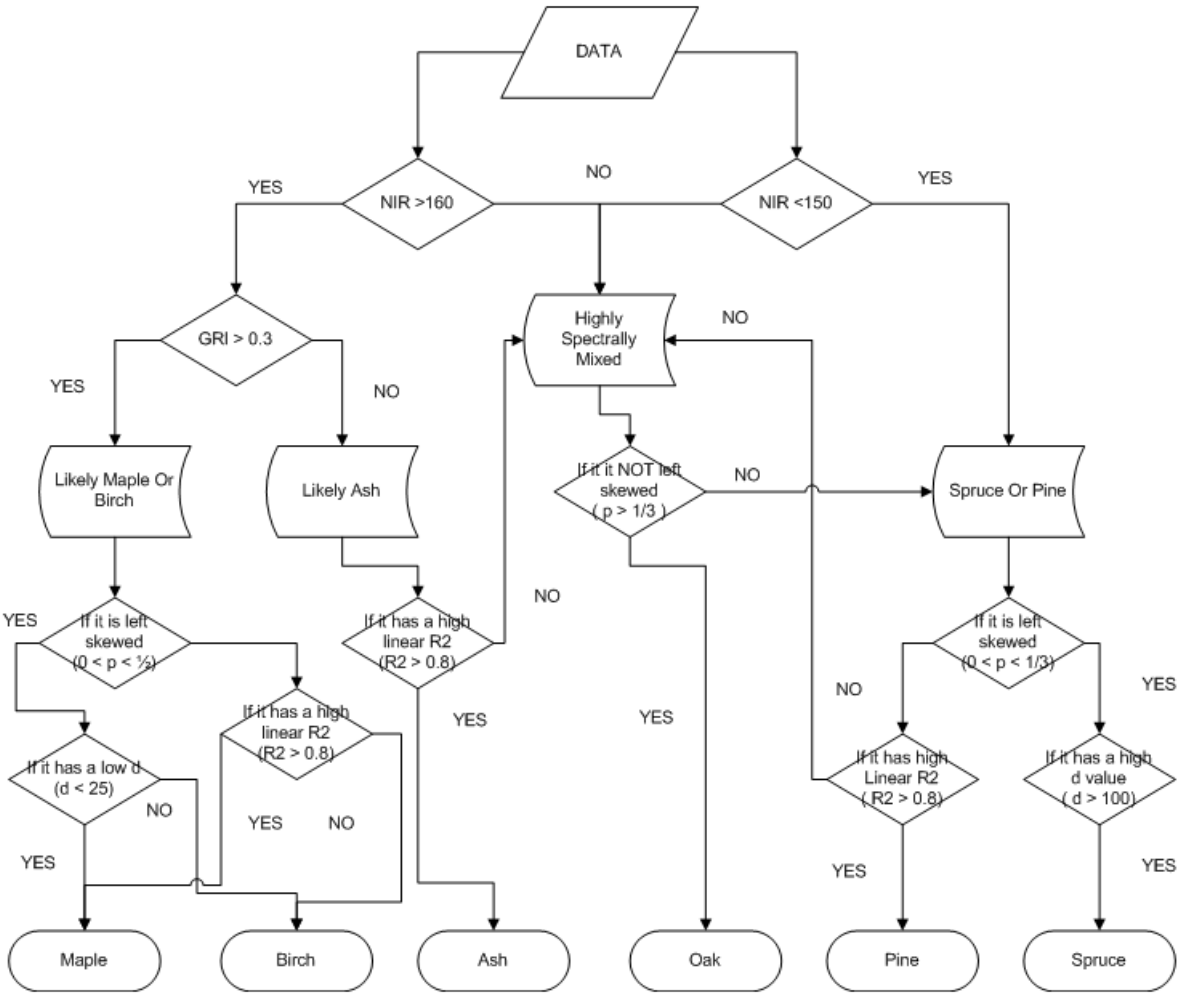

Figure 4.8: The knowledge-based decision tree constructed.

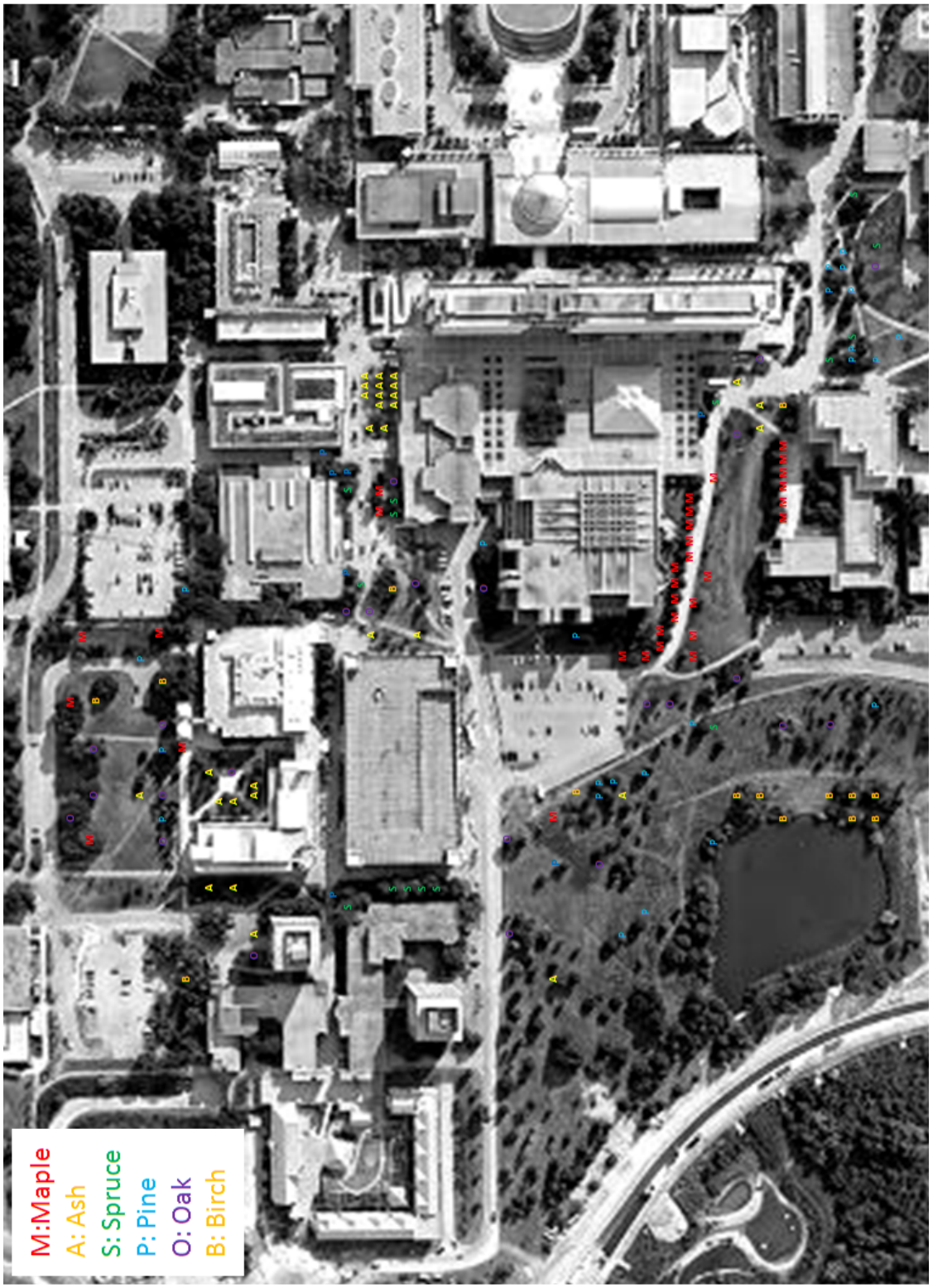

Figure 4.9: The indication map of knowledge based decision tree classification results (zoom into the central area for better view)

5 Early detection of Emerald Ash Borer (EAB) infestation using multi-sourced data

This chapter is based on the published journal paper:

Zhang, K., Hu, B., and Robinson, J., (2014), "Early detection of Emerald Ash Borer (EAB) infestation using multi-sourced data: a case study in the town of Oakville, Ontario, Canada", Journal of Applied Remote Sensing, 8(1), accepted on June 3, published on July 7, 2014.

It is a further development of the conference paper:

Zhang, K., Hu, B., Hanou, I. S., and Jin, L. (2012), "Early detection of ash Emerald Ash Borer (EAB) infestation using hyperspectral imagery", proceedings of the 2012 International Geoscience and Remote Sensing Symposium (IGARSS), 6360 - 6363, Munich, Germany.

5.1 Introduction

The Emerald Ash Borer (*Agrilus planipennis*, EAB) is one of the most destructive insects to affect ash species of the genus Fraxinus (Maloney et al., 2006; Sydnor et al., 2007). Ash is one of the most popular landscape trees in North America, replacing elm trees in new residential and commercial developments due to its high tolerance to environmental stresses and its resistance to pests(Gould et al., 2013). The invasion of EAB was first reported in 2002, in Michigan, USA. Despite substantial research and control efforts, the beetle has continued to spread to new areas, and today it is found in 14 states and has crossed the border to Southern Ontario, Canada (Kovacs et al., 2010).

The beetle has caused the death of millions of ash trees and billions of dollars in economic losses (Rose, 2010). The ash trees attacked by EABs often show serious decline within two years of initial infestation, and typically die within three to five years (Anulewicz et al., 2007). As such, early detection is especially valued, due to the aggressive nature of the EAB infestation.

Infestations are normally identified by tree owners and are confirmed by on-site tree branch sampling (Gould et al., 2013). Recent EAB studies have focused on biochemical and biological symptoms and treatments, such as tree leaf decline, woodpecker presence, chemical injection treatments, and tree removal (Gould et al., 2013; Ryall et al., 2011). However, each of these techniques is inherently concerned with late stage occurrences of the infestation. In order to improve in this multiple government agencies and environmental groups are exploring the use of remote sensing techniques for infestation detection over large areas, including city and provincial scales. Analysis of such data could offer workable results with improved cost and detectability efficiencies.

During EAB infestation, the larvae destroy the cambium layer under the bark responsible for transporting nutrients and water throughout the tree, therefore resulting in general stress (Ryall et al., 2011). Trees under general stress often experience changes in leaf pigment composition, particularly in leaf chlorophyll content. Thus, from a detection point of view, trees exhibiting general stress symptoms are much more likely to be infested (McCullough and Katovich, 2004). As a result, spectral features that are sensitive to leaf chlorophyll content can be potentially used for detecting EAB infestations with remote sensing technologies (Pontius et al., 2008). Current remote sensing approaches are focusing on such spectral features, but their success thus far has been limited, as described below.

In Pontius et al. (2008) a 6-parameter function was proposed, and a 97% correlation was reported between selected vegetation indices and tree decline caused by EAB infestations. However, this correlation can only be confirmed in the dieback stages, and the spectral-based variation is not sufficiently significant during the early infestation stage to allow unique identification.

Souci et al. (2009) presented an EAB detection project based in Milwaukee, Wisconsin, using high spatial resolution hyperspectral images and a pixel based vegetation index approach to map out the invasive species. They also used LiDAR (Light Detection And Ranging) to create a digital elevation model and applied GIS (Geographic Information System) buffer zone tools to highlight potential infested areas. However, no significant validation result was obtained, and this study is considered a pioneer work in multi-source data combination.

Hanou (2010) used a vegetation index to represent the correlation between infestation and tree crown pixels to map out ash infestation in Oakville, Ontario. It can

be expressed as:

$$VI = \frac{(R_{SWIR} + R_{Green})^2}{(R_{SWIR} - R_{Green})}, \tag{5.1}$$

where R_{SWIR} is the short wavelength infrared and R_{Green} is the green band. However, this pixel-based vegetation index approach can result in the misclassification of different tree species as ash, and struggles to identify tree canopy over different backgrounds, as well as being prone to spectral variations within individual trees. As a result, it was not able to successfully map infested ash trees using this method.

Our goal in this study is to make this difficult task of early stage EAB infestation identification possible, providing a methodology that can deliver a reasonable detectability for EAB infestation over large spatial scales. After background searches and literature reviews, we have determined that the clues associated with EAB infestation are widely varied and may be deeply buried in different data sources, and not just spectral data from hyperspectral imagery. As such, spectral and pixel-based analysis alone is not sufficient for early detection of EAB, as it is susceptible to considerable in-class spectral variation. It is necessary for us to broaden our range of information sources, which requires the precise identification of information correlated with EAB infestation, and their effective retrieval from different data sources. This additional information from varied sources can reduce the ambiguity and uncertainties caused by in-class spectral variation, and ultimately improve the accuracy of information retrieval.

First, we investigated spatial features as a potential information source. As suggested by (Smitley et al., 2008) there are a number of visual symptoms that can help to detect early stage infestation, such as the dieback of twigs, thinning of the crown, and

growth of new branches on the lower trunk. These symptoms can often be reflected in structural changes of the tree crowns (Cosmopoulos and King, 2004; Omari et al., 2013). For a mature and healthy ash tree, an oval shaped crown can be assumed. In the presence of EABs, an ash tree loses its leaves, starting from the top central branches, which leads to "holes" or "gaps" in the crown. In a high spatial resolution image, a healthy mature ash tree exhibits a smooth texture with "salt and pepper" patterning, which represents the gaps between leaves and branches. In contrast, certain patterns that derive from the presence of larger "holes" in the crown are expected in an EAB infested tree. Since spectral features do not typically consider the spatial patterning changes before and after infestation, this predictive information on tree morphology may help to determine the EAB infestation level.

We also recognize the natural spreading capacity of EAB. The mature beetle can migrate from one tree to its neighbors, within a 25 km radius (BenDor et al., 2006; Herms et al., 2009). Therefore, the known infested trees that have been previously documented are important contributors to the potential continuation of the infestation, which is a consideration that has been long neglected.

Further, following a comprehensive literature search and preliminary studies and testing of various data sources, we identify the leaf chlorophyll content as a potential indicator of infestation. Specifically, a significant drop compared to the surroundings, in addition to the tree crown degradation and distance from known infested trees may be considered key factors that can potentially lead to accurate estimation of the extent of infestation.

Despite recognition of these key factors, it remains a challenge to effectively assemble the diverse information, derived from multi-sourced data, in order to reach a

meaningful, consistent, and accurate conclusion. As a solution to this, we propose an object-oriented approach rooted in these key factors, and devise a weighted linear prediction score function. With proper calibration, this new infestation scoring approach can be applied to the detection of early to medium stage EAB infestations. Therefore, the overall outline of this study is as follows, also shown in detail in Table 5.1.

1) Comprehensive background search and literature review. 2) Extensive data collection and processing. 3) Prior-processing studies and testing. 4) Identification of the key factors for EAB infestation, which must be strongly correlated with infestation and must be extractable from our data. 5) Establish an operational workflow, which can effectively and robustly retrieve information from different sources and intelligently combine them to deliver a precise prediction. 6) Map out the health of individual ash trees within test areas using the proposed methodology.

5.2 Data specifications and pre-processing

5.2.1 Study area

The study area was the town of Oakville, Ontario (Figure 5.1). All ash trees within the township boundary were part of the study. However, due to data limitations, particularly related to ground data acquisition, we focused mainly on six sites within Oakville, which are indicated in the final infestation map. Oakville is the first town in Canada to use aerial-based imagery to compile and inventory public and private ash tree damage (Hanou, 2010). Oakville is located in the EAB infestation zone, and has multiple confirmed cases of EAB infestation. Therefore, this region has great interest in research into early detection of EAB for both environmental and economical reasons.

Table 5.1: Overall structure of this study

	$Spectral features$	$Spatial features$	$Prior-knowledge$
Background and literature review	Hanou (2010); Pontius et al. (2008); Souci et al. (2009)	Smitley et al. (2008); Zhang and Hu (2012)	BenDor et al. (2006); Herms et al. (2009),
Data sources	Hyperspectral data:	High spatial resolution data:	Community maps and paper documents
	1) Ground ASD measurements;	1) YUL Oakville imagery;	
	2) Airborne imagery	2) Google Earth imagery	
Prior-knowledge studies and testing	1) Ground ASD spectral signature separability study;	Spatial pattern visual interpretation	EAB natural spread capability
	2) Contribution analysis for vegetation indices band selection		
Key factors identified	Leaf chlorophyll content	Tree crown degradation	Distance from nearby known infested trees
Operational workflow	1) Three vegetation indices;	Longitudinal profiles	Distance constant
	2) Leaf chlorophyll content retrieved from model inversion	Longitudinal profiles	Distance constant

Figure 5.1: Location of the town of Oakville, Ontario, Canada and the ground survey results of individual tree distribution. Numbers in the inset are the IDs of trees with confirmed infestations.

5.2.2 Airborne and ground hyperspectral Data

Two sets of commercial hyperspectral remote sensing data were used:

1) Airborne hyperspectral imagery with a spatial resolution of 1 m was collected using a ProSpectTIR-VS2 in July 2010. In total, 360 spectral bands were recorded, ranging from 390 to 2400 nm with a band spacing of 5 nm. The raw imagery was converted into radiance by removing dark current, and was then corrected for atmospheric disturbances using ATCOR4 software. Precise geo-referencing and geometric correction was carried out using information provided by the on-board Internal Navigation System (INS) and Global Positioning System (GPS) (Hanou, 2010).

2) Ground-level hyperspectral data were also collected. The leaves from ash trees at different stages of infestation were measured using an Analytical Spectral Device (ASD) (ASD Inc., Boulder, CO, USA). Leaves were recorded as healthy, low, medium, and highly infested. This is a fundamental prior-processing study, used for separability assessment, which must be conducted before any further meaningful further research can be begun. If no significant differences are observed between ground level spectra of trees at different stages of infestation, then the likelihood of canopy-level spectra exhibiting sufficient differences for classification is very low.

5.2.3 High spatial resolution aerial imagery

High spatial resolution aerial imagery was provided by York University library. The data were collected during the winter of 2008, having 1 m resolution, and is orthorectified with Blue, Red and Green in three spectral bands. However, the absence of leaves at the time of image acquisition limited the use of these data in this study. We

therefore only use the images to validate the locations of trees and to confirm tree species identification.

5.2.4 Google Earth aerial imagery

The employment of Google Earth (GE) aerial imagery in scientific studies poses a dilemma. GE imagery is not quality assured with any known or documented geometric or radiometric corrections. However, the data are free and easy to access, and are potentially very powerful, containing, for example, multiple years of data from the same location. In the Oakville area, GE imagery has an average spatial resolution of 13-15 cm over our test sites. Before making use of the GE imagery, we made precise calculations of scale using known objects, such as rooftops. We also validated the geometric locations of trees, and the differences in the locations of our sampled trees. From this, we found that the GE imagery and the orthorectified images were within 0.5 m of the tree centers. We did not validate or calibrate the radiometric values of the GE imagery, as we were only concerned with the relative changes in the pixels.

5.2.5 Ground truthing

We used two sources of ground-based information to determine the likelihood of infestation from nearby infested or healthy trees, and to support ground validation. Firstly, most infestations were confirmed using a previously documented branch sampling approach (Ryall et al., 2011). Two branches, approximately 50 cm long and no less than 6 cm in diameter, of each targeted ash tree were obtained, and their bark was peeled off and the underlying cambium inspected for evidence of EAB infestation, such as serpentine galleries, larvae, and young beetles (Figure 5.2).

Figure 5.2: The branch sampling approach for EAB detection. A larva is found in this sample. Copyrighted at AMEC Inc, used with permission.

Secondly, nine community maps showing street and park tree layouts were supplied by the town of Oakville. In these maps, the infestation states of individual trees were recorded as "healthy", "low", "medium", and "high" infestation states, as indicated by ground-based survey. We manually transferred these locations and condition information into our imagery data.

Nine community maps with street and park tree layouts were supplied by the town of Oakville. In these maps, infestations of each individual tree were labelled with healthy, low, medium and high four infestation states. This was our second source of

ground truthing.

5.3 Operational workflow and detail procedures

We have identified three key factors that can potentially guide an estimation of the health of ash trees, supported by previous work and preliminary studies. These are the leaf chlorophyll content, tree crown degradation, and distance from nearby trees of known health state. An operational workflow must be established, with the objectives of: 1) effectively retrieving the targeted information from its associated data source; and 2) intelligently assembling all information to provide a final estimation.

Despite the convenience of pixel-based methods, we proposed an object-oriented approach, which ultimately forms a score-based prediction function. In this study, individual tree crowns were considered as the basic objects, instead of isolated pixels, and their spectral and spatial properties were analyzed. Using an object-oriented approach in this way is essential for the retrieval of distance and crown degradation information, while also improving the computing efficiency in the model inversion.

Our approach comprises four major steps: segmentation and identification of individual ash trees; information retrieval; information conversion; and final evaluation through score calculation. This operational workflow is graphically depicted in Figure 5.3. As shown in this figure, the airborne hyperspectral and the GE aerial imagery data underwent segmentation to outline tree boundaries. Then, the vegetation indices, leaf chlorophyll content derived from model inversion, and distance constants, originally from maps but transferred to imagery tree locations, were derived from the hyperspectral data, while the spatial patterns of crown degradation were obtained from the GE imagery. All "information" from this step was converted into normalized

numerical values between 0 and 5, and assembled into a score function, which provides a prediction score that can be used to determine the health state of individual trees.

5.3.1 Segmentation and identification of individual ash trees

To ensure the accuracy of the locations and boundaries of individual ash tree crowns, multi-scale automatic segmentation results from both the hyperspectral and high spatial resolution images were manually checked and corrected. In the hyperspectral image, the pixels within each tree crown were identified and classified into the same crown. Using ground surveys and the community maps provided by Oakville, all ash trees used in the following training and validation studies were checked and confirmed.

5.3.2 Information retrieval

5.3.2.1 Overview

As shown in Figure 5.3, four types of information, making up six indices or parameters, need to be retrieved from the varied data sources: three vegetation indices; the leaf chlorophyll content; the distance constant; and the longitudinal profile. The following sections will detail the individual methods used to extract each of these parameters.

5.3.2.2 Calculation of the selected vegetation indices (VIs) related to the health state of tree crowns from spectral features

Attempts have previously been made by many researchers to identify the health state of tree crowns from airborne and satellite images, through the design of a vegetation index (VI) sensitive to biochemical properties of leaves (e.g., (le Maire et al., 2004; Pontius et al., 2008; Thenkabail et al., 2012)). In these studies, four major categories

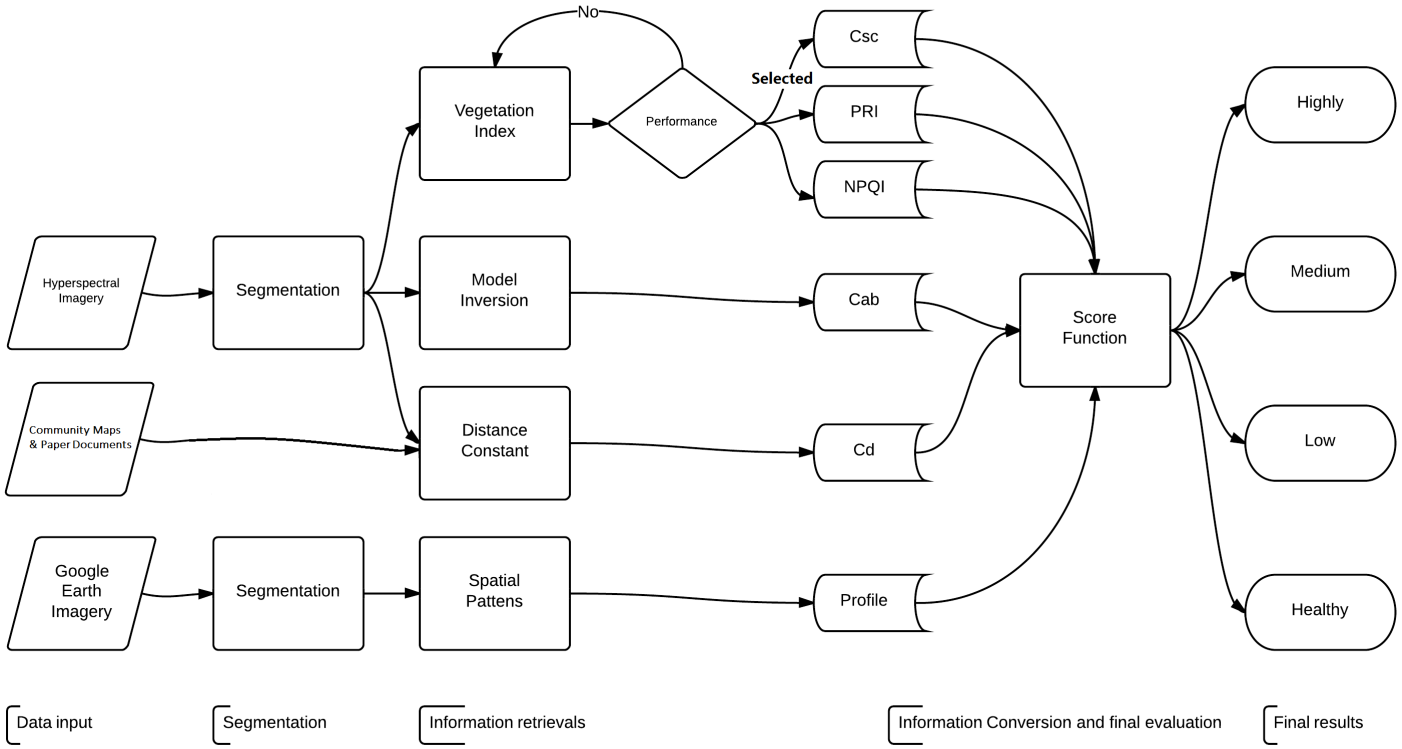

Figure 5.3: Graphical depiction of the operational workflow for this study, showing four major steps retrieving four types of information and six different parameters from three different data sources to derive the final health estimation.

of biochemical parameters have been considered: leaf chlorophyll content,(le Maire et al., 2004; Pontius et al., 2008; Zhang et al., 2008) carotenoids,(Sims and Gamon, 2002; Thenkabail et al., 2012) water content,(Barnes et al., 1992) and anthocyanins (Sims and Gamon, 2002). After a comprehensive review of these properties and their associated vegetation indices, a suite of indices were selected (Table 5.2) as candidates for detailed comparison and future selection. The existing indices were typically designed for specific sites and sensors, (Carter, 1994; le Maire et al., 2004; Pontius et al., 2008; Sims and Gamon, 2002) and it was found that using the same formula with a small change in the wavelength used in the index could result in a noticeable difference in the correlations between a vegetation index and its respective vegetation parameter (le Maire et al., 2004).

We applied a model-based site-independent band selection analysis called contribution analysis, theoretically equivalent to a sensitive study, to optimize the selection of vegetation indices. The contribution analysis calculates the CI, which provides detailed, quantitative measurements of the correlations between each observation band and the target parameters, solely based on the model that we use (Zhang et al., 2011). For this study, we calculated the CI for each spectral band based on the PROSPECT leaf model (Jacquemoud and Baret, 1990) due to the prevailing deciduous leaf type. PROSPECT is well validated and is known for successfully simulating deciduous trees situations. The model simulates leaf reflectance and transmittance at 400-2500 nm and takes four key input parameters: the leaf chlorophyll content, the water content, dry matter, and a parameter describing the internal structure of the leaf, denoted as N. We calculated CI using PROSPECT, which covers all the spectral bands for VIs listed in Table 5.2. CI is the most important criterion for VI band selection, and the

Table 5.2: Vegetation indices selected for investigation in this study.

Chlorophyll and Stress	**Vegetation Index Formula**	**Parameter Sensitive To**	**References**
Csc	$R605/R760$	Chlorophyll a	Carter and Miller (1994)
GI	$R554/R677$	LAI and total chlorophyll content	Smith et al. (2005)
$Vogb$	$FD715/FD705$	Total chlorophyll content	Vogelmann et al. (1993)
$NPQI$	$(R415 - R435)/(R415 + R435)$	Chlorophyll degradation	Barnes et al. (1992)
GMb	$R750/R700$	Total chlorophyll content	Gitelson and Merzlyak (1994)
$SR680$	$R800/R680$	Total chlorophyll content	Sims and Gamon (2002)
$TCARI/OSAVI$	TCARI $= 3(R700 - R670) - 0.2(R700 - R550)(R700/R670))$ OSAVI $= 1.16(R800 - R670)/(R800 + R670 + 0.16)$	Total chlorophyll content	Haboudane et al. (2002); Zhang et al. (2008)
$AMEC$	$(R_{SWIR} - R_G)^2/(R_{SWIR} + R_G)$	Direct infestation detection	Hanou (2010)
Cartenoids			
PRI	$(R531 - R570)/(R531 + R570)$	Cartenoids	Merzlyak et al. (1999)
Water Content			
WBI	$R970/R900$	Canopy water content	Carter (1994)
Anthocyanins			
$Red/Green$	$\sum_{i=600}^{699} R_i / \sum_{i=500}^{599} R_i$	Anthocyanins	Sims and Gamon (2002)

bands that have higher CIs are preferred over the lower scoring ones. In addition to this, we also conducted an actual performance evaluation. We used half of the known infested trees as a training data set, described in detail in the training section below, and the remainders were used as validators to evaluate the performance of the various VIs. From these analyses, the three top performing indices were chosen for the final infestation evaluation based on the following criteria: 1) Higher CI in those bands involved in the VI; 2) Higher separability in different health states; and 3) Lower in-class variation, which is quantified by the coefficient of variation (CV). CV measures the dispersion of the measurement, which is the extent of variability in relation to the mean of a population. For VI selection, this means that VI should have minimum class variation (e.g., low standard deviation) in each state. Essentially, the greater the separation shown between different stages, particularly the early and median stage, the better the candidate.

After determining the final three optimum VIs (PRI, CSc, and NPQI; the selection criteria are described in detail in later sections), we used them to calculate VI values from the hyperspectral spectra extracted from the airborne hyperspectral imagery. We used the average spectra of the sunlit portion of the tree crown only, but included any dark spots within that area.

5.3.2.3 Retrieving leaf chlorophyll content based on physical model inversion from spectral features

Physical model inversion is a sophisticated approach that can obtain accurate biophysical parameter estimations (Zhang et al., 2011). The observed and model-simulated spectra are compared using a pre-defined merit function to determine the best-estimated

model parameters.

In this study, the coupled PROSPECT and SAIL (Verhoef, 1984) models, known as the PROSAIL model, were used. Three variables were tested for, while the remaining parameters were fixed at typical values adapted from our earlier study.31 Since we used a Look-Up-Table (LUT) approach, the first variable, leaf chlorophyll content, was fixed within a range of 25-105 $\mu g cm^{-2}$, the parameter N, which is the leaf structural parameter from PROSPECT, was set at 0.5-4 (unitless), and LAI, the ratio of half total leaf size projected onto the area was set at 1-5 (unitless). The merit function was calculated based on a least square function implementing CI as a weighting. CI was used for band selection, in which we attempted to select those bands sharing a higher sensitivity to the targeted parameters. For a similar reason, we used CI here again as a weighting in the inversion to focus on the more highly sensitive bands.

After obtaining the leaf chlorophyll content values, they are classified into three potential risk levels of infestation, using threshold values derived from the model training. Those highly likely to be infested have a threshold of 2, a medium likelihood is assigned a value of 1, and the remainder has a value of 0, including uncertain or unknown cases.

5.3.2.4 Spatial pattern feature: longitudinal profile for tree crown delineation

Spatial information within a tree crown is useful in evaluating early leaf loss and shape change of the crown. The textural or structural anomalies in an infested crown during the early infestation stage are difficult to detect using traditional statistical textural analysis. Instead, in this study, a longitudinal profile along the solar principal plane,

end to end on the tree crown passing through the tree center, as developed by Zhang et al. (2011), was adopted. A sample longitudinal profile is given in Figure 5.4. In this figure, the tree crown boundary has already been segmented out, and the longitudinal profile is the line made up of digital values (e.g., reflectance) along the solar panel. To further reduce potential spectral variation and to minimize uncertainties in the GE image, the normalized relative differential values were used, wherein the differences in neighboring pixel values were divided by the average of all spectra within the crown. The numbers of significant drops in these longitudinal profiles were used to determine the possible infestation stage.

In this study, we used the following criteria to determine the infestation stage: crossing from the center of the tree, if there was at least one major drop in values on both sides, it was considered a low infestation state, with a score of 0.5; if there were at least four drops on both sides combined, it was classified as medium infestation, with a score of 1.5; and any case with more than six such drops was considered highly infested with a score of 2.5. The necessary size and significance of these drops was determined by a threshold value derived from training.

5.3.3 Distance from nearby known state trees from prior knowledge

As stated in BenDor et al. (2006) and Herms et al. (2009) the potential radius of infestation spread is 10-15 miles, or 16-24 km. Hence, in this study, the infestation likelihood was evaluated by considering the distance of the target tree from the known infested trees within a radius of 24 km. For calculating the distance constants, two different cases were considered in this study, street trees and natural park trees. Street trees were normally planted at linear and fixed intervals. Therefore, linear functions

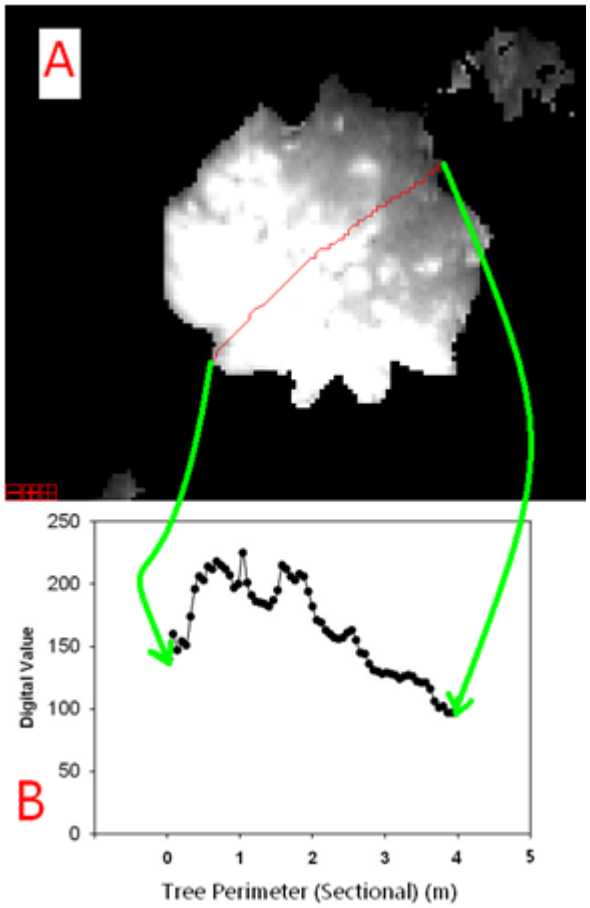

Figure 5.4: A sample longitudinal profile. The tree crown is segmented out and the profile is a line made up of digital values (e.g., reflectance) along the Sun illumination direction, end to end through the tree center.

were formed and each street may be considered as a linear line, which starts and ends with known infested or uninfested trees. All trees of unknown status in between then could be assigned scores of infestation likelihood. If a tree is covered by multiple such functions and receives conflicting information from different linear functions, then an average is calculated and used. The average is used instead of maximum likelihood due to the fact the actual distances are not considered. For naturally occurring and park trees, a normal distribution function was formed at the location of the trees of known status, and the standard deviation was set to 20 m. This value was considered as a constant in the final evaluation function.

5.3.4 Information conversion and final evaluation

5.3.4.1 Training and conversion of indices and parameters

We randomly selected half of the infested trees to obtain average values for thresholds and to generate regression functions. We used third order polynomial functions for the VIs, and a threshold values approach for the other parameters. The procedure was repeated multiple times to ensure consistency. Each parameter was then assigned a numerical score between 0 and 5, where 0 is healthy and uninfested and 5 represents a highly infested state.

5.3.4.2 Final evaluation

After conversion, all information was assembled into the prediction function for calculating the final score, which, as above, also ranged from 0 to 5, with 0 being healthy and 5 being highly infested. The infestation score was calculated as a weighted sum of all the parameter scores related to EAB infestation. The weight for each parameter

was determined based on its associated uncertainties. The final score can thus be expressed as follows:

$$Score = \frac{\sum \omega_i P_i}{N \sum \omega_i} + C, \tag{5.2}$$

where ω_i is the weight of i^{th} parameter, P_i is the score of the i^{th} parameter, N is the dimension of the information layers, or number of parameters used, and C is prior knowledge constants, which in this case is mainly dedicated to distance information derived from prior knowledge (Cd), such as the distance from trees with known infestation states.

5.4 Results and discussion

The results of this study are diverse and wide-ranging, and are reported in the following sections with their associated discussions alongside. Section 5.4.1 presents the prior-processing studies in ground level hyperspectral signature separability assessment and contribution sensitivity analysis. Section 5.4.2 details the performance evaluation for the selection of the final three vegetation indices, the final vegetation indices, and their score conversion functions. Section 5.4.3 outlines the leaf chlorophyll content retrieval results from the PROSAIL model inversion and its score settings. Section 5.4.4 presents the longitudinal profile tree crown degradation study and its score settings. Section 5.4.5 illustrates a sample tree calculation throughout the entire procedural workflow, as an example. Finally, section 5.4.6 presents the final ground validation result and the color-coded map of estimated ash tree health.

5.4.1 Prior-processing Studies

5.4.1.1 Ground level hyperspectral signature separability assessment

The ground level hyperspectral signature separability assessment is critical in spectral-based studies. As mentioned earlier, if no significant differences are observed between high detail (e.g., ground level) spectra of trees at different stages of infestation, then the likelihood of low detail (e.g., canopy level) spectra exhibiting sufficient differences for classification is very low. A set of sample reflectances for ash leaves from trees at different stages of infestation are shown in Figure 5.5. The figure shows that there are clear differences in leaf-level hyperspectral measurements throughout the spectral range. Therefore, it may be expected that information retrieved from spectral data, particularly entire spectra, will be informative.

5.4.1.2 Contribution sensitivity analysis and performance evaluation for selection of vegetation indices

To determine bands that are potentially more successful in the VI study, the leaf-level contribution sensitivity analysis was calculated based on the PROSPECT model, which was used to evaluate the performance of various vegetation indices. The contribution analysis calculates a contribution index that provides quantitative measurements of the "contribution" of each observation to the final retrieval of the targeted parameter. Therefore, a higher CI represents a higher correlation. As a result, those bands with high CI should be preferred during vegetation index band selection. We calculated a series of CI values for different leaf chlorophyll contents from the simulation studies of PROSPECT, which are shown in Figure 5.6. The outcomes of these

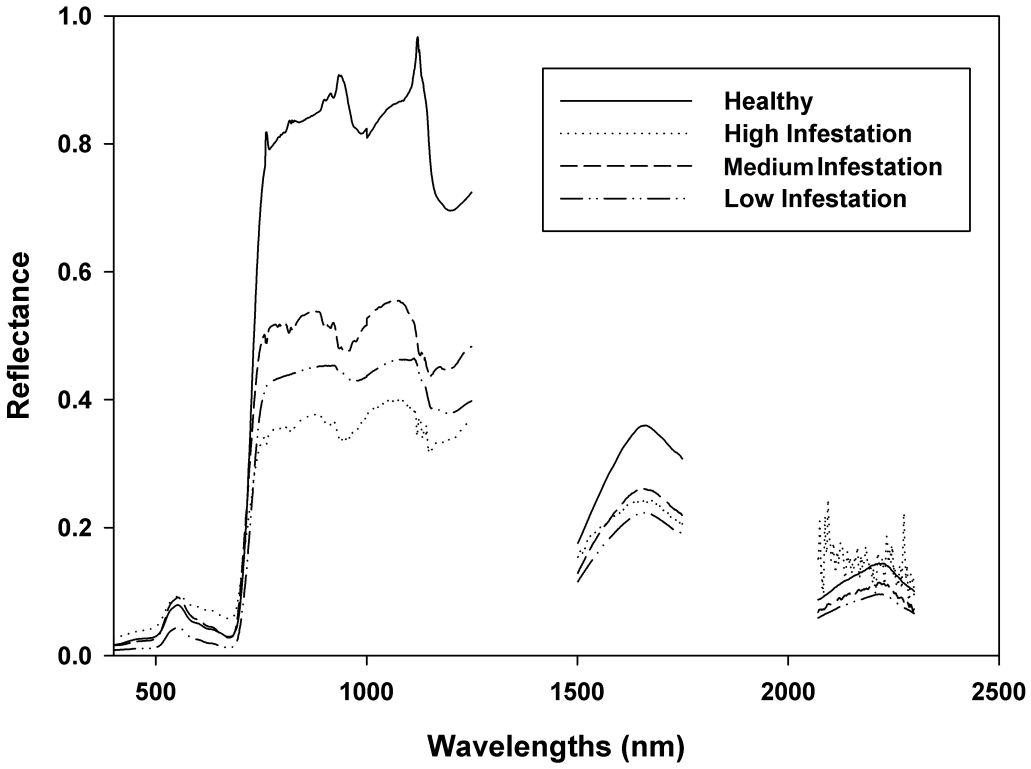

Figure 5.5: Average ASD measurements of leaves (each from 19-21 samples) from ash trees that are healthy, and which have low, medium, and highly infested states. There are clear differences between the different health states throughout the entire spectral range. However, we also note that the differences in different bands are not equal and some signals may be caused by noise.

CIs show strong agreement with the findings in Sims and Gamon (2002) and Pontius et al. (2008). Figure 5.6 illustrates the following: 1) there are two regions, 500-600 nm and 700-750 nm, showing significant increase with the increase in chlorophyll content; 2) at wavelengths of less than 500 nm, the CI only changes for cases with low chlorophyll content, typically less than 35 μgcm^{-2}; and 3) the region from 600-700 nm has moderate effect on the CI and decreases with increasing chlorophyll content. From this, it may be expected that vegetation indices within the ranges of 500-600 nm and 700-800 nm will perform better than indices spanning other ranges, such as PRI, SR680 (Table 5.2).

5.4.2 Vegetation indices and their infestation level scores

Besides the CI preference, the final selection of vegetation indices considered the index performance in each infestation state. We used information from trees of known infestation state to compare the performances of the various vegetation indices, as presented in Figure 5.7. In this figure, all vegetation index values were normalized by their averages. Greater variation between different infestation stages was considered representative of a good indicator. As such, PRI and CSc were clearly the two highest ranking, while NPQI, SR680, and TCARI/OSAVI all showed a similar level of performance. TCARI/OSAVI incorporated prefixed coefficients, which may need to be calibrated for different data sets, which is a relatively complex process. NPQI was less preferred by the CI measurements, but the bands of this index are in a different region of the spectra. The use of NPQI would thus increase the stability of this study, and hence it was chosen, but is given half the weight of CSc and PRI in the final function.

After examining each of the final selected vegetation indices, we found they are in

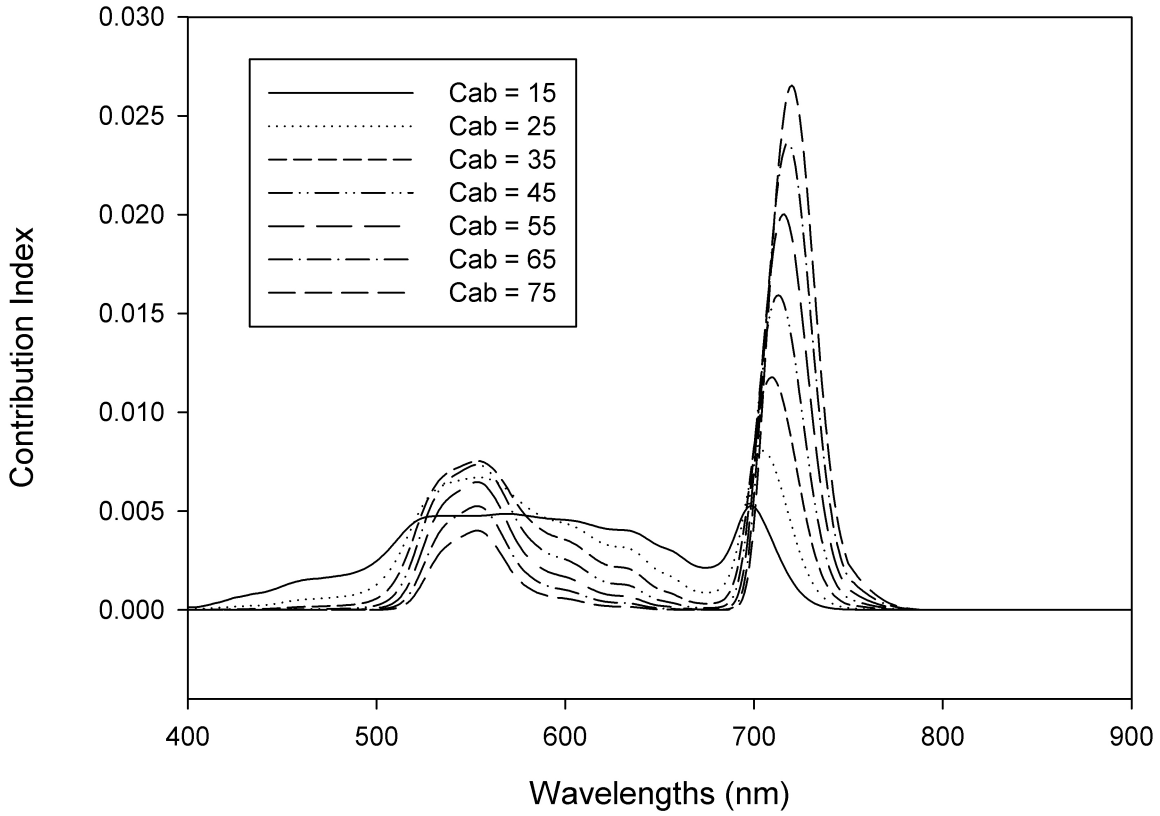

Figure 5.6: Calculated contribution index based on a PROSPECT simulation at different leaf chlorophyll contents. Leaf chlorophyll content varies from 15-75 $[gcm^{-2}]$. The other parameters used by PROSPECT were fixed, with at leaf structure parameter ($N[\,] = 1.4$), equivalent water thickness ($Cw[cm] = 0.025$), and leaf dry matter per area ($Cm[gcm^{-2}] = 0.005$).

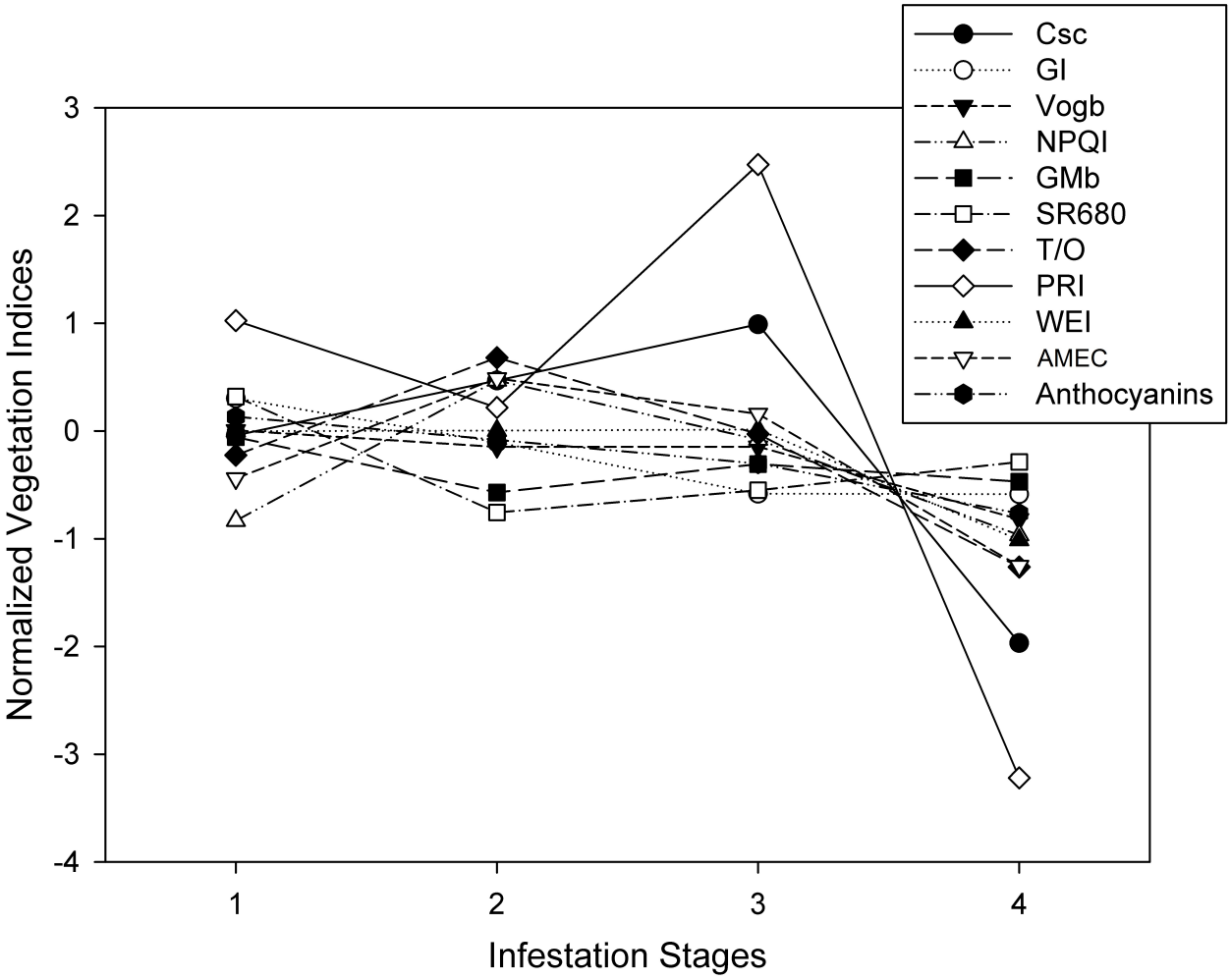

Figure 5.7: Performance of selected vegetation indices. T/O indicates the TCARI/OSAVI index and AMEC is the index proposed by AMEC. For the infestation stages, 1 is healthy, 2 represents low infestation, 3 is medium infestation, and 4 represents high infestation.

good agreement with previous reports in the literature: 1) CSc, originally from Carter and Miller (1994) was derived from eight different stress agents across six different plant species in laboratory studies. It was the best performing vegetation index in our study, which agreed with the results of (Pontius et al., 2008). 2) PRI, which was originally derived by Gamon et al. (1992) to estimate rapid changes in the relative levels of xanthophyll cycle pigments, thus serving as an estimation of photosynthetic light use efficiency (Sims and Gamon, 2002) which also performed well in this study, as expected. 3) The stress index NPQI (Barnes et al., 1992) which showed a positive correlation between EAB infestation and tree stress in le Maire et al. (2004), but was reported as less effective in Pontius et al. (2008) presented moderate performance in our analyses. However, it had relatively fewer data uncertainties than other indices, excepting CSc and PRI. We used it in the final estimation, but half weighted compared to other indices.

All results from the vegetation indices were converted into normalized scores ranging from 0-5. Their functions were derived from correlations with the data of known state trees using 3rd order polynomial or step linear functions. The CSc, PRI and NQPI conversion functions can be respectively given as:

$$P = -0.058CSc^3 + 3.503CSc^2 - 5.923CSc + 2.964 \tag{5.3}$$

$$P = -1.835PRI^3 + 12.543PRI^2 - 25.590PRI + 5.906 \tag{5.4}$$

$$P = \begin{cases} -6.739NPQI - 4.448 & (NPQI >= 0.5) \\ -4.099NPQI - 1.578 & (NPQI <= 0.5) \end{cases} \tag{5.5}$$

Vegetation indices have provided a convenient and robust methodology for EAB detection. However, calibrations are still required for each data set. Some indices,

such as NQPI, suffer from relatively low separation performance, and thus should be utilized with reduced weighting. We also compared pixel-based spectra against the tree crown average and found the shadow effect to cause major spectral variations in NIR band-related indices. This also corroborates the fact that the spectral based approach alone cannot sufficiently confirm the degree of EAB infestation.

5.4.3 Retrieved leaf chlorophyll content and its infestation state score

The absolute leaf chlorophyll content values were obtained by PROSAIL model inversion with a CI implemented LUT approach. Simply put, the hyperspectral spectra derived from the hyperspectral imagery was compared to the PROSAIL simulated spectra with CI as a weighting in the LUT inversion approach. In this study, we found that the leaf structure parameter N, ranging 1.7-2, and LAI, returning values of 3 and above, were slightly higher than reported elsewhere in the literature (e.g., Haboudane et al. (2004); Jacquemoud et al. (2009); Zarco-Tejada et al. (2001)). However, they are still considered to be within a reasonable range, as most of the ash trees in our study sites were mature. We found that leaf chlorophyll content retrieved from physical models has a much higher variation than the vegetation indices. However, relative decreases in leaf chlorophyll content compared with neighboring healthy trees were found in both approaches. As a result, we did not use a regression function as in the case of the vegetation indices, and instead employed a more general classification. We used two threshold values to separate the results into three classes. The threshold values used in this study were 65 and 37 [μgcm^{-2}], meaning that if the leaf chlorophyll content is greater than 65 [μgcm^{-2}], then a score of 0 is assigned, if the value is between 37 and 64 [μgcm^{-2}], it receives a score of 1, and if it is less than 36 [μgcm^{-2}],

then the score is 2.

Physical model inversion is a very time consuming process, and is prone to observation noise, thus it has not been adopted in other ash EAB infestation studies. In this study, however, since it is an object-oriented approach, average tree spectra were used instead of individual pixels, significantly reducing computation time and increasing the signal-to-noise ratio. More importantly, the model inversion approach evaluates the overall spectra, taking into consideration the quality of observations, including uncertainties, and providing the absolute values of target parameters. Although the parameter we calculated in this way is leaf chlorophyll content, it still can be considered a different approach and a fresh perspective compared to vegetation indices method, which focuses on only a few bands. We implemented CI as a weighting in the merit function to improve the retrieval accuracy. Hence, retrieving leaf chlorophyll content through physical model inversion can provide important information to be used in the final evaluation. Ideally, we seek consistent results with regard to leaf chlorophyll changes from both methods. We did confirm that the infested trees have lower leaf chlorophyll content than nearby healthy ones; however, the model inversion approach suffers from high saturation rates, which means it is fairly easy for results to converge on to the minimum or maximum values of the pre-set range.

5.4.4 Spatial patterns and their infestation state scores

We used a normalized differential value of 0.2 as the threshold value to determine major declines in the tree crown. We found that the normalized differential longitudinal profiles show better performance with regard to resistance to uncertainties, and partially to background and shadow effects. This method simply involves counting

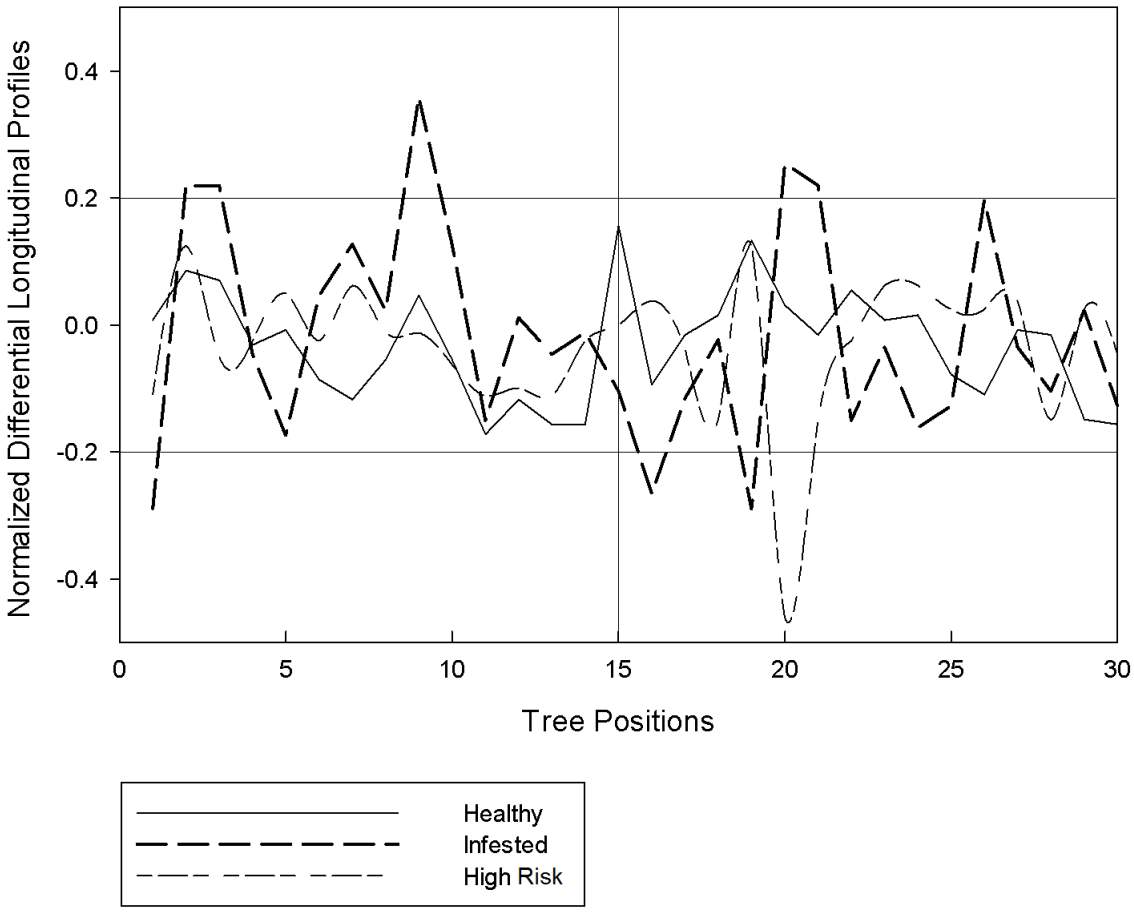

Figure 5.8: Normalized differential longitudinal profiles for different representative trees. Any declines that cross the two threshold lines are considered significant. The number of significant drops is used to form the infestation estimation.

the number of significant drops across the tree top crown profile. In Figure 5.8, all trees are resampled to 30 pixels in length to illustrate them together as a normalized size. This conversion ensures low levels of infestation can be detected, while highly infested interpretations should require further supportive evidence. We confirmed that the spatial patterning within the tree crown is a strong indicator of infestation, as previously reported (Rose, 2010; Smitley et al., 2008).

Figure 5.8 illustrates some typical examples for trees of different infestation stages. The healthy, or likely healthy, trees have a much smoother crown curve due to the healthy growing conditions, whereas the infested tree shows a clear alternating gap

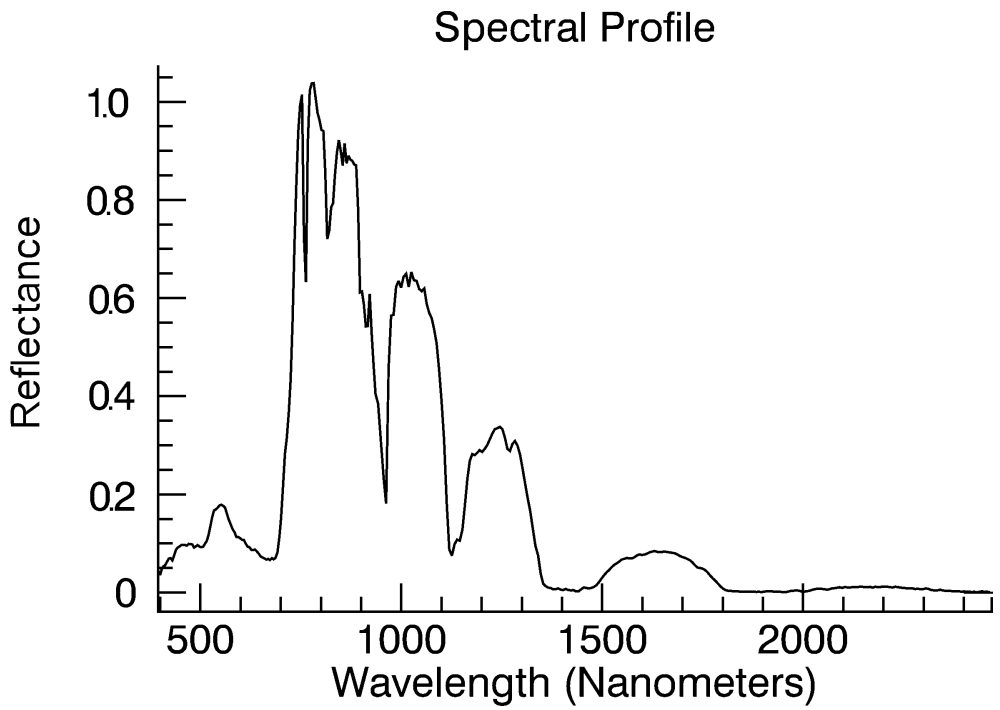

Figure 5.9: A typical hyperspectral profile from the sunlit portion of the tree crown.

pattern. This pattern is due to the leaf decline within the crown, which has been reported in Pontius et al. (2008). Spatial pattern can normally only be detected when the infestation is in the dieback stage, however. It is necessary to determine the optimal spectral band or vegetation index for this pattern to be obtained from, as it is also prone to variations in solar illumination conditions.

5.4.5 Complete sample calculation using the operational workflow

Let us perform a simple but complete calculation to illustrate the operational workflow introduced in this study, step by step. After segmenting each individual tree, regardless of whether this is done automatically or manually, then a spectral profile, like that shown in Figure 5.9, can be obtained. These spectra can be significantly altered if unnecessary pixels are included, and care must be taken to include all pixels in the sunlit portion of the tree crown, even the dark pixels.

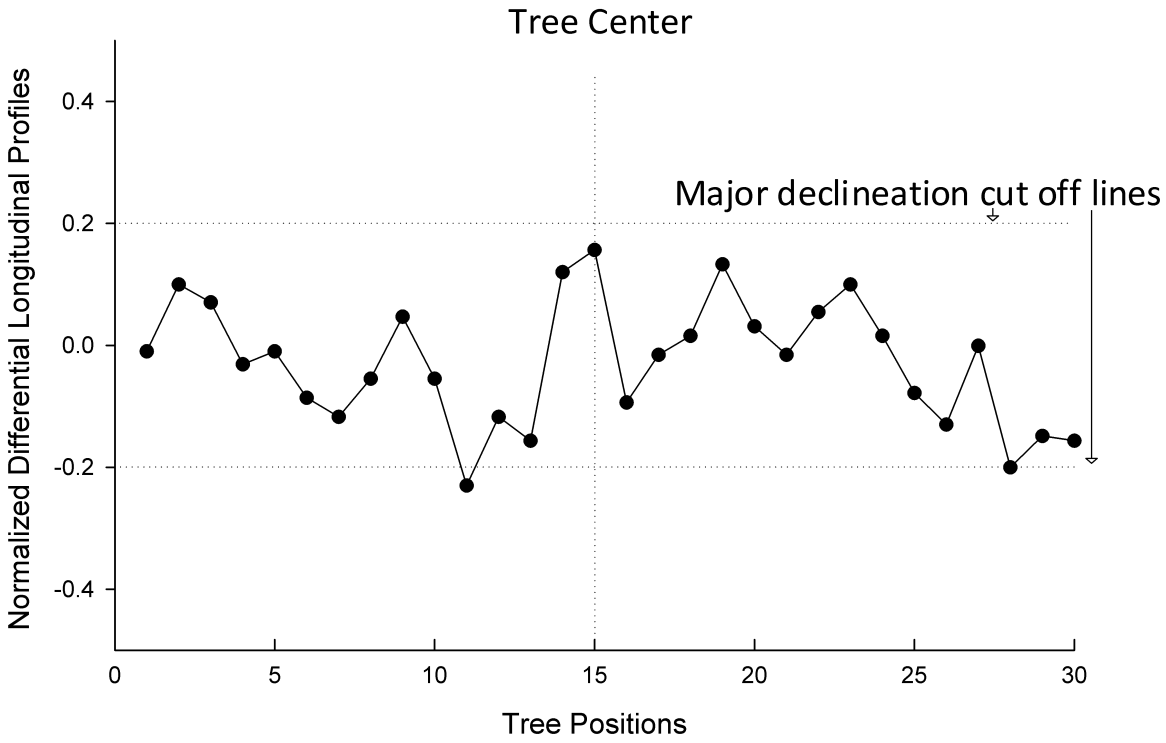

Figure 5.10: Normalized differential longitudinal profile for the same tree crown as in Fig 5.9. The threshold value in this study is 0.2, which means any declines that have an absolute value greater than 0.2, either positive or negative is considered major and significant.

By calculating the selected VI from the spectrum in Figure 5.9 and applying the expression functions listed in Equation 5.3, we find that Csc = 0.129, giving a score of 2.25, PRI =-0.241, which gives a core of 0.48; and NPQI is -0.201, with a score of 2.398. If this spectrum is input into the PROSAIL model, with three variables and the remaining parameters set to the values mentioned in the method section, then the inversion result, giving leaf chlorophyll content, is 65. Therefore, according to our threshold values, the score from model inversion is 0.

From Figure 5.10, it can be seen that there is only one major decline that crosses our threshold value. Therefore, the assigned score from the spatial pattern longitudinal

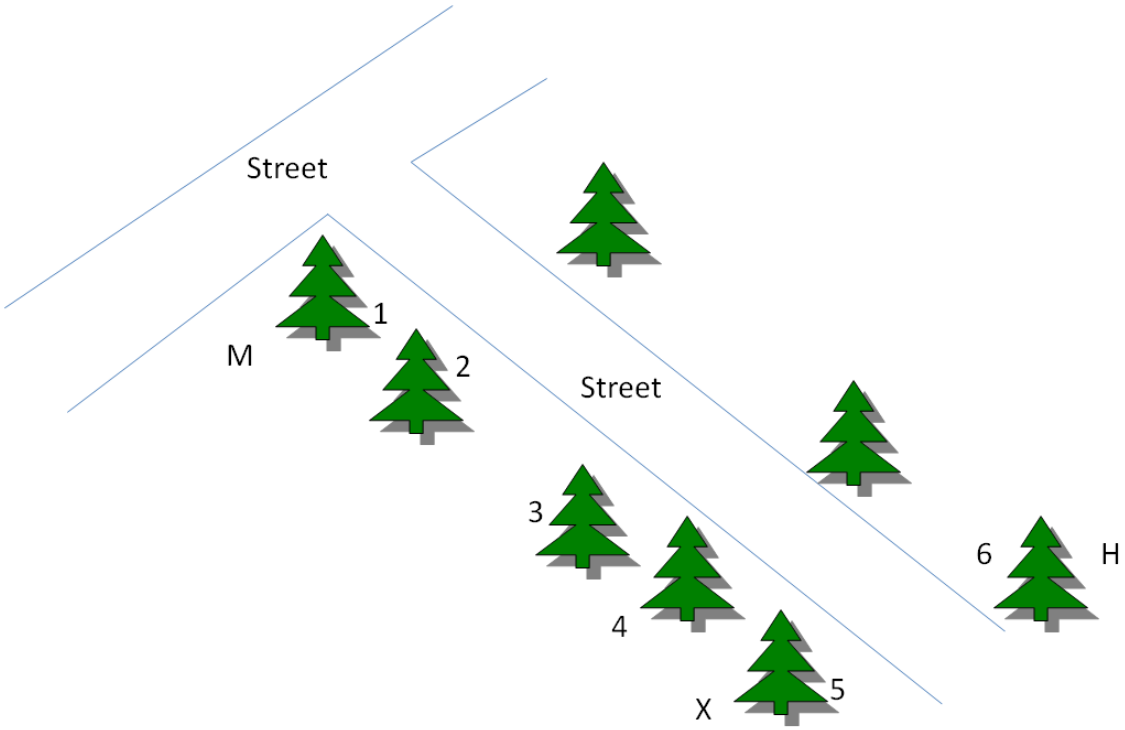

Figure 5.11: A sample street scenario for distance constant calculation. M is a medium infested tree, H is a known healthy tree, and X is the targeted tree. The numbers indicate the order of trees involved in this calculation.

profile is 0.5.

With regard to the distance from trees of known infestation state, this tree has a known medium infested tree nearby along the same street, and is spaced four trees away from it, while the nearest known healthy tree is across the street. These relationships are illustrated in Figure 5.11, in which M, H and X indicate the trees known to be medium infested, healthy, and the target tree, respectively. The target tree X is the fifth tree from the infested tree, and there is no tree between X and H, therefore, H is considered to be the sixth tree.

The final score for this individual tree marked is given as the solution from a linear

function $y = ax + b$, with the two known points (1,2.5) and (6,0) at x = 5, which equates to 0.5. Finally, the final estimation score of this individual tree, considering the score values and weightings, is given as:

$$score = \frac{1 * 2.250 + 1 * 0.480 + 0.5 * 2.398 + 1 * 0.500}{3 * 3.5} + 0.500 = 0.969 \qquad (5.6)$$

Since the score is less than 1, this tree is graded as currently healthy. Considering the typical green spectral signature attributes of a healthy living tree, the green peak, made by the green band being higher than both the blue and the red bands, and the red edge, from the NIR band being much higher than the red band, resulting a high NDVI value, are both clearly presented. In addition, the nearby neighbouring tree is currently known to be healthy. Thus, from raw observations, this tree is most likely currently healthy, which supports our calculation result. However, since there is an infested tree within the spread radius, this tree is potentially in high risk of future infestation. This is not in conflict with our score findings, since all of southern Ontario has been marked as a high risk zone. The score simply reflects the health state of the tree at the time of data acquisition.

5.4.6 Map of estimated ash tree health

Using this workflow to calculate infestation scores for all trees within our study area, the final results are collected and illustrated with ENVI (Exelis, Visual information solution, Boulder, CO, USA). The map of final results is shown in Figure 5.12, where different colors indicate different estimated levels of infestation. A comparison of 40 infested trees and 40 healthy trees for assessment of estimation accuracy is shown in Table 5.3. Columns show the predicted result (Pd), and the rows list data from ground

Table 5.3: Accuracy assessment of for estimated and ground observed tree health states for 80 sample trees

Predicted/Ground	***High***	***Medium***	***Low***	***Healthy***
High	10	0	0	0
Medium	2	8	1	5
Low	3	2	7	4
Healthy	1	1	5	31

truthing (GT). The overall accuracy, including healthy trees, is 70%, and 62.5% when healthy trees are excluded. The healthy tree omission error is 22.5%, and commission error is 18.5%.

5.5 Conclusions and future work

This study proposed an object-oriented approach to detecting early infestation of EAB from multi–sourced data, such as hyperspectral and high spatial resolution imagery. We derived different types of information from these data, which can be used together to detect EAB infestation. All information derived in this way is utilized in a weighted prediction function, in which all data are normalized into scores of 0-5.

The hypothesis of correlation between general stress and EAB infestation is confirmed. EAB infested trees show variation in leaf chlorophyll content, predominantly a reduction to, for example, less than 37 μgcm^{-2}, as a symptom of stress. From an observational point of view, stressed ash trees are more likely to be infested by EAB,

Figure 5.12: Color-coded result map, where Red indicates a score of 4 or higher, and highly infested trees; Yellow has a score of 2.5 to 4 and represents a medium infested tree; Blue, with a score of 1 to 2.5, shows low or early infested trees; and Green indicates a score of less than 1 and a current healthy tree.

and therefore stress-associated variations in leaf chlorophyll content, normally to values lower than found in nearby trees of the same species, are considered the primary indicator in detecting early infestations in ash trees. However, despite drops in leaf chlorophyll content having over 85% correlation with EAB infestation, the technique suffers from high omission errors. Thus, while the infested trees most likely have reduced leaf chlorophyll content, low leaf chlorophyll content does not always confirm an infestation.

We found that vegetation indices, leaf chlorophyll content, longitudinal profiles and paper documentation all have the potential to detect EAB infestation. While vegetation indices are the most convenient and robust, leaf chlorophyll content and longitudinal profiles may provide more precise results, but at the cost of computation time and the risk of considerable variation. Paper documents are considered as prior knowledge in this study, and represent the most reliable information. The synergy of web GIS and remote sensing techniques would be an interesting direction for future investigation.

Despite the weaknesses and limitations of Google Earth imagery, it is easy to access, free of charge, offering multiple years of availability, and in some cases provides better spatial resolution. These benefits make it a viable option for resource management and planning by governments and other agencies. Most importantly, GE imagery and the relative profile approach can easily be adopted and effectively employed by non-specialists.

In this study, all segmentations underwent manual corrections, which ensured that the initial tree boundary and location information were accurate. The manual correc-

tions included but not limited to merge and split tree objects, smooth and connect boundary lines and remove small objects. The manual segmentation and validation is very labour intensive and time consuming, and for this scheme to be applied over a larger area, automatic segmentation would be essential, which implicitly suggests that errors from segmentation could propagate and directly affect the accuracy of the final evaluation.

The PROSAIL model was chosen due to its simplicity, reliability, robustness, and effectiveness. In this study, PROSAIL served as a demonstration, which had been validated and reported with successful collaboration with CI-based optimization in (Zhang et al., 2011). This does not exclude other models from being adopted in this approach, and a comparison of the effectiveness and accuracy of different models would be an interesting future investigation.

The final accuracy validation is also limited by the data sources available, particularly in the number of confirmed infested trees. This and future studies could therefore be improved with further investigations and explorations.

This study presents a demonstration of a proof of concept and a prototype workflow. The vegetation indices chosen and the models used in parameter retrieval processing are not fixed, and may require future investigation for possible improvements. Other spatial information, such as texture, may also be considered for potential integration and expansion of the calculation.

6 Conclusions and recommendation for future work

This chapter summarises the achievements of the research described in Chapters 3, 4 and 5. My goal was to improve vegetation characterization from remote sensing data. More specifically, these studies focused on the retrieval or estimation of: 1) the biophysical parameters of vegetation canopies (Chapter 3), b) the species of individual trees (Chapter 4), and c) tree health state (Chapter 5). The results of these studies were published in three peer-reviewed journals. This chapter concludes by exploring new areas with potential for further development and breakthroughs.

6.1 Achievements of this research

First, in this study, a contribution index (CI) was derived to quantify the effect of a given observation on the retrieval of the model parameters of interest that accounted for both, the uncertainty of this observation and its sensitivity to the model parameters. Biophysical parameters, such as LAI and leaf chlorophyll content, appear to play crucial role in precision agriculture management, forest ecology monitoring, and global climate change studies. The CI shifts the focus of the retrieval of parameters onto most important and sensitive observations, e.g., bands in hyperspectral data, instead of taking all available ones equally.

One of the commonly used methods of biophysical parameter retrieval is based on the inversion of a physical canopy model. However, it is often an "ill-posed" problem, mainly due to the model complexity and observation uncertainties. In this study, the CI was used in the merit function to weight appropriately each observation to improve the stability of the inversion of the physical model. The CI, I adopted and introduced into remote sensing is a simple, effective and "universal" index that guarantees improvement to any parameter retrieval approaches at a very low computation cost. To evaluate the CI based merit function, the LUT model inversion was conducted using the coupled PROSPECT and SAIL model to retrieve LAI and leaf chlorophyll content. The results using both, simulated and real hyperspectral data showed that employing CI in the formulation of the merit function significantly improved the retrieval accuracy by reducing the prediction errors by at least 10% compared with the traditional and current state-of-the art LUT method. In another words, the more complex correlations between bands, and the more uncertainties in the observations, the more CI contributes to the final retrieval accuracy improvement.

Second, this study presents an new and innovative approach to improve the classification of individual tree species via longitudinal profiles from very high spatial resolution airborne imagery. Individual tree species identification is important for urban forest inventory and ecology management. Recent advances in remote sensing technologies facilitate more detailed estimation of individual urban tree characteristics. The longitudinal profiles represent the side view tree shape, which play a very important role in individual tree species on-site identification. Decision tree classification was employed to conduct the final classification result. Using this profile approach, six major species (Maple, Ash, Birch, Oak, Spruce, Pine) of trees on the York U-

niversity (Ontario, Canada) campus were successfully identified. Two decision trees were constructed, one knowledge-based and one derived from gain ratio criteria. The classification accuracy achieved was 84% and 86%, respectively. Compared to up to 65% classification accuracy reported in most recent literature, this is a very significant improvement. More importantly, this research extended the features used in multispectral image classification from traditional spectral based to spatial based ones. For the first time, the longitudinal profiles were successfully parameterized and adopted in multispectral image classification to achieve higher accuracy.

Third, in Chapter 5, I presented a new methodology using multi-sourced and heterogeneous data to predict potential infestations of EAB in the town of Oakville, ON, Canada. The Emerald Ash Borer (EAB) poses a significant economic and environmental threat to ash trees in Southern Ontario, Canada and the northern states of the USA. It is critical that effective technologies urgently be developed to detect, monitor and control the spread of EAB. The information effectively assimilated in this research included remotely sensed data, such as high spatial resolution aerial imagery, commercial ground and airborne hyperspectral data, and Google Earth imagery, in addition to non-remotely sensed data, such as archived paper maps and documents. A prediction function was developed to estimate the EAB infestation states of individual ash trees, using three major attributes: leaf chlorophyll content, tree crown spatial pattern, and prior knowledge. Comparison between these predicted values and a ground-based survey demonstrated an overall accuracy of 62.5%, with 22.5% omission and 18.5% commission errors. This is the first time that such a successful early detection of EAB has been reported. More importantly, it is a great general solution, which has great potential for other similar applications, as stated by the reviewer of my manuscript:

"it is a complete [step by step with numerical calculation samples] and comprehensive [used different types of data] remote sensing tree health state estimation workflow that have been clearly reported." and "I can see readers adopting individual parts of your workflow for similar applications."

6.2 What does the future hold?

Remote sensing has, and will continue to, serve as an important measurement and information acquisition method for a variety of applications, particularly in agriculture and forestry studies. The future work recommended in the sequel will ensure the accuracy of the object detection and segmentation.

In my studies, the manual corrections on the automatic segmentation results were still required (e.g., touch up tree boundaries, splitting close trees). This step had guaranteed the accuracy, but at the cost of labour and time. Obviously, the segmentation accuracy has a significant impact on the final classification or information retrieval accuracy. Without accurate segmentation inputs, it is impossible to obtain accurate classification results. The advantages of object oriented classification are quite significant compared to pixel based approaches; therefore, automatic segmentation research should be the next pressing matter. In fact, automatic segmentation is a current active research area showing promising future, e.g., Jing et al. (2012, 2011).

Spatial measurements and information are currently underused in tree species classification. The spatial pattern feature I explored, developed and demonstrated in this study, namely the longitudinal profiles, is just one of the spatial features that can be developed based on new data sets. Future work should investigate on other species related parameters, such as tree side shape, tree crown layer pattern, and tree diameter

at breast height (DBH). These parameters can directly be used for agricultural and forestry studies and can also be further developed for biomass and tree age estimation. All this information can be intelligently adapted into new classification schemes to obtain better species classification or individual tree characteristics.

The longitudinal profile of the tree crown simplifies the development of the tree crown into a 2D vector function, which can effectively present the significant top crown variations of different species. However, the parameterized variables are still too specific, and prone to in-class variations, which limit the number of applications. The next step is to develop algorithms that can adopt fuzzy similarity comparison, which means that the model parameters can allow high in-class variation and still be "similar". Also, in the longitudinal profile study, the analysis and results were validated only under a very high spatial resolution case. It is a noteworthy approach to investigate the minimum spatial resolution requirement for applying the longitudinal profile method. In other words, the next question to be answered is: "what would be the minimum spatial scale required by the longitudinal profile method to yield key information?"

Finally, current studies normally focus on a limited number of data sets that capture only the characteristics of the Earth's surface at the time of acquisition. It is critical to automatically detect anomalies in temporarily extensive data (Gray and Song, 2013). Since remote sensing data have been accumulated over decades, there needs to be studies dedicated to examining them under the same time series, e.g., for 40 years of Landsat data, a time series based study would be possible and valuable. However, data collection periods, sensors and analyses method have undergone significant improvements, such as bandwidths, signal processing methods, and different

data acquisition illumination and atmospheric conditions. I want to employ as much data as possible for maximum information. However, data fusion or intelligent information synergy will become another crucial matter in the future. Some issues can be resolved by developing new and improved instrumentation (Hakala et al., 2012; Morsdorf et al., 2009). More importantly, it should be resolved by improving data analysing, processing methodology as I demonstrated in this research.

A The flowchart of contribution index implementation in model inversion approach

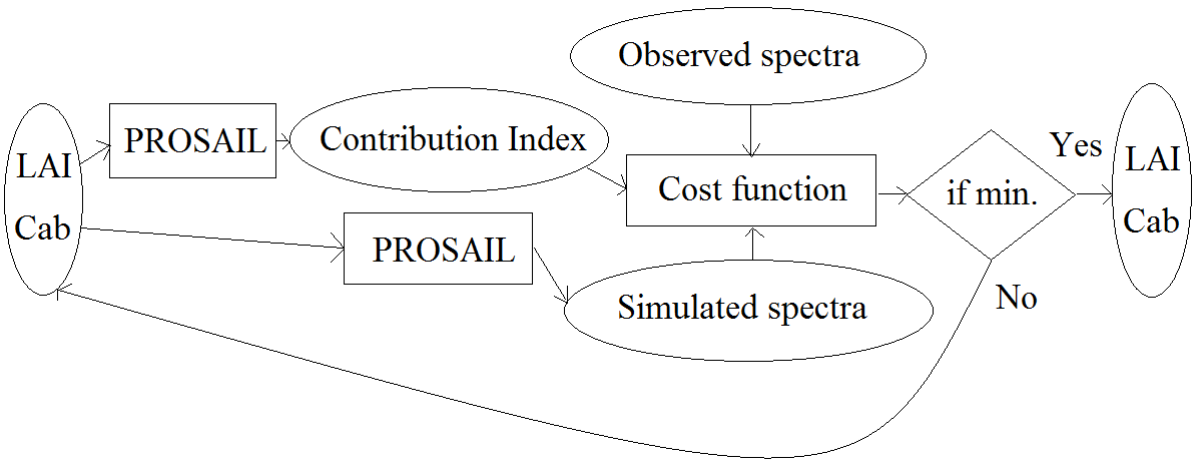

Figure A.1: The flowchart of contribution index implementation in model inversion approach. Only two parameters, LAI and Cab are considered variables in this study. All other PROSAIL parameters are fixed. Contribution index is derived solely based on model and is used as weighting to the cost function. Look-Up-Table method is used, which means an comprehensive search is conducted and the parameters combo that delivers the minimum cost is concluded as the retrieved result.

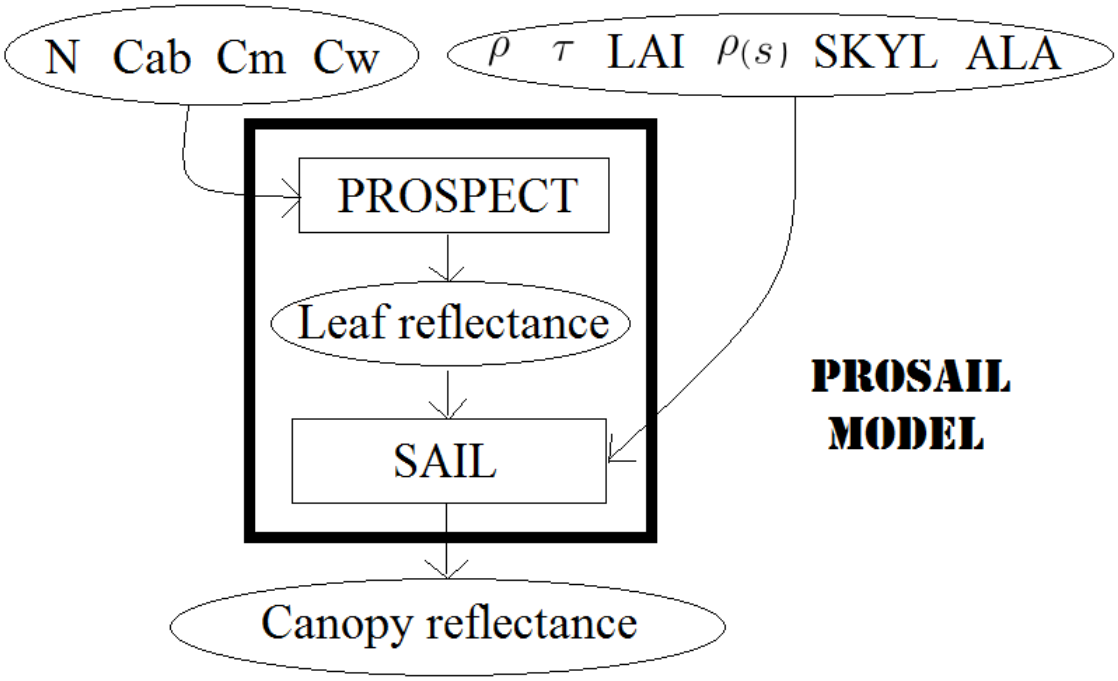

Figure A.2: PROSAIL model black box. Both PROSPECT and SAIL are provided by their original authors. PROSPECT is written in Matlab, while SAIL is in FORTRAN. The overall solution is in C++.

Bibliography

Ahamed, T., Tian, L., Zhang, Y., and Ting, K. C. (2011). A review of remote sensing methods for biomass feedstock production. *Biomass and Bioenergy*, 35(7):2455–2469.

Allen, W. A. and Richardson, A. H. (1968). Interaction of light with a plant canopy. *Journal of the Optical Society of America*, 58(8):1023–1028.

Antyufeev, V. S. and Marshak, A. L. (1990a). Inversion of monte carlo model for estimating vegetation canopy parameters. *Remote Sensing of Environment*, 33(3):201–209.

Antyufeev, V. S. and Marshak, A. L. (1990b). Monte carlo method and transport equation in plant canopies. *Remote Sensing of Environment*, 31:183–191.

Anulewicz, A. C., McCullough, D. G., and Cappaert, D. L. (2007). Emerald ash borer (agrilus planipennis) density and canopy dieback in three north american ash species. *Arboriculture and Urban forestry*, 33(5):338 – 349.

Aplin, P., Atkinson, P. M., and Curran, P. J. (1999). Fine spatial resolution satellite sensor imagery for land cover mapping in the united kingdom. *Remote Sensing of Environment*, 68:206–216.

Asrar, G. (1989). *Theory and application of optical remote sensing*. Wiley Interscience, Toronto, Canada.

Atzberger, C. (2013). Advances in remote sensing of agruculture: Context description, existing operational monitiring systems and major information needs. *Remote Sensing*, 5:949–981.

Barbezat, V. and Jacot, J. (1998). The clapa project: Automated classification of forest with aerial photographs. *Proceedings of the International Forum Automated Interpretation of High Spatial Resolution Digital Imagery for Forestry*.

Baret, F. and Guyot, G. (1991). Potentials and limits of vegetation indices for lai and apar assessment. *Remote Sensing of Environment*, 35:161 – 173.

Barnes, J. D., Balaguer, L., Manrique, E., Elvira, S., and Davsion, A. W. (1992). A reappraisal of the use of dmso for extraction and determination of chlorophylls a and b in lichens and higher plants. *Environmental and Experimental Botany*, 32(2):85 – 100.

Barnsley, M. J., Settle, J. J., Cutter, M. A., Lobb, D. R., and Teston, F. (2004). The proba/chris mission: A low cost smallsat for hyperspectral multiangle observations of the earth surface and atmosphere. *IEEE Transaction on Geoscience and Remote Sensing*, 42:1512–1502.

BenDor, T., Metcalf, S. S., Fontenot, L., Sangunett, L. E., and B., H. (2006). Modeling the spread of the emerald ash borer. *Ecological Model ling, Lethbridge, AB*, 2(6):222–236.

Bowyer, P. and Danson, F. M. (2004). Sensitivity of spectral reflectance to variation in live fuel moisture content at leaf and canopy level. *Remote Sensing of Environment*, 92:297–308.

Brandtberg, T. (2002). Individual tree-based species classification in high spatial resolution aerial images of forests using fuzzy sets. *Fuzzy Sets and Systems*, 132(3):371–387.

Brandtberg, T. and Walter, F. (1998). Automated delineation of individual tee crowns in high spatial resolution aerial images by multiple-scale analysis. *Machine Vision Application*, 11:64 –73.

Breda, N. J. (2003). Ground based measurements of leaf area index: a review of methods, instruments and current controversies. *Journal of Experimental Botany*, 54(392):2403–2417.

Broge, N. H. and Leblanc, E. (2000). Comparing preduction power and stability of broadband and hyperspectral vegetation indices for estimation of greeen leaf area index and canopy chlorophyll density. *Remote Sensing of Environment*, 76:156–172.

Brown, L., Chen, J., Leblanc, S., and Cihlar, J. (2000). A shortwave infrared modification to the simple ratio for lai retrieval in boreal forests: An image and model analysis. *Remote Sensing of Environment*, 71:16–25.

Bruegge, C., Chrien, N., and Haner, D. (2001). A spectralon brf data base for misr calibration application. *Remote Sensing of Environment*, 77(3):354–366.

Bruegge, C., Helmlinger, M., Conel, J., Gaitley, B., and Abdou, W. (2000). Parabola iii: A sphere scanning radiometer for field determination of surface anisotropic reflectance functions. *Journal of geophysical research.*

Carter, G. A. (1994). Ratio of leaf reflectance in narrow wavebands as indicators of plants stress. *Journal of International Remote Sensing*, 15:697–703.

Carter, G. A. and Miller, R. L. (1994). Early detection of plant stress by digital imaging within narrow stress-sensitive wavebands. *Remote Sensing of Environment*, 50:295–302.

Chatterjee, S. and Hadi, A. S. (1988). *Sensitivity analysis in linear regression.* John Wiley and Sons, New York, USA.

Chen, J. M. and Cihlar, J. (1997). A hotspot function in a simple bidirectional reflectance model for satellite applications. *Jounral of Geophysical Research*, 102(D22):25907–25913.

Chen, J. M. and Leblanc, S. (1997). A 4-scale bidirectional reflection model based on canopy architecture. *IEEE Transactions on Geoscience and Remote Sensing*, 35:1316–1337.

Chen, J. M. and Leblanc, S. G. (2001). Multiple-scattering scheme useful for geometric optical modelling. *IEEE Transactions on Geoscience and Remote Sensing*, 39:1061–1071.

Chen, J. M., Liu, J., Leblanc, S. G., Lacaze, R., and Roujean, J. (2003). Multi-angular optical remote sensing for assessing vegetation structure and carbon absorption. *Remote Sensing of Environment*, 84:516–525.

Chen, J. M., Menges, C. H., and Leblanc, S. G. (2005). Global mapping of foliage clumping index using multi-angular satellite data. *Remote Sensing of Environment*, 97:447–457.

Chen, J. M., Rich, P. M., Gower, T. S., Norman, J. M., and Plummer, S. (1997). Leaf area index of boreal forests: theory, techniques and measurements. *Journal of Geophysical Research*, 102(29):429–444.

Chen, X., Ma, W., and Paul, J. (2010). Cubic b-spline curve approximation by curve unclamping. *Comput.-Aided Des.*, 2:523–524.

Cho, M. A. and Skidmore, A. K. (2006). A new technique for extracting the red edge position from hyperspectral data: The linear extrapolation method. *Remote Sensing of Environment*, 101:181–193.

Chuang, S. and Kao, C. (1999). One-sided arc approximation of b-spline curves for interference-free offsetting. *Comput.-Aided Des.*, 31:111–118.

Clevers, J. G. P. W., De Jong, S. M., Epema, G. F., Van der Meer, F., Bakker, W. H., and Skidmore, A. K. (2002). Derivation of the red edge index using meris standard band setting. *International Journal of Remote Sensing*, 23:3169–3189.

Coburn, C. A. and Roberts, A. C. B. (2004). A multiscale texture analysis procedure for improved forest stand classification. *International Journal of Remote Sensing*, 130:40–50.

Coggins, S. B., Coops, N. C., Hilker, T., and Wulder, M. A. (2013). Augmenting forest inventory attributes with geometric optical modelling in support of regional susceptibility assessment to bark beetle infestations. *International Journal of Applied Earth Observation and Geoinformation*, 21:444–452.

Cosmopoulos, P. and King, D. J. (2004). Temporal analytsis of forest structural condition at an acid mine site using multispectral digital camera imagery. *International Journal of Remote Sensing*, 25(12):2259–2275.

Cracknell, A. P. and Hayes, L. (2007). *Introduction to Remote Sensing*. CRC Press, Taylor and Francis Group, Boca Raton, USA.

Cutter, M. A. (2000). Compact high resolution imaging spectrometer (chris). *RTO SET Symposium on Space based Observation Technology, Island o Samos, Greece*, MP-61.

Darvishzadeh, R. (2008). *Hyperspectral remote sensing of vegetation parameteres using statistical and physical models*. Ph.D. Thesis, Wageningen University, Netherlands.

Datcu, M. P. and Schwarz, G. (1998). Remote sensing of land, water and atmosphere: the role of forward modelling data analysis tool. *Proceeding of SPIE3500, Image and Signal Processing for Remote Sensing IV*, 180.

Dawson, B. and Parsons, A. (1994). Texture measures for the identification and monitoring of urban derelict land. *International Journal of Remote Sensing*, 5:1259–1271.

Dawson, T., Curran, P., and Plummer, S. (1998). Liberty: Modeling the effects of leaf biochemistry on reflectance spectra. *Remote Sensing of Environment*, 65(1):50–60.

Dawson, T. P. and Curran, P. J. (1998). A new technique for interpolating red edge position. *International Journal of Remote Sensing*, 19:2133–2139.

Erikson, M. (2004). Species classification of individually segmented tree crowns in high resolution aerial images using radiometric and morphologic image measures. *Remote Sensing of Environment*, 91:469–477.

Farrar, J. L. (1995). *Trees in Canada*. Fitzhenry and Whiteside Limited and the Canadian Forest Service Natural Resource Canada, Markham, Ontario, Canada.

Fourier, R., Edwards, G., and Eldridge, N. (1995). A catalogue of potential spatial discriminators for high spatial resolution digital images of individual crowns. *Canadian Journal of Remote Sensing*, 3:285–298.

Franklin, S., Wulder, M., and Gerylo, G. (2001). Texture analysis of ikonos panchromatic data for douglas-fir forest age class separability in british columbia. *International Jounral of Remote Sensing*, 22:2627–2632.

Gamon, J. A. and Bond, B. (2013). Effect of irradiance and photosynthetic downregulation on the photochemical reflectance index in douglas-fir and ponderosa pine. *Remote Sensing of Environment*, 135:141–149.

Gamon, J. A., Penuelas, J., and Field, C. B. (1992). A narrow-waveband spectral index that tracks diurnal changes in photosynthetic efficiency. *Remote Sensing of Environment*, 41:35–44.

Gastellu-Etchegorry, J. P., Zagolski, F., and Romier, J. (1996). A simple anisotropic reflectance model for homogeneous multilayer canopies. *Remote Sensing of Environment*, 57:22–38.

Gates, D. M., Keegan, J. J., Schleter, J. C., and Weidner, V. R. (1965). Spectral properties of plants. *Applied Optics*, 4(1):11–20.

Gebreslasie, M. T., Ahmed, F. B., and van Aardt, J. A. N. (2011). Extracting structural attributes from ikonos imagery for eucalyptus plantation forests in kwazulu-natal, south africa, using image texture analysis and artificial neural networks. *International Journal of Remote Sensing*, 32(22):7677–7701.

Gitelson, A. and Merzlyak, M. (1996). Signature analysis of leaf reflectance spectra algorithm development for remote sensing of chlorophyll. *Jounral of Plant Physiol.*, 148:494 – 500.

Gitelson, A. A. and Merzlyak, M. N. (1994). Quantitative estimation of chlorophyll-a using reflectance spectra experiments with autumn chestnut and maple leaves. *Journal of Photochemical Phytobiology*, 22:247–252.

Goel, N. S. and Grier, T. (1988). Estimation of canopy parameters from inhomogeneous vegetation canopies from reflentance data,iii:trim: A model for radiative tranfer in heterogeneous three-dimensional canopies. *Remote Sensing of Environment*, 25:255–293.

Goel, N. S. and Strebel, D. E. (1983). Inversion of vegetation canopy reflectance models for estimating agronomic variable. i. problem definition and initial results using the suits' model. *Remote Sensing of Environment*, 13:487–507.

Goel, N. S. and Thompson, R. L. (1984). Inversion of vegetation canopy reflectance models for estimating agronomic variables. v. estimation of leaf area index and average leaf inclination angle using measured canopy reflectance. *Remote Sensing of Environment*, 15:69–85.

Gong, J., Sui, H., Ma, G., and Zhou, Q. (2008). A review of multi-temporal remote sensing data change detection algorithms. *The International Archieves of Phtogrammetry, Remote Sensing and Spatial Information Sciences*, XXXVII(B7).

Gong, P., Pu, R., and Miller, J. R. (1995). Coniferous forest leaf area index estimation long the oregon trnasect using compact airborne spectrographic imager data. *Photogrammetric Engineering and Remote Sensing*, 61:1107–1117.

Gougeon, F. (1995). A crown-following approach to the automatic delineation of individual tree crown closure from airborne multispectral images. *Canadian Journal of Remote Sensing*, 25:274 – 284.

Gougeon, F. and Leckie, D. (2003). *Forest Information Extraction From High Resolution Images Using an Individual Tree Crown Approach.* Natural Resources Canada Information Report BC-X-396, Victoria, BC, Canada.

Gould, J. S., Bauer, L. S., Lelito, J., and Duan, J. (2013). Emerald ash borer, *Agrilus Planipennis* (fairmarire). *Biological control release and recovery guideline, United States Department of Agriculture, May.*

Gray, J. and Song, C. (2013). Consistent classification of image time series with automatic adaptive signature generalization. *Remote Sensing of Environment*, 134:333–341.

Haboudane, D., Miller, J., Pattey, E., Zarco-Tejada, P., and Strachan, I. (2004). Hyperspectral vegetation indices and novel algorithms for predicting green lai of crop canopies: Modeling and validation in the context of precision agriculture. *Remote Sensing of Environment*, 90:337–352.

Haboudane, D., Miller, J., Tremblay, N., Zarco-Tejada, P., and Dextraze, L. (2002). Integrated narrow-band vegetation indices for prediction of crop chlorophyll content for application to precision agriculture. *Remote Sensing of Environment*, 81:416–426.

Hakala, T., Suomalainen, J., Kaasalainen, S., and Chen, Y. (2012). Full waveform hyperspecral lidar for terrestial laser scanning. *Optics Express*, 20:7119–9127.

Hanou, I. (2010). 2010 town of oakville hyperspectral eab analysis. *Town of Oakville government document*.

Haralick, R. (2011). Statistical and structural approach to texture. *Proc. IEEE*, 67:786–804.

Hayes, J., Michie, D., and Richard, J., E. (1988). *Decision Trees and Multi-Valued Attributes, Machine Intelligence*. Oxford University Press, Oxford, UK.

Henderson, B. G., Theiler, J., and Villeneuve, P. (2003). The polarized emissivity of a wind-roughened sea surface: a moute carlo model. *Remote Sensing of Environment*, 88:453–467.

Herms, D. A., McCullough, D. G., Smitley, D. R., Sadof, C., Williamson, R. C., and Nixon, P. L. (2009). *Insecticide options for protecting ash trees from emerald ash borer*. North Central IPM Center Bulletin, Canada.

Heumann, B. (2012). An object based classification of mangroves using a hybrid decision tree support vector machine approach. *Remote Sensing*, 3:2440 –2460.

Hill, D. and Leckie, D. G. E. (1998). Proc. international forum: Automated interpretation of high spatial resolution digital imagery for forestry. *Victoria, Canada, Feb. 10 - 12*.

Hoaglin, D. C. and Welsch, R. E. (1978). The hat matrix in regression and anova. *The American Statistician*, 32.

Hoberg, R., Soegaard, H., and Boegh, E. (2007). Combining vegetation index and model inversion methods for the extraction of key vegetation biophysical parameteres using terra and aqua modis reflectance data. *Remote Sensing of Environment*, 93(1):18–29.

Hu, B., Zhang, K., and Wang, J. G. (2009). The retrieval of vegetation parameters from muti-anuglar hyperspectral remote sensing data. *the proceeding of IEEE Toronto International Conference, Toronto, ON, Canada*.

Hu, B., Zhang, K. F., Miller, J., Gray, L., and Zwick, H. (2007). The fifedom (frequent image frames enhanced digital ortho-rectified mapping) camera for acquiring multi-angular reflectance from the land surface. *IEEE Transaction on Geoscience and Remote Sensing*, 45:3110–3118.

Hunt, E. (1966). *Artificial Intelligence*. Academic Press, New York, NY, USA.

Jacquemoud, S., Bacour, C., Polive, H., and Fangi, J. (2000). Comparison of four radiative transfer models to simulate plant canopies reflectance: Direct and inverse mode. *Remote Sensing of Environment*, 74:417–481.

Jacquemoud, S. and Baret, F. (1990). Prospect: A model of leaf optical properties. *Remote Sensing of Environment*, 34(2):75–91.

Jacquemoud, S., Baret, F., Andrieu, B., Danson, F. M., and Jaggard, K. (1995). Extraction of vegetation biophysical parameters by inversion of the prospect sail models on sugar beet canopy reflectance data: application to tm and aviris sensors. *Remote Sensing of Environment*, 52:163–172.

Jacquemoud, S., Verhoef, W., Baret, F., Bacour, C., Zarco-Tejada, P., Asner, G., Francois, C., and Ustin, S. (2009). Prospect + sail models: A review of use for vegetation characterization. *Remote Sensing of Environment*, 113:S55 – S66.

Jensen, J. R. (2000). *Remote Sensing of the Environment: An Earth Resource Perspective, 2nd edition*. Prentice Hall, New Jersey, USA.

Jensen, J. R. (2005). *Introductory digital image processing: An remote sensing P-prspective, 3rd edition*. Prentice Hall, New Jersey, USA.

Jensen, J. R. (2007). *Remote Sensing of the Environment: An Earth Resource Perspective, 7th edition*. Prentice Hall, New Jersey, USA.

Jing, L. and Cheng, Q. M. (2012). An image fusion method based on object-oriented classification. *International Journal of Remote Sensing*, 33(8):2434–2450.

Jing, L., Hu, B., Li, L., Noland, T., and Guo, H. (2012). Automated tree crown delineation from imagery based on morphological techniques. *35th International Symposium o Remote Sensing of Environment, Beijing, China*.

Jing, L., Hu, B., Noland, T., and Li, J. (2011). An individual tree crown delineation method based on multi-scale segmentation of imagery. *ISPRS Journal of Photogrammmtry*, 70:88 – 98.

Kaufman1978 (1978). Influence of the atmosphere on contrast for zenith observation. *Journal of Geophysics Research*, 17:65–68.

Kershaw, L. (2001). *Trees of Ontario*. Lone Pine Publishing, Edmonton, Alberta, Canada.

Kimes, D., Knyazikhin, Y., Privette, J., Abuelgasim, A., and Gao, F. (2000). Inversion methods for physically-based models. *Remote Sensing Reviews*, 18:381–439.

Kimes, D. S. (1983). Dynamic of directional reflectance factor distribution for vegetation canopies. *Applied Optics*, 22(9):1364–1372.

Klassen, E., Srivastava, A., Mio, W., and Joshi, S. (2004). Analysis of planar shapes using geodesic paths on shape spaces. *IEEE transactions on pattern analysis and machines intelligence*, 26:372–383.

Kovacs, K. F., Haight, R. G., McCullough, D. G., Mercader, R. J., Siegert, N. W., and Liebhold, A. M. (2010). Cost of potential emerald ash borer damage in u.s. communities, 2009 - 2019. *Ecological Economics*, 3(69):569–578.

Kuenzer, C., Bluemel, A., Gebhardt, S., Vo Quoc, T., and Dech, S. (2011). Remote sensing of mangrove ecosystems: A review. *Remote Sensing*, 3:878–928.

Kulikova, M. (2009). *Shape Recognition for Image Scene Analysis*. Ph.D. Thesis, Universite de Nice, Sophia-Antipolis, Nice, France.

Kuusk, A. (1985). The hotspot effect of a uniform vegetation cover. *Sovit Journal of Remote Sensing*, 3:646–658.

Lallart, P., Kahn, R., and Tanre, D. (2008). Polder2/adeosii, misr and modis/terra reflectance comparisons. *Journal of Geophysics Research*, 113(D14S02).

Larsen, M. (1997). Crown modeling to find tree top positions in aerial photographs. *Proceedings of the Third International Airborne Remote Sensing Conference and Exhibition*.

Larsen, M. (2007). Sing tree species classification with a hypothetical multi-spectral satellite. *Remote Sensing of Environment*, 110:523–532.

Larsen, M. and Rudemo, M. (1998). Optimizing templates for finding trees in aerial photographs. *Pattern Recognition Letter*, 19:1153 – 1162.

Larsen, M. and Rudemo, M. (2004). Approximate bayesian estimation of a 3d point pattern from multiple views. *Pattern Recognition Letter*, 25:1359 – 1368.

le Maire, G., Francois, C., and Dufrene, E. (2004). Towards universal broad leaf chlrophyll indices using prospect simulated database and hyperspectral reflectance measurements. *Remote Sensing of Environment*, 89:1 – 28.

Leblanc, S. and Chen, J. M. (2000). A windows graphic user interface (gui) for the five-scale model for fast brdf simulations. *Remote Sensing Reviews*, 19:293–305.

Leckie, D., Gougeon, F., Tinis, S., Nelson, T., Burnett, C., and Paradine, D. (2004). Automated tree recognition in old growth conifer stands with high resolution digital imagery. *Remote Sensing of Environment*, 26:372–383.

Leckie, D. G., Gougeon, F. A., Walsworth, N., and Paradine, D. (2003). Stand delineation and composition estimation using automated individual tree crown analysis. *Remote Sensing of Environment*, 88:355–369.

Li, X. and Strahler, A. (1986). Geometric-optical bi-directional reflectance modeling of a coniferous forest canopy. *IEEE Transaction on Geoscience and Remote Sensing*, 24:906–919.

Li, X. and Strahler, A. H. (1992). Geometric-optical bi-directional reflectance modeling of the discrete crown vegetation canopy: effect of crown shape and mutual shadowing. *IEEE Transaction on Geoscience and Remote Sensing*, 30:276–292.

Li, X., Strahler, A. H., and Woodcock, C. E. (1995). A hybrid geometric optical-radiative transfer approach for modeling albedo and directional reflentance of discontinuous canopies. *IEEE Transaction on Geoscience and Remote Sensing*, 33(2):466–480.

Li, X., Wang, J., Hu, B., and Strahler, A. (1998). On utilization of a priori knowledge in inversion remote sensing models. *Science in China*, 41:6–10.

Liang, S. (2008). *Advance in Remote Sensing, System, Modeling, Inversion and Application*. Springer, USA.

Lillesand, T. M., Kiefer, R. W., and Chipman, J. W. (2008). *Remote Sensing and iamge interpretation, 6th edition*. John Wiley and Sons, New York, USA.

Makowski, D., Hiller, J., Wallach, D., Andrieu, B., and Jeuffroy, M. H. (2006). Parameters estimation for crop propose within the ceos land product validation subgroup. *IEEE Transaction on Geosciences and Remote Sensing*, 44:1804–1817.

Maloney, K., Boughton, J., and Schneeberger, N. (2006). *Emerald Ash Borer 2006 Brief, Newtown Square, PA, USDA Forest Service, Northeastern Area*. State and Private Forestry, USA.

Matinfar, H. R., Sarmadian, F., Alavi-Panah, S. K., and Heck, R. J. (2007). Comparisons of object-oriented and pixel based classification of land use/land cover types based on landsat 7, etm+ spectral bands (case study: Arid region of iran). *American-Eurasian Jounral of Agriculture and Environment Science*, 4(2):448–456.

Matzler, C. (2008). *Physical Principles of Remote Sensing*. University of Bern, Bern, Germany.

McCullough, D. G. and Katovich, A. S. (2004). *Emerald Ash Borer. Pest Alert.* Newtown Square, PA:USDA Forest Service NA-PR-02-04, USA.

Meroni, M., Colombo, R., and Panigada, C. (2004). Inversion of a radiotive transfer model with hyperspectral observaions for lai mapping in poplar plantations. *Remote Sensing of Environment*, 92:195–206.

Merzlyak, M. N., Gitelson, A. A., Chivkunova, O. B., and Rakitin, V. Y. (1999). Non-destructive optical detection of pigment changes during leaf senescence and fruit ripening. *Physiologia Plantarum*, 106:135–141.

Mitra, P., Murthy, C. A., and Pal, S. K. (2002). Unsupervised feature selection using feature similarity. *IEEE Transactions on Pattern Analysis and Machine Intelligence*, 24:301–312.

Moorthy, I., Miller, J. R., and Noland, T. L. (2008). Estimating chlorophyll concentration in conifer needles: An assessment at the needle and canopy level. *Remote Sensing of Environment*, 12(6):50 – 60.

Morsdorf, F., C., N., T., M., and I., W. (2009). Assessing forest structural and physiological information content of multi-spectral lidar waveforms by radiative transfer modelling. *Remote Sensing of Environment*, 113:2152–2163.

Mueller, R. W., Matsoukas, C., Gratzki, A., Behr, H. D., and Hollmann, R. (2009). The cm-saf operational scheme for the satellite based retrieval of solar surface irradiance - a lut based eigenvector hybird approach. *Remote Sensing of Environment*, 42:1012–1024.

Ni, W., Li, X., Woodcock, C. E., Caetano, M. R., and Strahler, A. H. (1999). An analytial hybrid gort model for bidirectional reflectance over discontinuous plant canopies. *IEEE Transaction on Geoscience and Remote Sensing*, 37(2):987–999.

Nicodemus, F. E. (1982). Geometric-optical bidirectional reflectance modeling of a conifer forest model for heterogeneous 3-d scenes. *Applied Optics*, 21:4119 – 4129.

Nicodemus, F. E., Richmond, J. C., Hsia, J. J., Ginsberg, I. W., and Limperis, T. (1977). Geometrical considerations and nomenclature for reflectance. *NBS Monograph (US)*, 160:1–52.

North, P. R. J. (1996). Three-dimensional forest light interaction model using a monte carlo method. *IEEE Transaction on Geoscience and Remote Sensing*, 34:946–956.

Omari, K., White, H. P., Staenz, K., and King, D. J. (2013). Retrieval of forest canopy parameters by inversion of the proflair leaf canopy reflectance model using the lut approach. *IEEE Journal of Selected Topics in Applied Earth Observations and Remote Sensing*, 6(2):715–723.

O'Neill, N., Zagolski, F., Bergeron, M., Royer, A., Miller, R., and Freemantle, J. (1997). Atmospheric correction validation of casi images acquired over the boreas southern study area. *Canadian Journal of Remote Sensing*, 23:143–162.

Ozdogan, M., Yang, Y., Allez, G., and Cervantes, C. (2010). Remote sensing of irrigated agriculture: Opportunities and challeges. *Remote Sensing*, 2:2274–2304.

Pattey, E., Strachan, I., Boisvert, J., Desjardins, R., and McLaughlin, N. (2001). Effect of nitrogen application rate and weather on corn using micrometeorological and hyperspectral reflectance measurements. *Agricultural and Forest Meteorology*, 108:85–99.

Peddle, D. R., Johnson, R. L., Cihlar, J., Leblanc, S. G., Chen, J. M., and Hall, F. G. (2007). Physically-based inversion modeling for unsupervised cluster labeling, independent forest classification and lai estimation using mfm-5-scale. *Canadian Journal of Remote Sensing*, 33(3):214–225.

Pena-Barragan, J. M., Ngugi, M. K., Plant, R. E., and Six, J. (2011). Object-based crop identification using multiple vegetation indices, textural features and crop phenology. *Remote Sensing of Environment*, 115:1301–1306.

Pinty, B., Gobron, N., Widlowshi, J., Gerstl, S. A. W., Verstraete, M. M., Antunes, M., Bacour, C., Gascon, F., Gastellu, J., Goel, N., Jacquemound, S., North, P., Qin, W., and Thompson, R. (2001). Radiation transfer model intercomparison (rami) exercise. *Journal of Geophysical Research*, 106(D11):11937–11956.

Pinty, B., Widlowshi, J., Taberner, M., Gobron, N., Verstraete, M. M., Disney, M., Gascon, F., Gastellu, J. P., Jiang, L., Kuusk, A., Lewis, P., Li, X., Ni-Meister, W., Nilson, T., North, P., Qin, W., Su, L., Tang, S., Thompson, R., Verhoef, W., Wang, H., Wang, J., Yan, G., and Zeng, H. (2004). Radiation transfer model intercomparison (rami) exercise: Results from the second phase. *Journal of Geophysical Research*, 109(D06210):19PP.

Pontius, J., Martin, M., Plourde, L., and Hallett, R. (2008). Ash decline assessment in emerald ash borer-infested regions: A test of tree-level, hyperspectral technologies. *Remote Sensing of Environment*, 112:2665 – 2676.

Privette, J. L., Emery, W. J., and Schimel, D. (1996). Inversion of a vegetation reflectance model with noaa avhrr data. *Remote Sensing of Environment*, 58:187–200.

Pu, R. and Gong, P. (2000). *Hyperspectral Remote Sensing and its applications (in Chinese)*. High Education Press, Beijing, China.

Puttonen, E., Litkey, P., and Hyypp, J. (2010). Individual tree species classification by illuminated shaded area separation. *Remote Sensing*, 2:19 – 35.

Quinlan, J. (1993). *C4.5 Programs for Machine Learning*. Morgan Kaufmann Publishers, Los Altos, USA.

Rich, R., Frelich, L., Reich, P., and Bauer, M. (2010). Detecting wind disturbance severity and canopy heterogeneity in boreal forest by coupling high spatial resolution satellite imagery and field data. *Remote Sensing of Environment*, 114:299–308.

Rivera, J. P., Verrelst, J., Leonenko, G., and Moreno, J. (2013). Multiple cost functions and regularization options for improved retrieval of leaf chlorophyll content and lai through inversion of the prosail model. *Remote Sensing*, 5(7):3280–3304.

Rose, J. (2010). *Landowners Guide for Woodlot threaded by Emerald Ash Borer*. Ontario Ministry of Natural Resource, Canada.

Rosenqvist, A., Milne, A., Lucas, R., and Dobson, C. (2003). A review of remote sensing technology in support of the kyoto protocol. *Environmental Science and Policy*, 6:441–455.

Rouse, J. W., Haas, R. H., Schell, J. A., and Deering, D. W. (1973). Monitoring vegetation systms in the great plains with erts. *in third ERTS Symposium*, pages 309 – 317.

Ryall, K. L., Fidgen, J. G., and Turgeon, J. J. (2011). Detectability of the emerald urban tree by using branch samples. *Environmental Entomology*, 40(3):679 – 688.

Shih, J.L.; Chuang, S. (2008). One-sided offset approximation of freeform curves for interference-free nurbs machining. *Comput.-Aided Des.*, 40:931–937.

Sibley, D. (2009). *The Sibley Guide to Trees*. Alfred, A., Ed. Knopf, New York, NY, USA.

Sims, D. A. and Gamon, J. A. (2002). Relationships between leaf pigment content and spectral reflectance across a wide range of species leaf structures and development stages. *Remote Sensing of Environment*, 81:337 – 354.

Smith, A., Nadeaum, C., Freemantle, J. I. H., Teillet, P., Kehler, I., Daub, N., Bourgeois, G., and de Jong, R. (2005). Leaf area index from chris satellite and application in plant yield estimation. *Proceeding of 26th Canadian Symposium on Remote Sensing, Wolfville, Nova Scotia*.

Smitley, D., Davis, T., and Rebek, E. (2008). Progession of ash canopy thinning and dieback outward from the initial infestation of emerald ash borer (coleoptera: Buprestidae) in southeastern michgan. *Journal of Economic Entormol*, 101:1643 – 1650.

Souci, J. S., Hanou, I., and Puchalski, D. (2009). High resolution remote sensing analysis for early detection and response planning for emerald ash borer. *Photogrammetric Engineering and Remote Sensing*, pages 905–911.

St-Louis, V., Pidgeon, A., Radeloff, V., Hawbaker, T., Tuceryan, M., and Jain, A. (1998). Handbook of pattern reorganization and computer vision. *Singapore World Scientific: Singapore*.

Strachan, I., Pattey, E., and Boisvert, B. (2002). Impact of nitrogen and environmental conditions on corn as detected by hyperspectral reflectance. *Remote Sensing of Environment*, 80:213–224.

Suits, G. H. (1972). The calculation of the directional reflectnace of vegetative canopy. *Remote Sensing of Environment*, 2:117–125.

Sydnor, T. D., Bumgardner, M., and Todd, A. (2007). The potential economicimpacts of merald ash borer on ohio us communities. *International Society of Arboriculture*, 33(1):45 – 54.

Terjund, H. W. and Louie, S. S. F. (1974). Enery input and output climate of the world. *Arch. Met. Geoph. Biokl*, 20:129–160.

Thenkabail, P. S. (2001). Optimal hyperspectral narrowbands for discriminating agricultural crops. *Remote Sensing Reviews*, 20(4):259–291.

Thenkabail, S., Lyon, J. G., and Huete, A. (2012). *Hyperspectral remote sensing of vegetation*. CRC Press, Taylor and Francis Group, USA.

Tooke, T., Coops, N., Goodwin, N., and Voogt, J. (2009). Extracting urban vegetation characteristics using spectral mixture analysis and decision tree classifications. *Remote Sensing of Environment*, 113:398–407.

Toutin, T. (2004). Review article: Geometric processing of remote sensing images: models, algorithms and methods. *International Journal of Remote Sensing*, 25(10):1893–1924.

Tso, B. and Mather, P. M. (2009). *Classifiaction methods for remotely sensed data*. CRC Press, Taylor and Francis Group, Boca Raton, USA.

Tucker, C. (1979). Red and photographic infrared linear combinations for monitoring vegetation. *Remote Sensing of Environment*, 8:12 –15.

Veganzones, M. A., Maldonado, J. O., and Grana, M. (2008). On content-based image retreival systems for hyperspectral remote sensing images. *Computational Intelligence for Remote Sensing, Studies in Computational Intelligence*, 133:123–144.

Verhoef, V. and Back, H. (2003). Simulation of hyperspectral and directional radiance images using coupled biophysical and atmospheric radiative transfer models. *Remote Sensing of Environment*, 87:23–41.

Verhoef, W. (1984). Light scattering by leaf layers with application to canopy reflectance modeling: The sail model. *Remote Sensing of Environment*, 23:125–141.

Vogelmann, J. E., Rock, B. N., and Moss, D. M. (1993). Red edge spectral measurements from sugar maple leaves. *International Journal of Remote Sensing*, 14:1563–1575.

Walter-Shen, E. A. and Biehl, L. L. (1990). Measuring vegetation spectral properties. *Remote Sensing Reviews*, 5(1):179–205.

Wang, J. G. (1987). Analysis of effects of observed elements in network (in chinese). *Journal of Wuhan Technical University of Surveying and Mapping*, 12:74–84.

Wang, Y. (2012). Regularization for inverse models in remote sensing. *Progress in physical geography*, 36(1):38–59.

Warner, T., Lee, J., and McGraw, J. (1998). Delineation and identification of individual trees in the eastern deciduous forest. *Proceedings of the International Forum Automated Interpretation of High Spatial Resolution Digital Imagery for Forestry.*

Waser, L., Ginzler, C., Kuechler, M., Baltsavias, E., and Hurni, L. (2011). Semi-automatic classification of tree species in different forest ecosystems by spectral and geometric variables derived from airborne digital sensor (ads40) and rs30 data. *Remote Sensing of Environment*, 115:76–85.

Watson, D. J. (1947). Comparative physiological studies in the growth of field crops. i. variation in net assimilation rate and leaf area between species and varieties and within and between years. *Annals of Botany*, page 41C76.

Weiers, S., Bock, M., Wissen, M., and Rossner, G. (2004). Mapping and indicator approaches for the assessment of habitats at different scales using remote sensing and gis methods. *Landscape and Urban Planning*, 67:43–65.

White, H. P. (1999). *Hyperspectral remote sensing of vegetation parameteres using statistical and physical models.* Ph.D. Thesis, York University, Toronto, Canada.

White, H. P., Miller, J. R., and Chen, J. M. (2002). Four-scale linear model for anisotropic reflectance (flair) for plant canopies ii: Partial validation and inversion using field measurements. *IEEE Transactions on Geoscience and Remote Sensing (Institute of Electrical and Electronics Engineers)*, 40(5):1038–1046.

Widlowski, J. L., Pinty, B., Clerici, M., Disney, M., Dai, Y., De Kauwe, M., de Ridder, K., Kallel, A., Kobayashi, H., Lavergne, T., Ni-Meister, W., Olchev, A., Quaife, T., Wang, S., Yang, W., Yang, Y., and Yuan, H. (2011). Rami4pilps: An intercomparison of formulations for the partitioning of solar radiation in land surface models. *Journal of Geophysical Research*, 116(D02019):25PP.

Widlowski, J. L., Taberner, M., Pinty, B., Bruniquel-Pinel, V., Disney, M., Fernandes, R., Gastellu-Etchegorry, J. P., Gobron, N., Kuusk, A., Lavergne, T., Leblanc, S., Lewis, P. E., Martin, E., Mottus, M., North, P., Qin, W., Robustelli, M., Rochdi, N., Soler, C., Thompson, R., Verhoef, W., Verstrete, M. M., and Xie, D. (2007). Third radiation transfer model intercomparison (rami) exercise: Documenting progress in canopy reflectance models. *Journal of Geophysical Research*, 112(D09111):28PP.

Wu, A. S., Xiong, X. X., and Angal, A. (2011). Evaluation of detector-to-detector and mirror side differences for terra modis reflective solar bands using simultaneous misr observations. *International Journal of Remote Sensing*, 32(2):299–312.

Wulder, M., Hall, R., Coops, N., and Franklin, S. (2004). High spatial resolution remotely sensed data for ecosystem characterization. *BioScience*, 54:511–521.

Yuksel, C., Schaefer, S., and Keyser, J. (2011). Parameterization and applications of catmull rom curves. *Comput.-Aided Des.*, 43:747 – 755.

Zarco-Tejada, P. J., Miller, J. R., Noland, T. L., Mohammed, G. H., and Sampson, P. H. (2001). Scaling-up and model inversion methods with narrow-band optical indices for chlorophyll content estimation in closed forest canopies with hyperspectral data. *IEEE Transactions on Geosciences and Remote Sensing*, 39:1491–1507.

Zhang, K. and Hu, B. (2012). Individual urban tree species classification using very high spatial resolution airborne multi-spectral imagery using longitudinal profiles. *Remote Sensing*, 4:1741–1757.

Zhang, K., Hu, B., Hanou, I. S., and Jin, L. (2012). Early detection of ash emerald ash borer (eab) infestation using hyperspectral imagery. *the proceeding of International Geoscience and Remote Sensing Symposium (IGARSS) 2012, Munich, Germany*, pages 6360 – 6363.

Zhang, K., Hu, B., and Robinson, J. (2014). Early detection of emerald ash borer (eab) infestation using multi-sourced data: a case study in the town of oakville, ontario, canada. *Journal of Applied Remote Sensing, in press*, 8(1).

Zhang, K., Hu, B., Wang, J., Pattey, E., and Smith, A. M. (2011). Improving the retrieval of the biophysical parameters of vegetation canopies by using the contribution index. *Canadian Journal for Remote Sensing*, 37(6):643–652.

Zhang, K., Hu, B., Wang, J., and Smith, A. (2009). Improving the canopy model inversion using a weighting function. *proceedings of the 30th Canadian Symposium of Remote Sensing, Lethbridge, AB.*

Zhang, S., Li, L., and Seah, H. (1998). Vectorization of digital images using algebraic curves. *Computer Graphy*, 22:91 – 101.

Zhang, Y., Chen, J. M., Miller, J. R., and Noland, T. L. (2008). Leaf chlorophyll content retrieval from airborne hyperspectral remote sensing imagery. *Remote Sensing of Environment*, 112:3234 – 3247.